Nanostrutture

Dipartimento di Fisica, UniTS

4 giugno 2019

1 Considerazioni generali

1.1 Nano che?

- Cosa significa nano? il prefisso nano implica una moltiplicazione per 10^{-9}. Con nanostrutture si intendono sistemi per i quali l'estensione (*size*) è su scala nanometrica almeno in una direzione.
- Come si ottiene una nano-struttura? Confinando il moto lungo una o più direzioni con mezzi opportuni (variazione della composizione del materiale (eterostrutture), applicando campi elettrici o magnetici, ...) . Daremo esempi di confinamento in una dimensione (sistema bidimensionale, in due dimensioni (sistema unidimensionale), in tre dimensioni (sistema zero dimensionale (punto quantistico, piccolo cluster).
- Perché nano è interessante? Perché con opportune tecniche di fabbricazione si possono ottenere sistemi con proprietà suscettibili di applicazioni tecnologiche, sistemi a volte non presenti in natura.

1.2 Rapporto superficie/volume in sistemi estesi ed in sistemi micrometrici e nanometrici

- Spesso in fisica statistica si argomenta dell'irrilevanza dei contributi di superficie rispetto a quelli di volume, in quanto nel limite termodinamico ($N \to \infty$, $V \to \infty$, $N/V = \varrho =$ cost) in generale il contributo di superfice è trascurabile rispetto a quello di volume.
  - Consideriano ad esempio il contributo di volume all'energia $E_V = eV$, ove e è l'energia per unità di volume ed il contributo di superficie all'energia $E_S = e'S$, ove e' è l'energia per unità di superficie dovuta ad una interfaccia; e ed e' sono quantità intensive. Evidentemente
  $$\frac{E_S}{E_V} \propto \frac{S}{V} \propto V^{-1/3} \to 0.$$
  - Consideriamo ora un sistema di taglia (estensione) finita. Cominciamo con un cubetto di spigolo $L = 1mm$. Assumendo un volume per atomo $v = 1/\varrho = 40\text{Å}^3$ si ottiene che il sistema contiene $N = 2.5 \cdot 10^{19}$ atomi. Semplici considerazioni portano al risultato che, se $N_S = S/v^{2/3}$ sono gli atomi in superficie e $N = V/v$,
  $$\frac{N_S}{N} = \frac{S/v^{2/3}}{V/v} = \frac{6V^{2/3}}{V/v^{1/3}} = \frac{6}{(V/v)^{1/3}} = \frac{6}{N^{1/3}}.$$
  - Quindi con $L = 1mm$ otteniamo $N_S/N = 2 \cdot 10^{-6}$, con $L = 1\mu m$ otteniamo $N_S/N = 2 \cdot 10^{-3}$ e con $L = 1nm$ c'è un solo atomo al centro circondato da 24 atomi di superficie.

- Ci possono essere casi nei quali si è interessati a massimizzare la superficie dei sistemi. Ad esempio nei catalizzatori i fenomeni d'interesse avvenogono alla superficie del catalizzatore che tipicamente è un metallo nobile molto costoso. Quindi la massimizzazione della superficie rispetto al volume risponde ad un'esigenzia di *economia*!

1.3 Dipendenza delle proprietà dei sistemi dalla dimensionalità

Supponendo di essere in grado di realizzare sistemi a dimensionalità ridotta, può essere interessante studiare come le proprietà dei sistemi dipendano dalla dimensionalità D. A questo scopo studiamo la densità di stati di elettroni non interagenti, ma con massa efficace per tener conto della presenza di un reticolo cristallino nel quale gli elettroni si muovono. Più avanti giustificheremo l'approssimazione di massa efficace e daremo cenni al modo di introdurre anche l'interazione tra gli elettroni.

Consideriamo nel seguito elettroni con massa m^* in D dimensioni in un dominio di spigolo L. La dispersione in energia degli stati di particella singola sarà quindi $\epsilon(k,\sigma) = \hbar^2k^2/2m^*$ ($\sigma = \pm 1$, per elettroni con proiezione di spin su/giù) e la densità di stati in energia (DOS) (per un sistema spolarizzato di spin, quindi con $\sum_\sigma = 2$) sarà

$$\begin{aligned} g(E) &= \frac{2}{L^D}\sum_{\mathbf{k}} \delta(E - \hbar^2k^2/2m^*) = \frac{2}{L^D}\int_0^\infty \frac{dk}{(2\pi/L)^D} k^{D-1}\Omega_D \delta(E - \hbar^2k^2/2m^*) \\ &= \frac{\Omega_D}{2^{D-1}\pi^D}\frac{m^*}{\hbar^2}k_*^{D-2}, \end{aligned}$$

ove $k_* = (2m^*E)^{1/2}/\hbar$ e $\Omega_D = D\pi^{D/2}/\Gamma(D/2+1)$. Quindi

$$g(E) = \frac{D}{\Gamma(D/2+1)}\left(\frac{m^*}{2\pi\hbar^2}\right)^{D/2} E^{D/2-1}\Theta(E).$$

1.4 Confinamento in una dimensione: sistema bidimensionale

1.4.1 L'Hamiltoniana di singola particella

Consideriamo ora l'Hamiltoniana $\hat{H}_0$ di singola particella in presenza di un potenziale $V(z)$

$$\hat{H}_0 = \frac{\hat{p}_x^2}{2m^*} + \frac{\hat{p}_y^2}{2m^*} + \frac{\hat{p}_z^2}{2m^*} + V(\hat{z}).$$

Supponiamo di conoscere le soluzioni del problema trasverso (moto lungo la direzione z)

$$\left[\frac{\hat{p}_z^2}{2m^*} + V(\hat{z})\right]\phi_n(z) = \varepsilon_n\phi_n(z) \qquad n = 0,1,2,....$$

La soluzione dell'equazione di Schrodinger completa

$$\hat{H}_0 \left|\psi_{\vec{k},n}\right\rangle = E_{\vec{k},n} \left|\psi_{\vec{k},n}\right\rangle$$

è

$$\psi_{\vec{k},n}(x,y,z) = \frac{1}{\sqrt{L}} e^{ik_x x} \frac{1}{\sqrt{L}} e^{ik_y y} \phi_n(z),$$

restringendosi alla componente spaziale dell'orbitale di singola particella, con

$$E_{\vec{k},n} = \frac{\hbar^2 k_x^2}{2m} + \frac{\hbar^2 k_y^2}{2m} + \varepsilon_n \equiv \frac{\hbar^2 k^2}{2m^*} + \varepsilon_n.$$

1.4.2 La densità di stati

Evidentemente la densità di stati in energia è

$$g(E) = \sum_n g_n(E),$$

con $(D = 2)$

$$\begin{aligned} g_n(E) &= \frac{2}{L^D} \sum_{\mathbf{k}} \delta(E - E_{\vec{k},n}) = \frac{2}{L^D} \sum_{\mathbf{k}} \delta(E - \varepsilon_n - \hbar^2 k^2/2m^*) = \frac{2}{\Gamma(2)} \frac{m^*}{2\pi\hbar^2} \Theta(E - \varepsilon_n), \\ &= \frac{m^*}{\pi\hbar^2} \Theta(E - \varepsilon_n). \end{aligned}$$

La densità di stati complessiva $g(E)$ è mostrata in Fig. 1.1.

1.4.3 Tipi di confinamento in una dimensione

Il potenziale $V(z)$ può avere varie forme. In un pozzo quantistico ha un profilo a buca (come mostrato in Fig. 1.1) e la buca (in 1 D) ha sempre almeno uno stato legato. Se la buca è abbastanza alta ne ha più d'uno. Una buca di larghezza L con pareti infinite ha infiniti stati legati con energie $\hbar^2\pi^2 n^2/(2m^* L^2)$ ed n interi non nulli. In tutti i casi i livelli energetici ϵ_n sono discreti, come pure nel caso di un confinamento armonico $(V(z) = m^*\omega^2 z^2/2)$.

1.5 Lunghezza di de Broglie ed effetti quantistici in sistemi confinati

La dinamica degli elettroni in un solido periodico è usualmente studiata in approssimazione semiclassica in termini di pacchetti di onde di Bloch. Nel caso in cui si sia interessati a pacchetti di stati di una singola banda centrati al minimo della banda e con componenti molto vicine al minimo è naturale ricorrere al concetto di massa efficace (m^*). Normalmente la massa efficace è un tensore reale, simmetrico e con autovalori positivi. In generale, a meno di affermazioni esplicite, in queste lezioni ci restringeremo a minimi sferici.

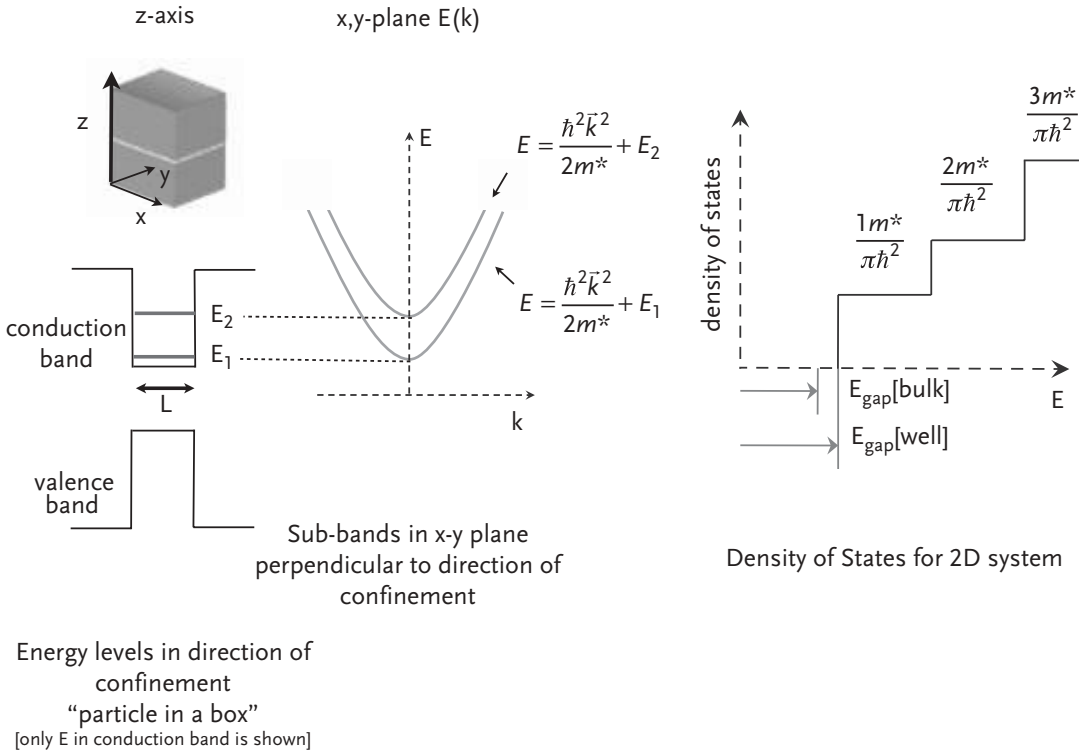

Figura 1.1: Densità di stati in un pozzo quantistico

Un modo di capire se il confinamento va ad inficiare la descrizione in termini di pacchetti è di confrontare la lunghezza di de Broglie termica

$$\lambda = h/\sqrt{2m^*E}$$

con la larghezza del potenziale $V(z)$, che nel caso della buca è L. Qui l'energia termica è stimata come $E = (3/2)K_BT$ e a temperatura ambiente ($T = 300^oK$)si ottiene

$$\lambda = \frac{6.02}{\sqrt{m^*/m_e}} nm,$$

con $m_e = 9.11 \cdot 10^{-28} g$, la massa dell'elettrone nel vuoto. Così si ottiene $\lambda = 24nm$ per una buca di GaAs, usando una massa efficace $m^* = 0.063m_e$. Perchè gli effetti di confinamento possano essere trascurati e si possa utilizzare l'approssimazione semiclassica bisogna che $L \gg \lambda$.

Notiamo che nella letteratura dei semiconduttori viene usata una definizione di lunghezza d'onda di de Broglie diversa da quella incontrata in meccanica statistica

$$\lambda = \frac{h}{\sqrt{2\pi m^* K_B T}}.$$

2 Envelope function approximation

Envelope functions and effective mass approximation

4

In this chapter we are interested in the quantum mechanical motion of electrons in the crystal if the periodic lattice potential is perturbed. This can occur as a result of the presence of lattice defects, impurities, or doping atoms. It can also arise due to the incorporation of interfaces between different layers of materials. Other reasons could be the presence of external electric or magnetic fields, or internal fields arising from time-dependent lattice distortions or vibrations such as those caused by phonons or surface acoustic waves. In this chapter, we will restrict ourselves to static perturbations small enough to be treated in lowest order perturbation theory, and of a spatial range much larger than the lattice constant of the underlying material. We will see that this restriction leads to considerable simplifications leading us to an effective mass Schrödinger equation for electrons in conduction bands with parabolic dispersion.

4.1 Quantum mechanical motion in a parabolic band

Weak and long-range perturbations of perfect crystal symmetry can be caused, for example, by an external electric field, or by the presence of a charged doping atom. Figure 4.1 shows schematically the perturbed

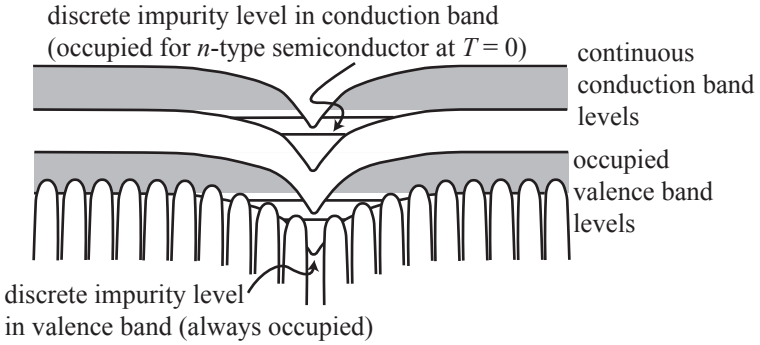

Fig. 4.1 Continuum and discrete energy levels in the vicinity of a doping atom in a semiconductor. E_1 is the energy of a discrete level below the conduction band edge; E_2 is the energy of a state in the continuum. (Reprinted with permission from Slater, 1949. Copyright 1949 by the American Physical Society.)

lattice potential in the presence of a positively charged doping atom.

There are a number of different ways of solving this quantum mechanical problem for the electronic motion. The methods differ essentially in the set of basis functions used as a starting point for a perturbation treatment. People have used Bloch-states (Enderlein and Schenk, 1992), band edge states from $\mathbf{k}\cdot\mathbf{p}$-theory (Luttinger and Kohn, 1955), and the so-called Wannier states (Wannier, 1937; Zinman, 1972; Kittel, 1970). In order to give some insight into the derivation of the equation of motion, we will work in the Bloch-state basis and restrict the discussion to a perturbation of a parabolic conduction band with minimum at Γ as it is found, for example, in GaAs.

The problem on the basis of Bloch-states. Assume that we have solved Schrödinger's equation for the unperturbed crystal. The corresponding dispersion relations $E_n(\mathbf{k})$ and the Bloch-functions $\psi_{n\mathbf{k}}(\mathbf{r}) = e^{i\mathbf{kr}}u_{n\mathbf{k}}(\mathbf{r})$ are known. Now we seek the solution of the perturbed Schrödinger equation

$$[H_0 + U(\mathbf{r})]\,\Psi(\mathbf{r}) = E\Psi(\mathbf{r}), \tag{4.1}$$

where H_0 is the hamiltonian of the unperturbed lattice and $U(\mathbf{r})$ is the perturbing potential. We expand the wave function $\Psi(\mathbf{r})$ on the basis of Bloch-states:

$$\Psi(\mathbf{r}) = \sum_{n,\mathbf{k}} F_n(\mathbf{k})\psi_{n\mathbf{k}}(\mathbf{r}).$$

Inserting this expansion into Schrödinger's equation gives

$$\sum_{n\mathbf{k}} \psi_{n\mathbf{k}}(\mathbf{r})\,[E_n(\mathbf{k}) - E + U(\mathbf{r})]\,F_n(\mathbf{k}) = 0.$$

Multiplying by $\psi^\star_{n'\mathbf{k}'}(\mathbf{r})$ and integrating over $\mathbf{r}$ leads to

$$\sum_{n,\mathbf{k}} \left[(E_n(\mathbf{k}) - E)\,\delta_{n\mathbf{k},n'\mathbf{k}'} + U_{n'\mathbf{k}',n\mathbf{k}}\right] F_n(\mathbf{k}) = 0, \tag{4.2}$$

where we have used the orthogonality of Bloch-states and introduced the matrix elements of the perturbing potential

$$U_{n'\mathbf{k}',n\mathbf{k}} = \int d^3r\;\; \psi^\star_{n'\mathbf{k}'}(\mathbf{r})U(\mathbf{r})\psi_{n\mathbf{k}}(\mathbf{r}).$$

The matrix elements of the perturbation. We will now further simplify the matrix elements of the perturbation. To this end we introduce the Fourier transform of $U(\mathbf{r})$ (see Appendix A.2) and obtain

$$U_{n'\mathbf{k}',n\mathbf{k}} = \int d^3q\;\; U(\mathbf{q}) \int d^3r\;\; e^{i(\mathbf{k}-\mathbf{k}'+\mathbf{q})\mathbf{r}} u^\star_{n'\mathbf{k}'}(\mathbf{r})u_{n\mathbf{k}}(\mathbf{r}).$$

In this expression we can expand the lattice periodic function $u^\star_{n'\mathbf{k}'}(\mathbf{r})u_{n\mathbf{k}}(\mathbf{r})$ into a Fourier series and obtain for the matrix element

$$U_{n'\mathbf{k}',n\mathbf{k}} = \int d^3q\;\; U(\mathbf{q}) \sum_{\mathbf{K}} C^{n'\mathbf{k}'}_{n\mathbf{k}}(\mathbf{K}) \int d^3r\;\; e^{i(\mathbf{k}-\mathbf{k}'+\mathbf{q}+\mathbf{K})\mathbf{r}}$$

with the so-called Bloch integral

$$C_{n\mathbf{k}}^{n'\mathbf{k}'}(\mathbf{K}) = \frac{1}{V_0}\int_{EZ} d^3r \;\; e^{-i\mathbf{K}\mathbf{r}} u^{\star}_{n'\mathbf{k}'}(\mathbf{r}) u_{n\mathbf{k}}(\mathbf{r}).$$

The spatial integral in the expression for the matrix element $U_{n'\mathbf{k}',n\mathbf{k}}$ contributes only if the exponent vanishes, i.e., if $\mathbf{q} = \mathbf{k}' - \mathbf{k} - \mathbf{K}$. As a matter of fact, the integral is a representation of Dirac's delta function. Therefore the matrix element simplifies to

$$U_{n'\mathbf{k}',n\mathbf{k}} = (2\pi)^3 \sum_{\mathbf{K}} U(\mathbf{k}' - \mathbf{k} - \mathbf{K}) C_{n\mathbf{k}}^{n'\mathbf{k}'}(\mathbf{K}). \tag{4.3}$$

So far we have used the periodicity of the crystal lattice without using any approximation.

Simplifying approximations. For further simplifications to the problem we make the following assumptions about the perturbation:

(1) We assume that the perturbing potential changes slowly on the scale of the lattice constant, i.e., $U(\mathbf{q})$ is significant only for $q \ll \pi/a$.

(2) We assume that the perturbation is small compared to typical energy separations of bands in the crystal.

(3) We assume that the coefficients $F_n(\mathbf{k})$ have significant values only for small values of $\mathbf{k}$.

According to the third assumption, we consider only states near the nondegenerate Γ-minimum. As a consequence of this and the first assumption, in the sum over $\mathbf{K}$ only $\mathbf{K} = 0$ is retained and the matrix element simplifies to

$$U_{n'\mathbf{k}',n\mathbf{k}} \approx (2\pi)^3 U(\mathbf{k}' - \mathbf{k}) C_{n\mathbf{k}}^{n'\mathbf{k}'}(0).$$

Now we would like to simplify the Bloch integral $C_{n\mathbf{k}}^{n'\mathbf{k}'}(0)$. Based on the third assumption, we employ the expansion of the Bloch-functions near the conduction band minimum, eq. (3.19). We obtain

$$C_{n\mathbf{k}}^{n'\mathbf{k}'}(0) = \frac{1}{V_0}\int_{EZ} d^3r \;\; u^{\star}_{n'\mathbf{k}'}(\mathbf{r}) u_{n\mathbf{k}}(\mathbf{r}) \approx \frac{1}{(2\pi)^3}\delta_{nn'} + \mathcal{O}(k^2),$$

and therefore

$$U_{n'\mathbf{k}',n\mathbf{k}} \approx U(\mathbf{k}' - \mathbf{k})\delta_{nn'}.$$

This means that, given our assumptions, the perturbation does not mix states of neighboring bands, but only states of different $\mathbf{k}$ near the Γ-minimum. With the above result for the matrix element, the equation of motion (4.2) simplifies to

$$\sum_{\mathbf{k}} \left[(E_n(\mathbf{k}) - E)\,\delta_{\mathbf{k},\mathbf{k}'} + U(\mathbf{k}' - \mathbf{k}) \right] F_n(\mathbf{k}) = 0.$$

Simplification of the wave function. The wave function in real space now reads

$$\Psi(\mathbf{r}) = \sum_{\mathbf{k}} F_n(\mathbf{k}) e^{i\mathbf{kr}} u_{n\mathbf{k}}(\mathbf{r}).$$

Only small wave vectors $\mathbf{k}$ are important here, due to the long-range nature of $U(\mathbf{r})$. We therefore approximate $u_{n\mathbf{k}}(\mathbf{r}) \approx u_{n0}(\mathbf{r})$ and obtain for the wave function

$$\Psi(\mathbf{r}) = u_{n0}(\mathbf{r}) \sum_{\mathbf{k}} F_n(\mathbf{k}) e^{i\mathbf{kr}} = u_{n0}(\mathbf{r}) F_n(\mathbf{r}).$$

In the last step we have interpreted the sum over $\mathbf{k}$ as the Fourier series of a real space function $F_n(\mathbf{r})$. This function is of long range compared to the lattice period and is called the *envelope function* of the wave function.

Approximating the dispersion. We now approximate the dispersion relation $E_n(\mathbf{k})$ accordingly by using an approximation for small $\mathbf{k}$. Near the Γ-minimum we have [cf. eq. (3.22)]

$$E_{\mathrm{c}}(\mathbf{k}) = E_{\mathrm{c}} + \frac{\hbar^2 k^2}{2m^\star},$$

where $m^\star$ is the effective mass of electrons in the conduction band. With these simplifications the equation of motion for electrons reads

$$\frac{\hbar^2}{2m^\star} k^2 F_{\mathrm{c}}(\mathbf{k}) + \sum_{\mathbf{k}'} U(\mathbf{k}-\mathbf{k}') F_{\mathrm{c}}(\mathbf{k}') = (E - E_{\mathrm{c}}) F_{\mathrm{c}}(\mathbf{k}).$$

Equation of motion in real space. This equation determines the Fourier components of the envelope function $F_{\mathrm{c}}(\mathbf{r})$. Transformation from Fourier space into real space is straightforward. The first term on the left-hand side corresponds to the second derivative of the envelope function in real space. The second term is a convolution integral which transforms into the product of the two corresponding functions in real space. We therefore obtain the following differential equation determining the envelope function $F_{\mathrm{c}}(\mathbf{r})$:

$$\Big[-\frac{\hbar^2}{2m^\star}\Delta + \underbrace{E_{\mathrm{c}} + U(\mathbf{r})}_{:=E_{\mathrm{c}}(\mathbf{r})} \Big] F_{\mathrm{c}}(\mathbf{r}) = E F_{\mathrm{c}}(\mathbf{r}). \tag{4.4}$$

This is exactly Schrödinger's equation (4.1) where the periodic lattice potential hidden in H_0 has disappeared, but the free electron mass in H_0 has been replaced by the effective mass of the conduction band electrons. Introducing the local band edge energy $E_{\mathrm{c}}(\mathbf{r})$, this function acts as the effective potential in which the conduction band electrons move.

The envelope function $F_{\mathrm{c}}(\mathbf{r})$ brings about very convenient simplifications. For example, matrix elements of a quantum mechanical quantity, which have to be calculated using the complete electronic wave function,

can usually be expressed as integrals over the envelope function alone. As an example, we consider the electron density. Assume that the envelope functions $F_i(\mathbf{r})$ are solutions of eq. (4.4) with energies E_i. The electron density of the system is then given by

$$n(\mathbf{r}) = \sum_i |\psi_i(\mathbf{r})|^2 f(E_i) = |u_{c0}(\mathbf{r})|^2 \sum_i |F_i(\mathbf{r})|^2 f(E_i),$$

where $f(E)$ is the Fermi distribution function. The envelope function and the lattice periodic function $u_{c0}(\mathbf{r})$ vary on different length scales. Within a primitive cell at position $\mathbf{R}$ of the lattice $F_i(\mathbf{r}) \approx F_i(\mathbf{R})$ is essentially constant. If we are interested only in the mean density in the primitive cell at $\mathbf{R}$, it is given by

$$n(\mathbf{R}) = \underbrace{\frac{N}{V_{EZ}} \int_{EZ} dV\, |u_{c0}(\mathbf{r})|^2}_{=1} \sum_i |F_i(\mathbf{R})|^2 f(E_i) = \sum_i |F_i(\mathbf{R})|^2 f(E_i).$$

On a length scale that is large compared to the lattice constant, the electron density is given by the envelope function alone and we can neglect the lattice periodic function $u_{n0}(\mathbf{r})$.

Hydrogen-like impurities. A simple application of the concept of the envelope function is the determination of the energy levels of a hydrogen-like impurity in a semiconductor. It has indeed been shown that modern fabrication techniques have the potential to allow a precise incorporation of single doping atoms at predefined locations. Figure 4.2 shows scanning tunneling microscope images of a hydrogen passivated Si(001) surface. Using the tip of the scanning tunneling microscope, hydrogen atoms can be locally desorbed. Such a spot of about 1 nm size is shown in Fig. 4.2(a). If the surface is then exposed to PH_3, the molecules are preferentially adsorbed at those positions, where the hydrogen passivation has been removed. A thermal annealing step lets the P atom diffuse into the top layer of the Si substrate where it forms a substitutional doping site as shown in Fig. 4.2(b).

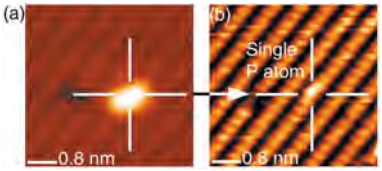

Fig. 4.2 STM images of atomically controlled single phosphor atom incorporation into Si(001). (a) Hydrogen terminated Si(001) surface with a hydrogen desorption point. (b) The same area after PH_3 dosing and annealing showing a single P atom incorporated at the location defined by the H-desorption point. (Reprinted with permission from Schofield, 2003. Copyright 2003 by the American Physical Society.)

As an example for the use of the effective mass equation, we consider a silicon atom sitting on the Ga site in a GaAs lattice. The silicon atom can satisfy all bonds with neighboring arsenic atoms using only three of its four valence electrons. As a consequence, one excess electron and an excess positive elementary charge in the silicon nucleus remain. Such a silicon atom is called a donor, because it can give away the excess electron. However, the positively charged donor ion will bind the excess electron, and the Coulomb interaction between them will appear in the equation for the envelope function:

$$\left[-\frac{\hbar^2}{2m^\star}\Delta - \frac{e^2}{4\pi\varepsilon\varepsilon_0 r} \right] F_c(\mathbf{r}) = (E - E_c) F_c(\mathbf{r}).$$

The important point is that the relative dielectric constant of the host crystal, in our case GaAs, enters in the Coulomb potential. It accounts

for the polarization of the lattice by the charged donor, which effectively reduces the interaction strength. The solution of this quantum problem is that of the hydrogen problem, in which the Rydberg energy $E_{\mathrm{Ry}} = 13.6$ eV is replaced by an effective Rydberg energy $E^{\star}_{\mathrm{Ry}}$ and Bohr's radius $a_{\mathrm{B}} = 0.53$ Å by an effective radius $a^{\star}_{\mathrm{B}}$:

$$\begin{aligned} E^{\star}_{\mathrm{Ry}} &= \frac{e^4 m^{\star}}{2(4\pi\varepsilon\varepsilon_0)^2\hbar^2} = E_{Ry}\frac{m^{\star}}{m_{\mathrm{e}}}\frac{1}{\varepsilon^2} \\ a^{\star}_{\mathrm{B}} &= \frac{4\pi\varepsilon\varepsilon_0\hbar^2}{m^{\star}e^2} = a_{\mathrm{B}}\frac{m_{\mathrm{e}}}{m^{\star}}\varepsilon. \end{aligned}$$

For GaAs, with $\varepsilon = 12.53$ and $m^{\star} = 0.067 m_{\mathrm{e}}$, we find $E^{\star}_{\mathrm{Ry}} = 5.7$ meV and $a^{\star}_{\mathrm{B}} = 100$ Å. The energy levels of the hydrogen-like impurity are then

$$E_n = E_{\mathrm{c}} - \frac{E^{\star}_{\mathrm{Ry}}}{n^2}.$$

These states are discrete and lie below the conduction band edge of the unperturbed crystal as schematically shown in Fig. 4.3. As in the hydrogen atom, the excitation energy $E^{\star}_{\mathrm{Ry}}$ from the ground state to the lower edge of the conduction band (continuum) is called the binding energy. Measured binding energies of donors in GaAs are 5.789 meV for $\mathrm{Se_{As}}$, 5.839 meV for $\mathrm{Si_{Ga}}$, 5.870 meV for $\mathrm{S_{As}}$, 5.882 meV for $\mathrm{Ge_{Ga}}$, and 5.913 meV for $\mathrm{C_{Ga}}$. These values agree quite well with the theoretical prediction for $E^{\star}_{\mathrm{Ry}}$.

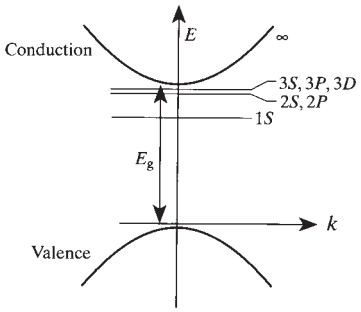

Fig. 4.3 Energy levels of a hydrogen-like impurity in GaAs (Yu and Cardona, 2001).

Figure 4.4 shows the total wave function of the ground state including the Bloch part emphasizing that the envelope function determines the shape of the probability density distribution on length scales large compared to the lattice constant.

Equation of motion at the Γ-minimum of the conduction band in the presence of a magnetic field. The equation of motion of an electron at the conduction band minimum under the influence of a

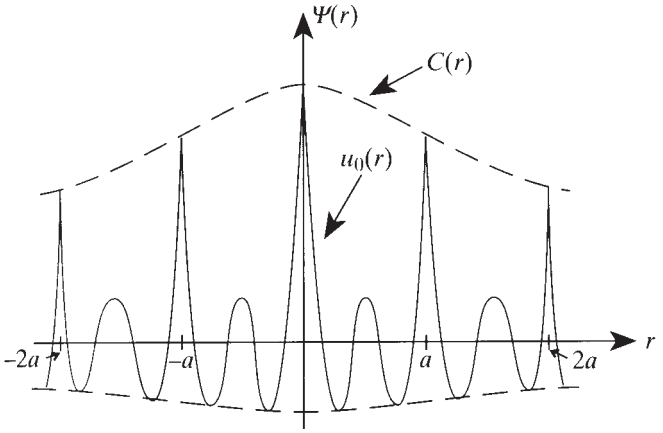

Fig. 4.4 Total wave function of the hydrogen-like impurity in GaAs including the Bloch contribution (Yu and Cardona, 2001).

magnetic field has been derived by Luttinger (1951), and by Luttinger and Kohn (1955) using similar methods. It was also found that, in this case, the equation for the envelope function is identical to the effective mass Schrödinger equation for a free particle in a magnetic field. Under the simultaneous influence of a vector potential $\mathbf{A}(\mathbf{r})$ and an electrostatic potential $U(\mathbf{r})$ the equation of motion for electrons at the Γ-minimum of the conduction band (see, e.g., Winkler 2003) reads

$$\left[\frac{1}{2m^\star}\left(\frac{\hbar}{i}\nabla + |e|\mathbf{A}(\mathbf{r})\right)^2 + U(\mathbf{r}) + \frac{1}{2}g^\star\mu_\mathrm{B}\boldsymbol{\sigma}\mathbf{B}\right]F_\mathrm{c}(\mathbf{r}) = (E - E_\mathrm{c})F_\mathrm{c}(\mathbf{r}). \tag{4.5}$$

Here, the elementary charge $|e| = 1.6 \times 10^{-19}$ C is taken to be a positive number. In the following chapters of the book we will frequently call the envelope function $F_\mathrm{c}(\mathbf{r})$ simply the *wave function* of the electron, because its equation of motion is identical with that of an electron with mass $m^\star$ in vacuum. We will further use the convention that all energies are measured from the conduction band edge of the unperturbed crystal, such that $E_\mathrm{c} = 0$ in the above equation. The effective mass $m^\star$ and the effective $g^\star$-factor entering in the above equation can be calculated from the knowledge of the band edge parameters given in Table 3.6 using eqs. (3.30) and (3.31).

Equation (4.5) is of great importance for semiconductor nanostructures. Methods of structuring and patterning materials allow the fabrication of tailored potential landscapes $U(\mathbf{r})$. Magnetic fields can be created in the laboratory that influence the electronic motion as they do in the free electron case. Solving the equations of motion is greatly facilitated by the existence of many analytical solutions and approximative schemes from quantum mechanics textbooks.

The considerations leading to eq. (4.5) for conduction band electrons near Γ can be extended to semiconductors with conduction band minima at other points in the first Brillouin zone (e.g., silicon or germanium). In this case, the wave function is expanded at the corresponding conduction band minima rather than at Γ. More complicated equations of motion result due to the valley degeneracy and the anisotropic effective masses. The theory for valence band holes is also much more demanding, because there are degenerate states at Γ.

4.2 Semiclassical equations of motion, electrons and holes

Conduction band electrons. With the validity of the effective mass Schrödinger equation (4.5) for the crystal electron, the semiclassical limit of quantum mechanics (i.e., the motion of wave packets) must have its range of application in semiconductor physics. Wave packets can be constructed from the envelope functions $F_\mathrm{c}(\mathbf{r})$ and the dynamics of its center of mass can be investigated. The result is Newton's equation of

motion

$$m^\star \ddot{\mathbf{r}} = -|e|(\mathbf{E} - \dot{\mathbf{r}} \times \mathbf{B}), \tag{4.6}$$

where $\mathbf{E}$ is the electric field and $\mathbf{B}$ is the magnetic field at the location of the electron. As a consequence, there is a variety of possibilities in the physics of semiconductor nanostructures to investigate the borderlines between classical and quantum physics. Examples are investigations of the relation between classical and quantum chaos, or the transition from quantum to classical mechanics in the presence of decoherence.

Valence band holes. We will now briefly discuss the dynamics of holes, i.e., missing electrons near a maximum of the valence band, in the classical limit. The convex curvature of the valence band could be interpreted using a negative effective mass. Newton's equation of motion reads in this case

$$-m^\star \ddot{\mathbf{r}} = -|e|(\mathbf{E} - \dot{\mathbf{r}} \times \mathbf{B}).$$

However, a negative effective mass is physically not very intuitive. We can reinterpret this equation of motion by multiplying it by -1:

$$m^\star \ddot{\mathbf{r}} = +|e|(\mathbf{E} - \dot{\mathbf{r}} \times \mathbf{B})$$

This can be interpreted as the equation of motion for particles with positive mass $m^\star$, but with *positive charge* $+|e|$. The occurrence of a positive charge at the top of the valence band is also intuitive from another point of view. In the electrically neutral, uncharged semiconductor crystal the valence band is completely filled. Removing an electron from the top of the valence band, an initially localized positive charge remains. Such a missing electron is called a hole. According to the above equation of motion, the effective mass $m^\star$ and the charge $+e$ are properties of this hole which appears to move through the crystal like a classical particle.

Further reading

- Papers: Slater 1949; Luttinger 1951; Luttinger and Kohn 1955.
- Effective mass from $\mathbf{k} \cdot \mathbf{p}$-theory: Davies 1998; Kittel 1970; Yu and Cardona 2001.
- Effective mass from quasi-classical considerations with group velocity and Newton's equation of motion: Kittel 2005; Kittel 1970; Singleton 2001; Ashcroft and Mermin 1987.
- Effective mass from the hydrogen problem in semiconductors, doping: Davies 1998.
- Band structure of semiconductors: Winkler 2003.

Exercises

(4.1) Consider the differential equation for the envelope function, eq. (4.5), with a magnetic field $\mathbf{B} = (0, 0, B)$ and the Coulomb potential $U(\mathbf{r}) = e^2/4\pi\epsilon\epsilon_0 r$.

(a) Give reasons why the solution of the problem can be separated in that of the orbital motion and that of the spin dynamics.

(b) Discuss qualitatively the effects of the magnetic field on the spin dynamics.

(c) Discuss qualitatively how the magnetic field affects the orbital energy levels and wave functions.

(4.2) In silicon, the hamiltonian for the conduction band envelope function in the effective mass equation is given by

$$H = \frac{\hbar^2}{2m_{\mathrm{L}}}\frac{\partial^2}{\partial x^2} + \frac{\hbar^2}{2m_{\mathrm{T}}}\left(\frac{\partial^2}{\partial y^2} + \frac{\partial^2}{\partial z^2}\right) + V_{\mathrm{c}}(r),$$

where $V_{\mathrm{c}} = e^2/4\pi\epsilon\epsilon_0 r$ is the Coulomb potential, and m_{L} and m_{T} are the longitudinal and transverse effective masses, respectively. Consider the case $m_{\mathrm{L}} = m_{\mathrm{T}} + \Delta m$, where $\Delta m/m_{\mathrm{T}} \ll 1$. Calculate the effect of the presence of Δm on the energies of the 1s-, 2s-, and 2p-states of a hydrogen-like impurity using perturbation theory.

3 Interazioni effettive - singola sottobanda occupata

3.1 Gas di elettroni 2D - buca infinita di larghezza a e potenziale triangolare

Consideriamo pochi elettroni interagenti in banda di conduzione ed in presenza di un potenziale confinante lunfo z, descritti quindi dall'Hamiltoniana

$$\begin{aligned} H = H_1 + H_2 &\equiv \sum_{i=1}^{N} \left[\frac{-\hbar^2 \nabla_i^2}{2m^*} + V(z_i) \right] + \sum_{i<j} v(|\mathbf{r}_i - \mathbf{r}_{j|}) \\ &= \sum_i \left[-\frac{\hbar^2}{2m^*} \frac{\partial^2}{\partial z^2} + V(z) \right] + \sum_i \left[-\frac{\hbar^2}{2m^*} \left(\frac{\partial^2}{\partial x^2} + \frac{\partial^2}{\partial y^2} \right) \right] + \sum_{i<j} v(|\mathbf{r}_i - \mathbf{r}_j|) \\ &\equiv H_z + \tilde{H}, \end{aligned}$$

ove evidentemente

$$H_z = \sum_i \left[-\frac{\hbar^2}{2m^*} \frac{\partial^2}{\partial z^2} + V(z) \right],$$

$$\tilde{H} = \sum_i \left[-\frac{\hbar^2}{2m^*} \left(\frac{\partial^2}{\partial x^2} + \frac{\partial^2}{\partial y^2} \right) \right] + \sum_{i<j} v(|\mathbf{r}_i - \mathbf{r}_j|),$$

$\mathbf{r} = (x, y, z) = (\mathbf{s}, z)$, con $\mathbf{s} = (x, y)$ e $V(z)$ è il potenziale di confinamento trasverso. Vogliamo studiare ora il problema agli autovalori per l'hamiltoniana H:

$$H\Psi(\mathbf{s}_1,\, \mathbf{s}_1,\, ...,\mathbf{s}_N;\, z_1,\, z_2,\, ...,\, z_N) = E\Psi(\mathbf{s}_1,\, \mathbf{s}_1,\, ...,\mathbf{s}_N;\, z_1,\, z_2,\, ...,\, z_N). \tag{3.1}$$

Evidentemente conosciamo le soluzioni del problema di singola particella con hamiltoniana

$$h = -\frac{\hbar \nabla^2}{2m^*} + V(z);$$

esse sono, restringendosi alla componente spaziale dell'orbitale di singola particella,

$$\phi_{k,n}(\mathbf{r}, z) = \frac{e^{i\mathbf{k}\cdot\mathbf{s}}}{\sqrt{A}} \varphi_n(z),$$

con

$$-\frac{\hbar^2\varphi_n^{"}(z)}{2m^*}+V(z)\varphi_n(z)=\epsilon_n\varphi_n(z),$$

e $\mathbf{k}=(k_x,k_y)$.

Ora gli orbitali $\{\varphi_n(z)\}$ costituiscono una base completa rispetto a ze possiamo sviluppare le soluzioni dell'eq. 3.1 come

$$\Psi(\mathbf{s}_1,\,\mathbf{s}_1,\,...,\mathbf{s}_N;\,z_1,\,z_2,\,...,\,z_N)=\sum_{n_1,n_2,...,n_N}\psi_{n_1,n_2,...,n_N}(\mathbf{s}_1,\,\mathbf{s}_1,\,...,\mathbf{s}_N)\varphi_{n_1}(z_1)\varphi_{n_2}(z_N)\ldots\varphi_{n_N}(z_N).$$

Se i livelli ϵ_n sono ben separati ($\varepsilon_{n_2}-\varepsilon_{n_1}\gg\varepsilon_F$), ove ε_F è l'energia di Fermi del problema bidimensionale nel piano (x,y), si può approssimare

$$\begin{aligned}\Psi(\mathbf{s}_1,\,\mathbf{s}_1,\,...,\mathbf{s}_N;\,z_1,\,z_2,\,...,\,z_N)&\approx\psi_{n_1,n_1,...,n_1}(\mathbf{s}_1,\,\mathbf{s}_1,\,...,\mathbf{s}_N)\varphi_{n_1}(z_1)\varphi_{n_1}(z_N)\ldots\varphi_{n_1}(z_N)\\&\equiv\psi(\mathbf{s}_1,\,\mathbf{s}_1,\,...,\mathbf{s}_N)\varphi_{n_1}(z_1)\varphi_{n_1}(z_N)\ldots\varphi_{n_1}(z_N),\end{aligned}$$

mettendo tutte le particelle nell'orbitale trasverso più basso in energia, ovvero $\phi_{n_1}(z)$, ottenendo

$$\begin{aligned}H\psi(\mathbf{s}_1,\,\mathbf{s}_1,\,...,\mathbf{s}_N)\varphi_{n_1}(z_1)\varphi_{n_1}(z_N)\ldots\varphi_{n_1}(z_N)&=(\tilde{H}+N\varepsilon_{n_1})\psi(\mathbf{s}_1,\,\mathbf{s}_1,\,...,\mathbf{s}_N)\varphi_{n_1}(z_1)\varphi_{n_1}(z_N)\ldots\varphi_{n_1}(z_N)\\&=E\psi(\mathbf{s}_1,\,\mathbf{s}_1,\,...,\mathbf{s}_N)\varphi_{n_1}(z_1)\varphi_{n_1}(z_N)\ldots\varphi_{n_1}(z_N),\end{aligned}$$

che implica

$$(\tilde{H}\psi(\mathbf{s}_1,\,\mathbf{s}_1,...,\mathbf{s}_N)\varphi_{n_1}(z_1)\varphi_{n_1}(z_N)\ldots\varphi_{n_1}(z_N)=E_{2D}\psi(\mathbf{s}_1,\,\mathbf{s}_1,...,\mathbf{s}_N)\varphi_{n_1}(z_1)\varphi_{n_1}(z_N)\ldots\varphi_{n_1}(z_N),\tag{3.2}$$

ove $E_{2D}=E-N\epsilon_1$. Attenzione: l'hamiltoniana $\tilde{H}$ dipende ancora dalle intere coordinate spaziali $\mathbf{r_i}=(\mathbf{s}_{i,},z_i)$, $i=1,N$.

Possiamo però proiettare l'eq. 3.2 su $\varphi_{n_1}(z_1)\varphi_{n_1}(z_N)\ldots\varphi_{n_1}(z_N)$ moltiplicandola sulla sinistra per $\varphi^*_{n_1}(z_1)\varphi^*_{n_1}(z_N)\ldots\varphi^*_{n_1}(z_N)$ ed integrando rispetto a $z_{1.}z_{2,}\ldots,\,z_N$. Evidentemente in questa operazione bisogna valutare integrali del tipo

$$\int_{-\infty}^{\infty}dz|\varphi_{n_1}(z)|^2,$$

che valgono 1 (gli orbitali sono normalizzati ad 1) ed integrali del tipo

$$u(|\mathbf{s_i}-\mathbf{s}_j|)=\int_{-\infty}^{\infty}dz_i\int_{-\infty}^{\infty}dz_j|\varphi_{n_1}(z_i)|^2|\varphi_{n_1}(z_j)|^2v(|\mathbf{r}_i-\mathbf{r}_j)|,\tag{3.3}$$

con $\mathbf{r}=(\mathbf{s},z)$. Consideriamo il caso di elettroni in un mezzo con costante dielettrica ϵ,

$$v(r)=\frac{e^2}{\epsilon r}=\frac{e^2}{\epsilon\sqrt{s^2+z^2}},$$

e sviluppiamo il potenziale di interazione di coppia in trasformata di Fourier:

$$\int \frac{d\mathbf{q}}{(2\pi)^2} e^{i\mathbf{q}\cdot\mathbf{s}} \int \frac{dQ}{2\pi} e^{iQz} \frac{4\pi e^2}{\epsilon(q^2+Q^{2)}}. \tag{3.4}$$

È facile mostrare con il metodo dei residui che

$$\int \frac{dQ}{2\pi} e^{iQz} \frac{4\pi e^2}{\epsilon(q^2+Q^{2)}} = \frac{2\pi e^2}{\epsilon q} e^{-qz}. \tag{3.5}$$

Utilizzando le eq. 3.4 e 3.5 nell'eq. 3.3si ottiene

$$\begin{aligned} u(|\mathbf{s_i}-\mathbf{s}_j|) &= \int_{-\infty}^{\infty} dz_i \int_{-\infty}^{\infty} dz_j |\varphi_{n_1}(z_i)|^2 |\varphi_{n_1}(z_j)|^2 \int \frac{d\mathbf{q}}{(2\pi)^2} e^{i\mathbf{q}\cdot(\mathbf{s}_i-\mathbf{s}_j)} \frac{2\pi e^2}{\epsilon q} e^{-q|z_i-z_j|} \\ &= \int \frac{d\mathbf{q}}{(2\pi)^2} e^{i\mathbf{q}\cdot(\mathbf{s}_i-\mathbf{s}_j)} \frac{2\pi e^2}{\epsilon q} \int_{-\infty}^{\infty} dz_i \int_{-\infty}^{\infty} dz_j |\varphi_{n_1}(z_i)|^2 |\varphi_{n_1}(z_j)|^2 e^{-q|z_i-z_j|} \\ &\int \frac{d\mathbf{q}}{(2\pi)^2} e^{i\mathbf{q}\cdot(\mathbf{s}_i-\mathbf{s}_j)\mathbf{r}} \frac{2\pi e^2}{\epsilon q} F(q) \equiv \int \frac{d\mathbf{q}}{(2\pi)^2} e^{i\mathbf{q}\cdot(\mathbf{s}_i-\mathbf{s}_j)\mathbf{r}} u(q), \end{aligned}$$

ove, chiaramente il fattore di forma $F(q)$ è dato da

$$F(q) = \int_{-\infty}^{\infty} dz_i \int_{-\infty}^{\infty} dz_j |\varphi_{n_1}(z_i)|^2 |\varphi_{n_1}(z_j)|^2 e^{-q|z_i-z_j|}$$

e

$$u(q) = \frac{2\pi e^2}{\epsilon q} F(q).$$

E quindi la proiezione fornisce l'equazione

$$H_{2D}\psi(\mathbf{s}_1,\, \mathbf{s}_1,\, ...,\mathbf{s}_N) = E_{2D}\psi(\mathbf{s}_1,\, \mathbf{s}_1,\, ...,\mathbf{s}_N),$$

ove

$$H_{2D} = \sum_i \left[-\frac{\hbar^2}{2m^*} \left(\frac{\partial^2}{\partial x^2} + \frac{\partial^2}{\partial y^2} \right) \right] + \sum_{i<j} u(|\mathbf{s}_i - \mathbf{s}_j|).$$

Abbiamo ottenuto in questo modo un'hamiltoniana bidimensionale con un'interazione di coppia effettiva, che si ottiene dall'originaria interazioine tridimensionale, attraverso la proiezione sull'orbitale del moto trasverso più basso in energia. L'interazione effettiva ha una forma particolarmente semplice in termini della trasformata di Fourier che risulta essere il prodotto di $u(q) = u_{2D}(q)F(q)$, con $u_{2D}(q) = 2\pi e^2/(\epsilon q)$ l'interazione per un sistema strettamente bidimensionale (corrisponente a $|\varphi_{n_1}(z)|^2 = \delta(z)$). Il fattore di forma $F(q)$, che tiene conto della forma del potenziale di localzzazione, dipende dalla particolare scelta di $V(z)$. Per una buca di altezza infinita e larghezza a (pozzo quantistico) si ottiene il risultato esatto

$$F(q) = \frac{1}{4\pi^2 + q^2a^2} \left(3qa + \frac{8\pi^2}{qa} - \frac{32\pi^4}{q^2a^2} \frac{1-e^{-qa}}{4\pi^2+q^2a^2} \right).$$

Per una buca triangolare

$$V(z) = \begin{cases} \infty & z < 0 \\ eFz & z > 0 \end{cases},$$

con F l'intensità del campo elettrico trasverso nella regine d'interesse, un trattamento variazionale per l'equazione di singola particella fornisce

$$F(q) = [1 + \frac{9}{8}\frac{q}{b} + \frac{3}{8}\frac{q^2}{b^2}][1 + \frac{q}{b}]^{-3},$$

ove il vettore d'onda b contiene parametri del dispositivo (HIGFET) nel caso in cui la costante dielettrica dei due materiali che costituiscono l'interfaccia siano identiche (caso GaAs - AlGaAs). Nel caso del MOSFET (composto da un'interfaccia Si- Ossido di Si) l'espressione è leggermente più complicata, dalla presenza delle due costanti dielettriche che sono apprezzabilmente diverse. Nei due casi il limite strettamente bidimensionale $F(q) = 1$ è ottenuto rispettivamente per $a \to 0$ e $b \to \infty$.

4 Graphene - additions to Foa-Torres

This is followed by the improved description provided by *first-principles* calculations within density functional theory (DFT) and beyond using *many-body perturbation theory within the GW approximation*, which leads to a renormalized Fermi velocity close to the Dirac point. The next part focuses on the specificities of graphene nanoribbons (GNRs), with a description of the formation of confinement-induced energy gaps which increase linearly with reducing the lateral size. These GNR structures are shown to share some commonalities with their folded versions, since carbon nanotubes (CNTs) are often pictured as the geometrical result of rolling up a graphene ribbon. Carbon nanotubes are found to be either metallic or semiconducting depending on their helical symmetry. Metallic (armchair) nanotubes are actually the best existing one-dimensional ballistic conductors, almost insensitive to the Peierls dimerization mechanism, and exhibiting quantized conductance when appropriately connected to metals such as palladium. The energy gaps in semiconducting tubes downscale linearly with the tube diameter, and eventually close for the limit of very large diameter (in accordance with the zero-gap limit of a graphene monolayer). Finally, note that there is currently great interest in analyzing the effects of chemical doping and structural defects in graphene-based materials, given the possibility to tailor the electronic properties and add novel functionalities to the related devices, to improve or complement the silicon-based CMOS technologies.

2.2 Electronic properties of graphene

2.2.1 Tight-binding description of graphene

In two-dimensional graphene, carbon atoms are periodically arranged in an infinite honeycomb lattice (Fig. 2.1(a)). Such an atomic structure is defined by two types of bonds within the sp^2 hybridization, as described in Chapter 1. From the four valence orbitals of the carbon atom (the $2s$, $2p_x$, $2p_y$, and $2p_z$ orbitals, where z is the direction perpendicular to the sheet), the (s, p_x, p_y) orbitals combine to form the inplane σ (bonding or occupied) and σ^* (antibonding or unoccupied) orbitals. Such orbitals are even with respect to the planar symmetry. The σ bonds are strongly covalent bonds determining the energetic stability and the elastic properties of graphene (Fig. 2.1(a)). The remaining p_z orbital, pointing out of the graphene sheet as shown in Fig. 2.1(a), is odd with respect to the planar symmetry and decoupled from the σ states. From the lateral interaction with neighboring p_z orbitals (called the $pp\pi$ interaction), localized π (bonding) and π^* (antibonding) orbitals are formed (Wallace, 1947). Graphite consists of a stack of many graphene layers. The unit cell in graphite can be primarily defined using two graphene layers translated from each other by a C-C distance ($a_{cc} = 1.42$ Å). The three-dimensional structure of graphite is maintained by the weak interlayer van der Waals interaction between π bonds of adjacent layers, which generate a weak but finite out-of-plane delocalization (Charlier, Gonze & Michenaud, 1994*b*).

The bonding and antibonding σ bands are actually strongly separated in energy (> 12 eV at Γ), and therefore their contribution to electronic properties is commonly

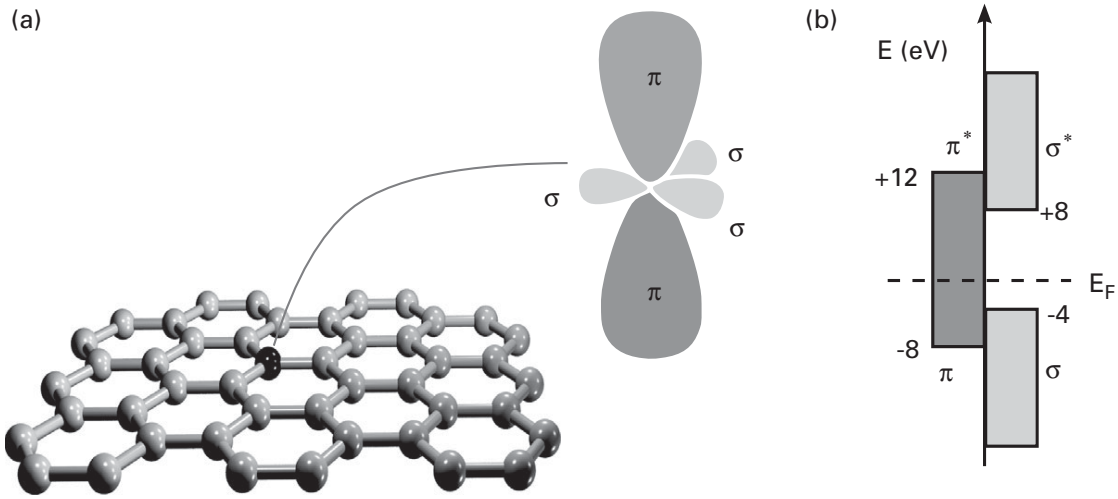

Figure 2.1 The carbon valence orbitals. (a) The three σ orbitals in graphene and the π orbital perpendicular to the sheet. The σ bonds in the carbon hexagonal network strongly connect the carbon atoms and are responsible for the binding energy and the structural properties of the graphene sheet. The π bonds are perpendicular to the surface of the sheet. The corresponding bonding and antibonding σ bands are separated by a large energy gap of $\sim$12 eV; while (b) the bonding and antibonding π states lie in the vicinity of the Fermi level (E_F). Consequently, the σ bonds are frequently neglected for prediction of the electronic properties of graphene around the Fermi energy.

disregarded (Fig. 2.1(b)). The two remaining π bands completely describe the low-energy electronic excitations in both graphene (Wallace, 1947) and graphite (Charlier *et al.*, 1991). The bonding π and antibonding π^* orbitals produce valence and conduction bands (Fig. 2.1(b)) which cross at the charge neutrality point (Fermi level of undoped graphene) at vertices of the hexagonal Brillouin zone.

Carbon atoms in a graphene plane are located at the vertices of a hexagonal lattice. This graphene network can be regarded as a triangular Bravais lattice with two atoms per unit cell (A and B) and basis vectors $(\mathbf{a}_1, \mathbf{a}_2)$:

$$\mathbf{a}_1 = a\left(\frac{\sqrt{3}}{2}, \frac{1}{2}\right), \quad \mathbf{a}_2 = a\left(\frac{\sqrt{3}}{2}, -\frac{1}{2}\right). \tag{2.1}$$

Note that $a = \sqrt{3}a_{cc}$, where $a_{cc} = 1.42$ Å is the carbon–carbon distance in graphene. In Fig. 2.2(a) A-type and B-type atoms are represented by full and empty dots respectively. From this figure we see that each A- or B-type atom is surrounded by three atoms of the opposite type.

By using the condition $\mathbf{a}_i \cdot \mathbf{b}_j = 2\pi\delta_{ij}$, the reciprocal lattice vectors $(\mathbf{b}_1, \mathbf{b}_2)$ can be obtained,

$$\mathbf{b}_1 = b\left(\frac{1}{2}, \frac{\sqrt{3}}{2}\right), \quad \mathbf{b}_2 = b\left(\frac{1}{2}, -\frac{\sqrt{3}}{2}\right), \tag{2.2}$$

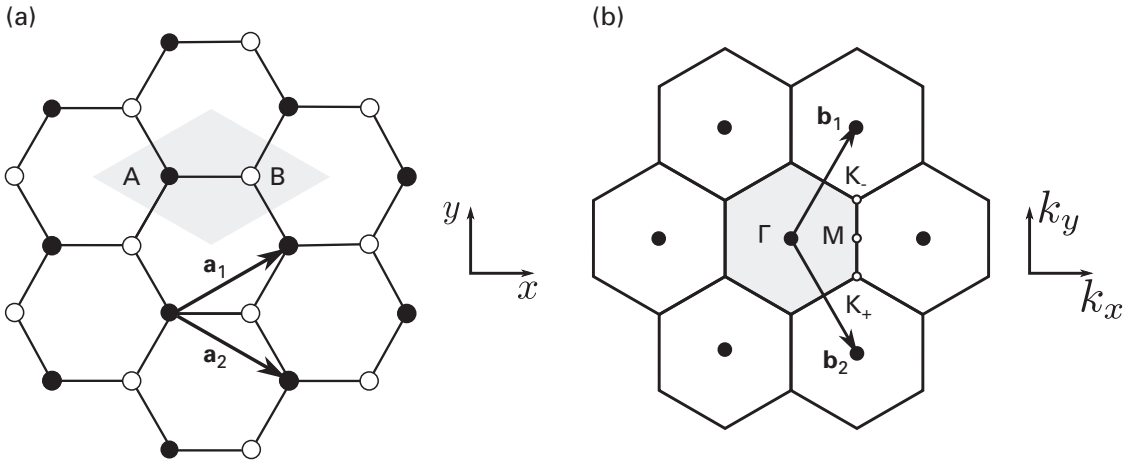

Figure 2.2 (a) Showing the basis vectors $\mathbf{a}_1$ and $\mathbf{a}_2$ in the hexagonal network of graphene. This network is a triangular Bravais lattice with a two atom-basis: A (full dots) and B (empty dots). (b) The reciprocal lattice points corresponding to the triangular Bravais lattice (full dots) as well as the associated basis vectors $\mathbf{b}_1$ and $\mathbf{b}_2$. The unit cell/Brillouin zone are shown shaded gray in a and b respectively. Highly symmetric points labeled with Γ (zone center), K_+, K_-, and M are also indicated in b.

with $b = 4\pi/(3a_{cc}) = 4\pi/a\sqrt{3}$. These vectors are shown in Fig. 2.2(b) together with the first Brillouin zone (shaded gray). This hexagonal-shaped Brillouin zone[1] is built as the Wigner–Seitz cell of the reciprocal lattice. Out of its six corners, two of them are inequivalent (the others can be written as one of these two plus a reciprocal lattice vector). These two special points are denoted with K_+ and K_-. Another high symmetry point is the one labeled with M in Fig. 2.2(b). They can be chosen as:

$$\mathbf{K}_+ = \frac{4\pi}{3a}\left(\frac{\sqrt{3}}{2}, -\frac{1}{2}\right), \quad \mathbf{K}_- = \frac{4\pi}{3a}\left(\frac{\sqrt{3}}{2}, \frac{1}{2}\right), \quad \mathbf{M} = \frac{2\pi}{\sqrt{3}a}(1, 0)\,. \tag{2.3}$$

When the carbon atoms are placed onto the graphene hexagonal network (Fig. 2.2(a)), the electronic wavefunctions from different atoms overlap. However, because of symmetry the overlap between the p_z orbitals and the s or the p_x and p_y electrons is strictly zero. Therefore, the p_z electrons which form the π bonds in graphene can be treated independently from the other valence electrons. Within this π-band approximation, the A atom (or B atom) is uniquely defined by one orbital per atom site $p_z(\mathbf{r} - \mathbf{r}_A)$ (or $p_z(\mathbf{r} - \mathbf{r}_B)$).

To derive the electronic spectrum of the total Hamiltonian, the corresponding Schrödinger equation has to be solved. According to Bloch's theorem, the eigenfunctions evaluated at two given Bravais lattice points $\mathbf{R}_i$ and $\mathbf{R}_j$ differ from each other in just a phase factor, $\exp(\mathrm{i}\mathbf{k}\cdot(\mathbf{R}_i - \mathbf{R}_j))$. Because of the two-atom basis, the Bloch *ansatz*

[1] Note that the hexagonal shape of the Brillouin zone is a consequence of the triangular Bravais lattice. It is by no means connected with the two-atom basis which does not enter into the definition of the Brillouin zone.

for the eigenfunctions is a linear combination of Bloch sums[2] on each sublattice:

$$\Psi(\mathbf{k},\mathbf{r}) = c_A(\mathbf{k})\tilde{p}_z^A(\mathbf{k},\mathbf{r}) + c_B(\mathbf{k})\tilde{p}_z^B(\mathbf{k},\mathbf{r}), \tag{2.4}$$

where

$$\tilde{p}_z^A(\mathbf{k},\mathbf{r}) = \frac{1}{\sqrt{N_{\text{cells}}}}\sum_j \mathrm{e}^{\mathrm{i}\mathbf{k}.\mathbf{R}_j} p_z(\mathbf{r}-\mathbf{r}_A-\mathbf{R}_j), \tag{2.5}$$

$$\tilde{p}_z^B(\mathbf{k},\mathbf{r}) = \frac{1}{\sqrt{N_{\text{cells}}}}\sum_j \mathrm{e}^{\mathrm{i}\mathbf{k}.\mathbf{R}_j} p_z(\mathbf{r}-\mathbf{r}_B-\mathbf{R}_j), \tag{2.6}$$

where $\mathbf{k}$ is the electron wavevector, N_{cells} the number of unit cells in the graphene sheet, and $\mathbf{R}_j$ is a Bravais lattice point. In the following we will neglect the overlap $s = \langle p_z^A | p_z^B \rangle$ between neighboring p_z orbitals. Then, the Bloch sums form an orthonormal set:

$$\langle \tilde{p}_z^\alpha(\mathbf{k}) \mid \tilde{p}_z^\beta(\mathbf{k}') \rangle = \delta_{\mathbf{k},\mathbf{k}'}\delta_{\alpha,\beta}, \tag{2.7}$$

where $\alpha,\beta = A,B$. Using these orthogonality relations in the Schrödinger equation, $\mathcal{H}\Psi(\mathbf{k},\mathbf{r}) = E\Psi(\mathbf{k},\mathbf{r})$, one obtains a 2×2 eigenvalue problem,

$$\begin{pmatrix} \mathcal{H}_{AA}(\mathbf{k}) & \mathcal{H}_{AB}(\mathbf{k}) \\ \mathcal{H}_{BA}(\mathbf{k}) & \mathcal{H}_{BB}(\mathbf{k}) \end{pmatrix} \begin{pmatrix} c_A(\mathbf{k}) \\ c_B(\mathbf{k}) \end{pmatrix} = E(\mathbf{k}) \begin{pmatrix} c_A(\mathbf{k}) \\ c_B(\mathbf{k}) \end{pmatrix}. \tag{2.8}$$

The matrix elements of the Hamiltonian are given by:

$$\mathcal{H}_{AA}(\mathbf{k}) = \frac{1}{N_{\text{cells}}}\sum_{i,j} \mathrm{e}^{\mathrm{i}\mathbf{k}.(\mathbf{R}_j-\mathbf{R}_i)} \langle p_z^{A,\mathbf{R}_i} \mid \mathcal{H} \mid p_z^{A,\mathbf{R}_j} \rangle, \tag{2.9}$$

$$\mathcal{H}_{AB}(\mathbf{k}) = \frac{1}{N_{\text{cells}}}\sum_{i,j} \mathrm{e}^{\mathrm{i}\mathbf{k}.(\mathbf{R}_j-\mathbf{R}_i)} \langle p_z^{A,\mathbf{R}_i} \mid \mathcal{H} \mid p_z^{B,\mathbf{R}_j} \rangle, \tag{2.10}$$

with $\mathcal{H}_{AA} = \mathcal{H}_{BB}$ and $\mathcal{H}_{AB} = \mathcal{H}_{BA}^*$, and introducing the notation $p_z^{A,\boldsymbol{\tau}} = p_z(\mathbf{r}-\mathbf{r}_A-\boldsymbol{\tau})$ and $p_z^{B,\boldsymbol{\tau}} = p_z(\mathbf{r}-\mathbf{r}_B-\boldsymbol{\tau})$. After simple manipulations, and by restricting the interactions to first-nearest-neighbors only, one gets:

$$\begin{aligned} \mathcal{H}_{AB}(\mathbf{k}) &= \langle p_z^{A,0}|\mathcal{H}|p_z^{B,0}\rangle + \mathrm{e}^{-\mathrm{i}\mathbf{k}.\mathbf{a}_1}\langle p_z^{A,0}|\mathcal{H}|p_z^{B,-\mathbf{a}_1}\rangle + \mathrm{e}^{-\mathrm{i}\mathbf{k}.\mathbf{a}_2}\langle p_z^{A,0}|\mathcal{H}|p_z^{B,-\mathbf{a}_2}\rangle \\ &= -\gamma_0\alpha(\mathbf{k}), \end{aligned} \tag{2.11}$$

where γ_0 stands for the transfer integral between first neighbor π orbitals (typical values for γ_0 are 2.9–3.1 eV (Charlier *et al.*, 1991, Dresselhaus *et al.*, 2000)), and the function $\alpha(\mathbf{k})$ is given by:

$$\alpha(\mathbf{k}) = (1 + \mathrm{e}^{-\mathrm{i}\mathbf{k}.\mathbf{a}_1} + \mathrm{e}^{-\mathrm{i}\mathbf{k}.\mathbf{a}_2}). \tag{2.12}$$

Taking $\langle p_z^{A,0}|\mathcal{H}|p_z^{A,0}\rangle = \langle p_z^{B,0}|\mathcal{H}|p_z^{B,0}\rangle = 0$ as the energy reference, we can write $\mathcal{H}(\mathbf{k})$ as:

$$\mathcal{H}(\mathbf{k}) = \begin{pmatrix} 0 & -\gamma_0\alpha(\mathbf{k}) \\ -\gamma_0\alpha(\mathbf{k})^* & 0 \end{pmatrix}. \tag{2.13}$$

[2] Alternatively, one may proceed by writing the Hamiltonian and the eigenfunctions in matrix form, as shown in the supplementary material on the authors' website.

This 2×2 Hamiltonian is very appealing and may also be written in terms of Pauli matrices as in (Haldane, 1988), thereby emphasizing the analogy with a spin Hamiltonian.[3] Section 2.2.2 derives in detail the consequences of the A/B bipartite lattice structure on the (pseudo)-spinor symmetry of (four-component) electronic eigenstates. The energy dispersion relations are easily obtained from the diagonalization of $\mathcal{H}(\mathbf{k})$ given by Eq. (2.13):

$$E_{\pm}(\mathbf{k}) = \pm\gamma_0|\alpha(\mathbf{k})| \tag{2.14}$$

$$= \pm\gamma_0\sqrt{3 + 2\cos(\mathbf{k}.\mathbf{a}_1) + 2\cos(\mathbf{k}.\mathbf{a}_2) + 2\cos(\mathbf{k}.(\mathbf{a}_2 - \mathbf{a}_1))}, \tag{2.15}$$

which can be further expanded as

$$E_{\pm}(k_x, k_y) = \pm\gamma_0\sqrt{1 + 4\cos\frac{\sqrt{3}k_x a}{2}\cos\frac{k_y a}{2} + 4\cos^2\frac{k_y a}{2}}. \tag{2.16}$$

The wavevectors $\mathbf{k} = (k_x, k_y)$ are chosen within the first hexagonal Brillouin zone (BZ). Clearly, the zeros of $\alpha(\mathbf{k})$ correspond to the crossing of the bands with the $+$ and $-$ signs. One can verify that $\alpha(\mathbf{k} = \mathbf{K}_+) = \alpha(\mathbf{k} = \mathbf{K}_-) = 0$ and therefore the crossings occur at the points $\mathbf{K}_+$ and $\mathbf{K}_-$. Furthermore, with a single p_z electron per atom in the π-π^* model (the three other s, p_x, p_y electrons fill the low-lying σ band), the $(-)$ band (negative energy branch) in Eq. (2.16) is fully occupied, while the $(+)$ branch is empty, at least for electrically neutral graphene. Thus, the Fermi level E_F (or charge neutrality point) is the zero-energy reference in Fig. 2.3 and the Fermi surface is composed of the set of K_+ and K_- points. Graphene displays a metallic (zero-gap) character. However, as the Fermi surface is of zero dimension (since it is reduced to a discrete and finite set of points), the term semi-metal or zero-gap semiconductor is usually employed. Expanding Eq. (2.16) for $\mathbf{k}$ in the vicinity of $\mathbf{K}_+$ (or $\mathbf{K}_-$), $\mathbf{k} = \mathbf{K}_+ + \delta\mathbf{k}$ ($\mathbf{k} = \mathbf{K}_- + \delta\mathbf{k}$), yields a linear dispersion for the π and π^* bands near these six corners of the 2D hexagonal Brillouin zone,

$$E_{\pm}(\delta\mathbf{k}) = \pm\hbar v_F|\delta\mathbf{k}|, \tag{2.17}$$

where

$$v_F = \frac{\sqrt{3}\gamma_0 a}{2\hbar} \tag{2.18}$$

is the electronic group velocity. Graphene is thus highly peculiar for this linear energy–momentum relation and electron–hole symmetry. The electronic properties in the vicinity of these corners of the 2D Brillouin zone mimic those of *massless* Dirac fermions (developed in Section 2.2.2) forming "Dirac cones" as illustrated in Fig. 2.3. The six points where the Dirac cones touch are referred to as the Dirac points. The electronic

[3] Writing the Hamiltonian in terms of Pauli matrices allows us also to classify the terms according to their symmetries. A particularly important one is electron–hole symmetry. The Hamiltonian is said to have electron–hole symmetry if there is a transformation $\mathcal{P}$, such that $\mathcal{P}^\dagger\mathcal{H}\mathcal{P} = -\mathcal{H}$. This guarantees that if Ψ is an eigenstate of $\mathcal{H}$ with a positive energy E (electron function), then $\mathcal{P}\Psi$ is also an eigenstate with energy $-E$ (hole function) and the spectrum is symmetric with respect to $E = 0$. For a Hamiltonian as the one here, a term proportional to σ_z (such as a staggering potential which breaks A-B symmetry) opens a gap but preserves electron–hole symmetry.

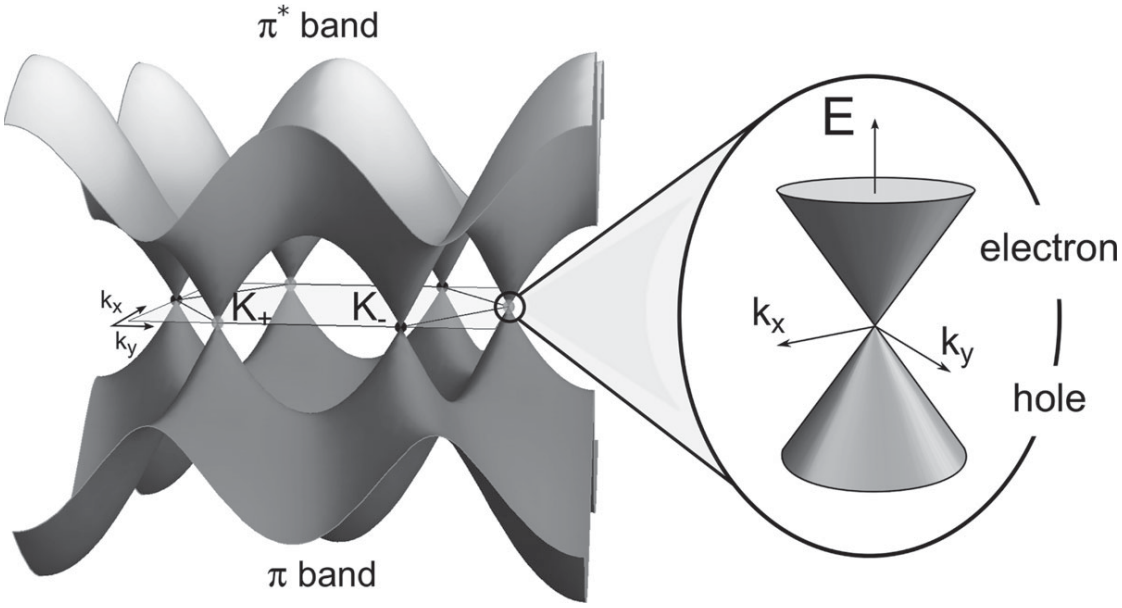

Figure 2.3 Graphene π and π^* electronic bands. In this simple approach, the π and π^* bands are symmetric with respect to the valence and conduction bands. The linear dispersion relation close to the K_+ (light grey dots) and K_- (black dots) points of the first 2D Brillouin zone gives rise to the "Dirac cones" as shown on the right. Note that close to these cones k_x and k_y are used to denote the shift from the corresponding K point.

group velocities close to those points are quite high at $\sim 8.5 \times 10^5$ m/s, and within the massless Dirac fermions analogy represent an effective "speed of light."

This simple orthogonal *tight-binding* model (Wallace, 1947) yields π and π^* zone-center Γ energies which are symmetric ($\pm\gamma_0$) with respect to E_F. In fact, the anti-bonding (unoccupied) π^* bands are located at a higher energy if the overlap integral S is not set to zero (as illustrated in Fig. 2.1(b)). A better (but more complicated) $\pi - \pi^*$ parameterization could lead to analogous results (Reich *et al.*, 2002), as well as more accurate first-principles calculations. In the following, after a presentation of the effective massless Dirac fermion model, we comment on the effects beyond nearest neighbor interactions and the so-called trigonal warping correction.

2.2.2 Effective description close to the Dirac point and massless Dirac fermions

By expanding Eq. (2.13) for the Hamiltonian around K_+ and K_- (the two inequivalent corners of the Brillouin zone) we get an approximation close to those points. To keep a compact notation in what follows, $\mathbf{k}$ measures the deviations from those points. A linear expansion then gives

$$\mathcal{H}_{K_+} = \hbar v_F \begin{pmatrix} 0 & k_x - ik_y \\ k_x + ik_y & 0 \end{pmatrix} = v_F(p_x\sigma_x + p_y\sigma_y), \tag{2.19}$$

where $p_{x(y)} = \hbar k_{x(y)}$ and the Pauli matrices are defined as usual:

$$\sigma_x = \begin{pmatrix} 0 & 1 \\ 1 & 0 \end{pmatrix}, \quad \sigma_y = \begin{pmatrix} 0 & -i \\ i & 0 \end{pmatrix}, \quad \sigma_z = \begin{pmatrix} 1 & 0 \\ 0 & -1 \end{pmatrix}. \tag{2.20}$$

The effective Hamiltonian can also be written in the more compact form:

$$\mathcal{H}_{K_+} = v_F \hat{\sigma}.\mathbf{p}, \tag{2.21}$$

where $\hat{\sigma} = (\sigma_x, \sigma_y, \sigma_z)$. For the inequivalent K point one has the transposed Hamiltonian

$$\mathcal{H}_{K_-} = \mathcal{H}^t_{K_+}. \tag{2.22}$$

Substituting $\mathbf{p}$ by the corresponding operator $\hat{\mathbf{p}} = -\mathrm{i}\hbar\hat{\nabla}$ in Eq. (2.21) (this is equivalent to the $\boldsymbol{k}.\boldsymbol{p}$ or effective mass approximation Ajiki 1993, DiVicenzo and Mele, 1984), a form equivalent to the Dirac–Weyl Hamiltonian in two dimensions is obtained, which in quantum electrodynamics follows from the Dirac equation by setting the rest mass of the particle to zero. Therefore, the low-energy excitations mimic those of massless Dirac particles of spin 1/2 (such as a massless neutrino), with velocity of light c, and inherent chirality as explained below. However, in contrast to relativistic Dirac particles, low-energy excitations of graphene have a Fermi velocity v_F about 300 times smaller than the light velocity, whereas the Pauli matrices appearing in the low-energy effective description operate on the sublattice degrees of freedom instead of spin, hence the term *pseudospin*. The low-energy quasiparticles in graphene are often referred to as massless Dirac fermions.

One of the most interesting properties of the Dirac–Weyl equation is its helical or chiral nature[4] which is a direct consequence of the Hamiltonian being proportional to the helicity operator, which here for the case of the Hamiltonian in Eq. (2.21) is defined as:

$$\hat{h} = \hat{\sigma} \cdot \frac{\mathbf{p}}{|\mathbf{p}|}. \tag{2.23}$$

The quantity $\hat{h}$ is essentially the projection of the sublattice pseudospin operator $\hat{\sigma}$ on the momentum direction. Interestingly, since $\hat{h}$ commutes with the Hamiltonian, the projection of the pseudospin is a well-defined conserved quantity which can be either positive or negative, corresponding to pseudospin and momentum being *parallel* or *antiparallel* to each other (see Fig. 2.4). At the K_- point, the Hamiltonian is proportional to $\hat{\sigma}^t.\mathbf{p}$ and involves the *left-handed* Pauli matrices $\hat{\sigma}^t$ (in contrast to the right-handed matrices $\hat{\sigma}$). Therefore, one says that chirality is inverted when passing from K_+ to K_- as represented in Fig. 2.4.

To explore this in more detail, let us rewrite once more the Hamiltonian as:

$$\mathcal{H}_\xi(\mathbf{p}) = v_F|\mathbf{p}| \begin{pmatrix} 0 & \mathrm{e}^{-\mathrm{i}\xi\theta_p} \\ \mathrm{e}^{+\mathrm{i}\xi\theta_p} & 0 \end{pmatrix}, \tag{2.24}$$

where $p_x + \mathrm{i}p_y = \sqrt{p_x^2 + p_y^2}\mathrm{e}^{\mathrm{i}\theta_p}$, $\theta_p = \arctan(p_y/p_x)$ and ξ can take the values $\xi = +1$ which corresponds to K_+ and $\xi = -1$ to K_-. Then, one can verify that this Hamiltonian is diagonalized by the unitary operator

$$\mathcal{U}_\xi = \frac{1}{\sqrt{2}} \begin{pmatrix} -\mathrm{e}^{-\mathrm{i}\xi\theta_p} & \mathrm{e}^{-\mathrm{i}\xi\theta_p} \\ 1 & 1 \end{pmatrix}. \tag{2.25}$$

[4] For massless particles the two are identical and the terms are used interchangeably.

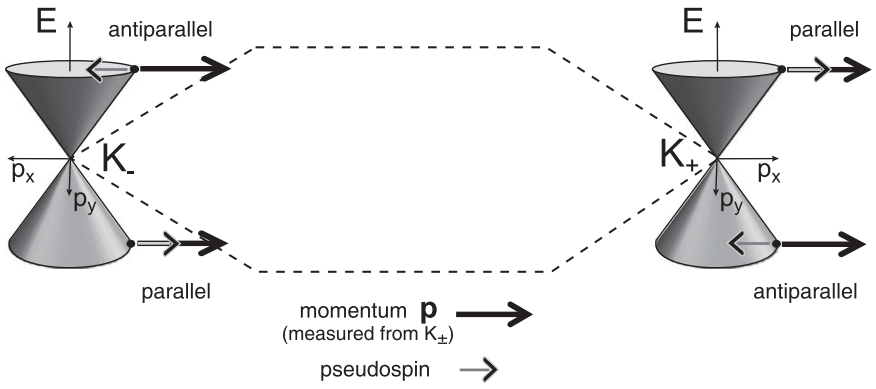

Figure 2.4 The two inequivalent Dirac cones at K_+ and K_- points of the first Brillouin zone, together with direction of the pseudospin parallel or antiparallel to the momentum $\mathbf{p}$ of selected energies in conduction and valence bands.

Indeed,

$$\mathcal{U}_\xi^\dagger(\mathbf{p})\mathcal{H}_\xi(\mathbf{p})\mathcal{U}_\xi(\mathbf{p}) = v_F \begin{pmatrix} -|\mathbf{p}| & 0 \\ 0 & |\mathbf{p}| \end{pmatrix} = -v_F|\mathbf{p}|\sigma_z, \tag{2.26}$$

which makes explicit the linear energy dispersion $E_\pm(\mathbf{p}) = \pm v_F|\mathbf{p}|$ and the electron–hole symmetry.[5] On the other hand, the eigenstates of Eq. (2.24) can be written as:

$$|\Psi_{\xi,s}\rangle = \frac{1}{\sqrt{2}} \begin{pmatrix} 1 \\ s\mathrm{e}^{+\mathrm{i}\xi\theta_p} \end{pmatrix}. \tag{2.27}$$

The index $s = \pm 1$ is the band index ($s = +1$ for the conduction band and $s = -1$ for the valence band) and ξ the valley index as stated before ($\xi = +1$ (K_+), $\xi = -1$ (K_-)). Using this explicit form for the eigenstates we can directly verify that they are also eigenstates of the appropriate helicity operator (also called chirality operator) with eigenvalues ± 1.

Around K_+ ($\xi = +1$), the pseudospin of eigenstates in the conduction band is parallel to the momentum and antiparallel for eigenstates in the valence band. The chirality in this case is simply the band index. The property around K_- ($\xi = -1$) is reversed as illustrated in Fig. 2.4. This peculiarity has a strong influence in many of the most intriguing properties of graphene. For example, for an electron to backscatter (i.e. changing $\mathbf{p}$ to $-\mathbf{p}$) it needs to reverse its pseudospin. But as the pseudospin direction is locked to that of momentum, backscattering is not possible if the Hamiltonian is not perturbed by a term which flips the pseudospin (this is also termed *absence of backscattering* (Ando, Nakanishi & Saito, 1998)).

Although we are dealing all the time with both valleys separately, it is important to keep in mind that the full structure of the eigenstates is described by a four-component spinor wavefunction, $(|\Psi_{K_+,A}\rangle, |\Psi_{K_+,B}\rangle, |\Psi_{K_-,A}\rangle, |\Psi_{K_-,B}\rangle)^t$. The full Hamiltonian of

[5] Also, by comparison with the relativistic expression, $E(p) = \pm\sqrt{p^2v_F^2 + m^{*2}c^4}$ enforces a zero effective mass.

ideal graphene is given by,

$$\hat{\mathcal{H}} = v_F \begin{pmatrix} 0 & \pi^\dagger & 0 & 0 \\ \pi & 0 & 0 & 0 \\ 0 & 0 & 0 & \pi \\ 0 & 0 & \pi^\dagger & 0 \end{pmatrix}, \tag{2.28}$$

with $\pi = p_x + \mathrm{i}p_y$ and $\pi^\dagger = p_x - \mathrm{i}p_y$. Although for this ideal case the states at both k points are decoupled, one should be aware that any perturbation which is not smooth at the atomic scale (e.g. impurities) will couple them.

Phase ambiguity and Berry phase

The existence of an inherent phase ambiguity of the quantum wavefunction is well illustrated through the Bloch theorem, which states that the eigenstates of a given Hamiltonian $\mathcal{H}$ (defining the energetics of the atomic unit cell with periodic boundary conditions) can generally be written as $|\Psi_k\rangle = \mathrm{e}^{\mathbf{ik.r}}|\psi_k\rangle$, with $|\psi_k\rangle$ defined inside the unit cell (invariant under any transformation such as $|\psi_k\rangle \rightarrow \mathrm{e}^{\varphi_k}|\psi_k\rangle$, with e^{φ_k} an arbitrary phase function in k-space). To leave the phase ambiguity and capture the phase interferences in physical observables, one has to define the so-called Berry connection (equivalent to a vector potential) as $\mathbf{A} = \mathrm{i}\langle\psi_k|\hat{\nabla}_k|\psi_k\rangle$. All physical quantities will be invariant under any gauge transformation $\mathcal{A} \rightarrow \mathcal{A} + \hat{\nabla}_k\varphi_k$, while the Berry phase defined as a gauge-invariant quantity

$$\gamma_c = \oint \mathbf{A}.d\mathbf{k} \tag{2.29}$$

measures the total phase accumulated upon a transformation (rotation) of the wavefunction in k-space along a closed loop. The Berry curvature $\mathbf{F} = \hat{\nabla}_k.\mathbf{A}$ is analogous to the magnetic field, while $\gamma_c = \iint \mathbf{F}.d^2k$ gives the Berry flux. The existence of a nontrivial Berry phase has been demonstrated to have many profound consequences in quantum physics (Thouless, 1998, Xiao, Chang & Niu, 2010), and in graphene and carbon nanotubes it conveys phenomena such as absence of backscattering in nanotubes, Klein tunneling, weak antilocalization, zero-energy Landau level, and an anomalous quantum Hall effect, as described in the following chapters.

Under 2π rotation, the eigenstates of the Dirac excitations get a π phase factor. Using the rotation operator $\mathcal{R}(\theta) = \mathrm{e}^{-\mathrm{i}\theta.\mathbf{S}/\hbar}$, with $\mathbf{S} = \hbar/2\hat{\sigma}_z$ for spin-1/2 particles, it is indeed readily shown that $\mathcal{R}(\theta = 2\pi)|\Psi_{\mathrm{K}_\pm}(s = \pm 1)\rangle = \mathrm{e}^{\mathrm{i}\pi\hat{\sigma}_z}|\Psi_{\xi,s}\rangle = -|\Psi_{\xi,s}\rangle$ (using $\mathrm{e}^{-\mathrm{i}\theta(\hat{n}.\hat{\sigma})/\hbar} = \cos\theta + \mathrm{i}(\hat{n}.\hat{\sigma})\sin\theta$).

One can also directly compute the Berry phase from the general definition as

$$\mathbf{A} = -\mathrm{i}\langle\psi_k|\hat{\nabla}_k|\psi_k\rangle = \frac{-\mathrm{i}}{2}(1, \mathrm{e}^{-\mathrm{i}\theta}).\begin{pmatrix} 0 \\ \mathrm{i}\nabla_k\theta\mathrm{e}^{\mathrm{i}\theta} \end{pmatrix} = \frac{\mathbf{e}_\theta}{2|\mathbf{k}|}, \tag{2.30}$$

($\mathbf{e}_\theta$ is a unit vector perpendicular to $\mathbf{p}$) while

$$\gamma_c = \oint \mathbf{A}.d\mathbf{k} = \int_0^{2\pi} d\mathbf{k}.\frac{\mathbf{e}_\theta}{2|\mathbf{k}|} = \pi\,. \tag{2.31}$$

4.1 Bands, valley degree of freedom and pseudospin

4.1.1 Bands, band filling and valley degree of freedom

In neutral graphene (no doping and no additional charges due to gates) in the (Wigner-Seitz) unit cell there are 2 carbon atoms with a total of 8 valence electrons.

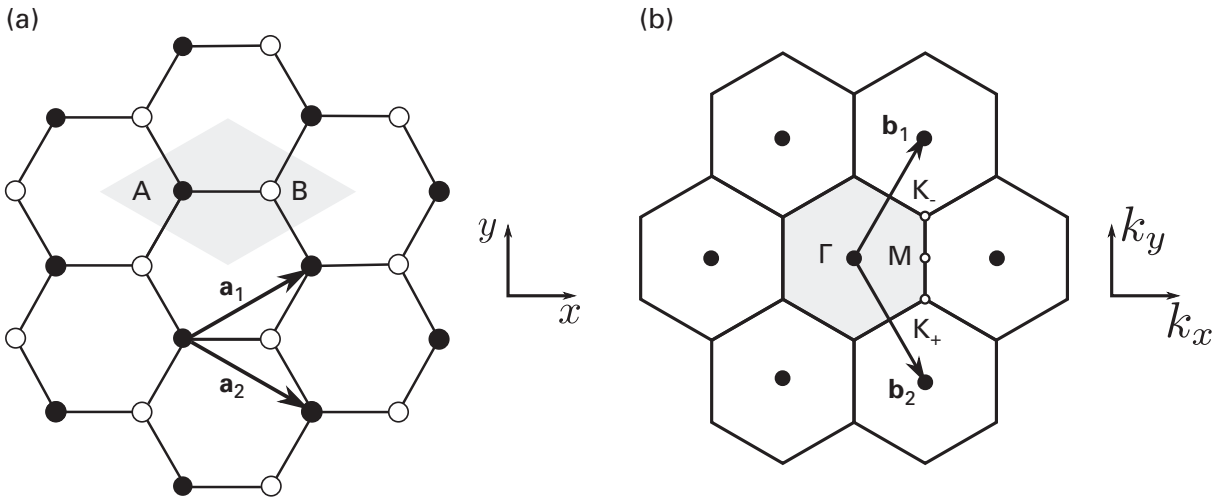

Figure 4.1:

In order to study the valence and the (lowest) conduction bands, one diagonalizes the crystal Hamiltonian on the basis set of the eight Bloch sums, formed with 2s, $2p_x$, $2p_y$, and $2p_z$ orbitals for each of the two carbon atoms in the unit cell. Since there are eight valence electrons per unit cell, we expect four completely occupied bands (if the four lowest lying bands do not overlap in energy with upper lying four energy bands). The band wavefunctions originated from the six s, p_x , and p_y orbitals (σ bands) are even under reflection in the plane of graphite; they do not mix with band wavefunctions originated from the two p_z orbitals (π bands), which are odd under reflection in the plane of graphene. Thus σ -bands and π -bands can be studied separately. One finds three bonding σ bands, separated by a substantial gap ($\approx$ 6eV) from the three antibonding σ^* bands and 2 π bands, with the bonding π band *separated* by *a zero energy gap* from the antibonding π^* band at the 3 $\mathbf{K}_-$ and 3 $\mathbf{K}_+$ points in the First Brillouin Zone (FBZ) (see, e.g., Fig. 4.1).

The lowest lying bands are shown as obtained in older (Fig. 4.2) and newer (Fig. 4.3) tight-binding calculations. The qualitative energy plot given in Fig. 2.1 (b) of Foa-Torres (FT) does not really agree with the results shown above.

For the sake of clarity and with reference to Fig. 4.1 let's observe that in the FBZ there are 3 $\mathbf{K}_-$ points (the one shown plus the additional two obtained by reciprocal lattice translation) that however belong to the FBZ only for 1/3 (they are shared between 3 different unit cells in k-space); similarly for the $\mathbf{K}_+$ points. In the end in the FBZ there is only *one full* $\mathbf{K}_-$ point and similarly there is only *one full* $\mathbf{K}_+$ point. Thus, if the chemical potential is slightly above the neutrality value $\mu = 0$, one has few electrons occupying the two inequivalent pockets (inverted

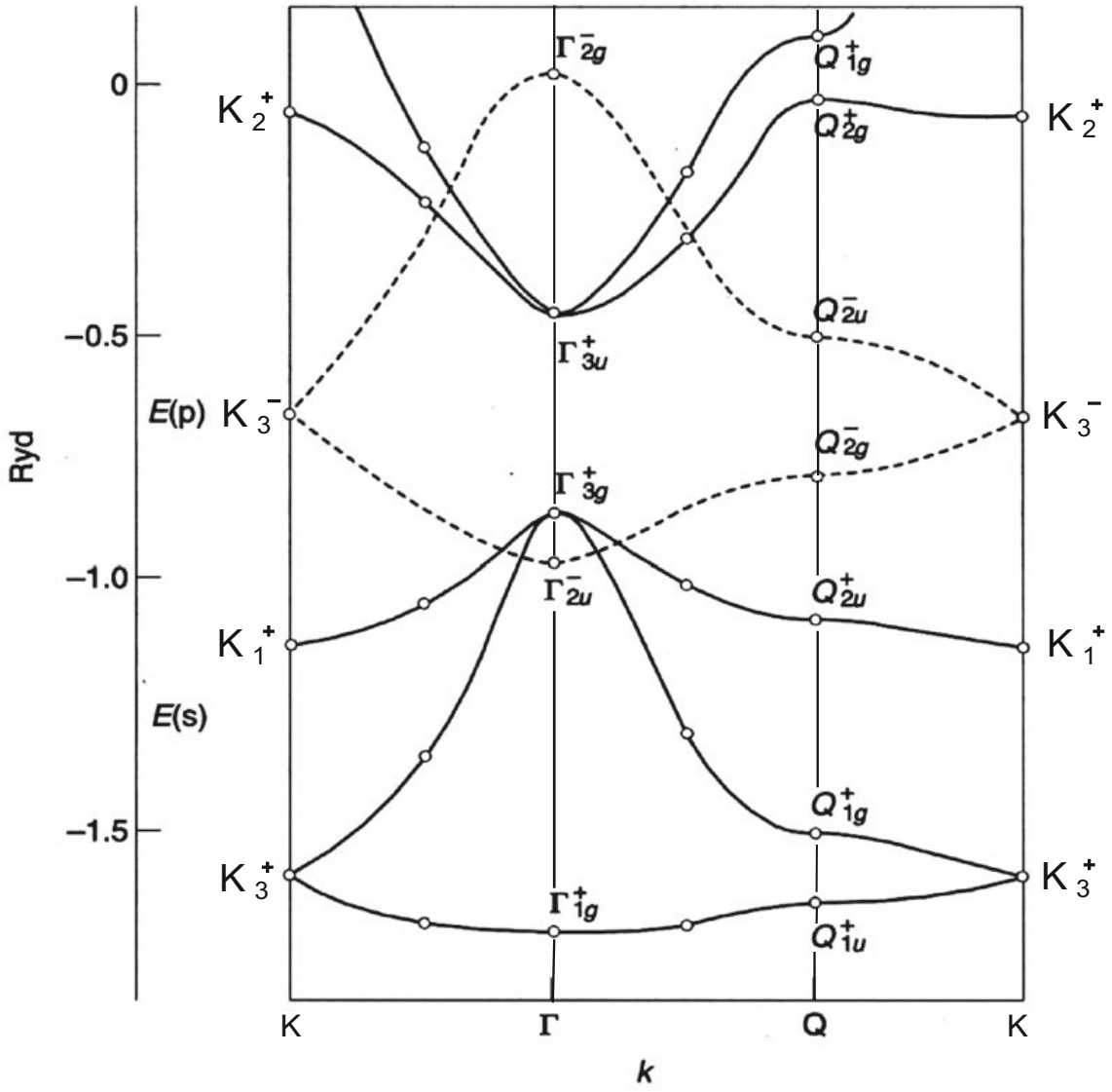

Figure 6.17 Band structure of graphene, obtained with the tight-binding method. Bands which are even and odd under reflection in the plane of graphene are indicated with continuous and broken lines respectively. The energies of the valence states of the carbon atom are also indicated. The values of $\mathbf{k}$ at the points Γ, K, and Q, are $\mathbf{k} = 0, \mathbf{k} = (2\pi/a)(2/3, 0)$, and $\mathbf{k} = (2\pi/a)(1/2, \sqrt{3}/6)$, respectively [from F. Bassani and G. Pastori Parravicini, Nuovo Cimento *50* B, 95 (1967); with kind permission from Società Italiana di Fisica].

Figure 4.2:

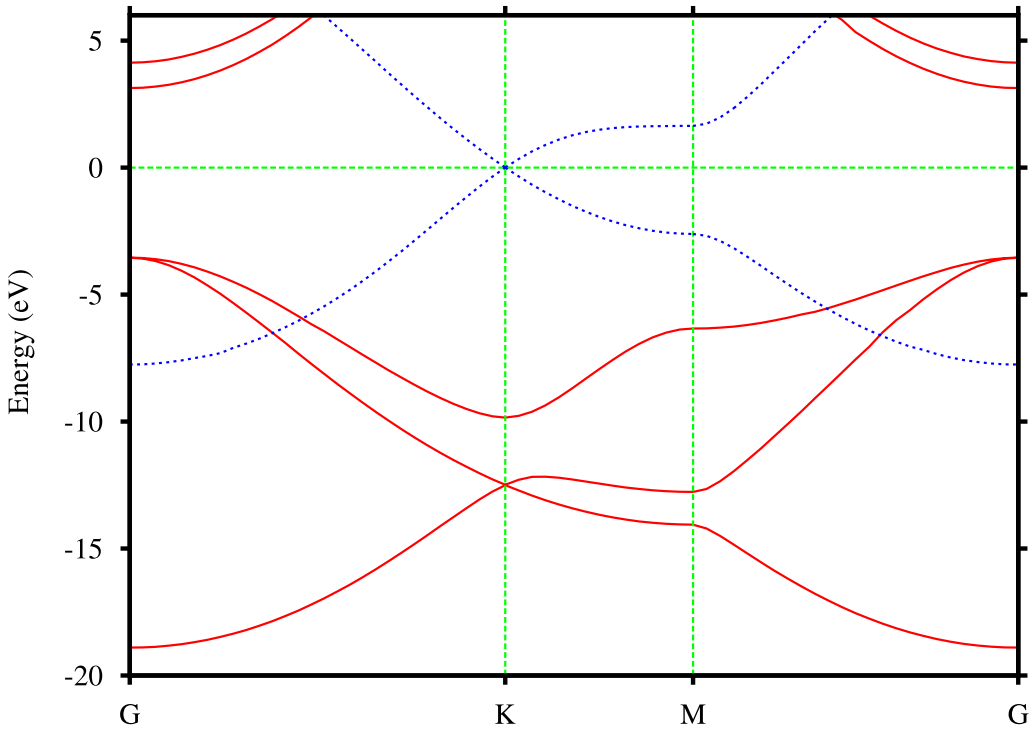

FIG. 1. (Color online) Band structure of a single graphene layer. Solid red lines are σ bands and dotted blue lines are π bands.

Figure 4.3:

cones) at $\mathbf{K}_-$ and $\mathbf{K}_+$. The electrons in the two pockets or *valleys* are distinguishable in the absence of intervalley transition, thus one has an additional degree of freedom (the *valley degree of freedom*) to label the electrons! Thus, if you like, we have red (at $\mathbf{K}_-$) and black (at $\mathbf{K}_+$) electrons!

4.1.2 Linearized Hamiltonian, pseudospin, helicity

4.1.2.1 Linearization

With reference to eqs. 2.12, 2.13 of FT, we have

$$\alpha(\mathbf{k}) = 1 + e^{-i\mathbf{k}\cdot\mathbf{a_1}} + e^{-i\mathbf{k}\cdot\mathbf{a_2}},$$

with $\mathbf{a}_1 = a(\sqrt{3}/2,1/2)$, $\mathbf{a}_2 = a(\sqrt{3}/2,-1/2)$, which gives

$$\alpha(\mathbf{k}) = 1 + e^{-ik_x a\sqrt{3}/2}e^{-ik_y a/2} + e^{-ik_x a\sqrt{3}/2}e^{ik_y a/2} = 1 + 2e^{-ik_x a\sqrt{3}/2}\cos\left(\frac{k_y a}{2}\right).$$

Note that in the following we shall change to the usual definition of the Dirac points $\mathbf{K}_\pm = (4\pi/3a)(\sqrt{3}/2, \pm 1/2)$, so as to make contact with some of the existing literature. The choice of FT appears to be a mistake. See, for example, Rev. Mod. Phys. 81, 109 (2009) by Castro Neto and coworkers, Rev. Mod. Phys. 83, 1193 (2011) by M. O. Goerbig, and the book by (i) G. Grosso e G. Pastori Parravicini (2014).

Let's now put $\mathbf{k}_\pm = \mathbf{K}_\pm + \mathbf{q}$, with $\mathbf{K}_\pm = (4\pi/3a)(\sqrt{3}/2, \pm 1/2)$ and $q \ll K_\pm$, $qa \ll 1$. Considering that $k_x a\sqrt{3}/2 = \pi + q_x a\sqrt{3}/2$ and $k_y a/2 = \pm\pi/3 + q_y a/2$, We get

$$\alpha(\mathbf{k}_\pm) = 1 + 2e^{-i\pi - iq_x a\sqrt{3}/2}\cos\left(\pm\frac{\pi}{3} + \frac{q_y a}{2}\right) \simeq 1 - 2\left(1 - i\frac{q_x a\sqrt{3}}{2}\right)\left(1/2 \mp \frac{\sqrt{3}}{2}\frac{q_y a}{2}\right),$$

which yields, to leading order in qa,

$$\alpha(\mathbf{k}_\pm) = 1 - 1 + iq_x a\frac{\sqrt{3}}{2} \pm \frac{\sqrt{3}}{2}q_y a = a\frac{\sqrt{3}}{2}(iq_x \pm q_y) = ia\frac{\sqrt{3}}{2}(q_x \mp iq_y). \tag{4.1}$$

In order to recover a result similar to the one in eq. 2.19 of FT we resort to a unitary transformation, which we choose already diagonal on the basis of the two orbitals $\tilde{p}_z^A(\mathbf{k},\mathbf{r})$ and $\tilde{p}_z^B(\mathbf{k},\mathbf{r})$ as

$$P = \begin{pmatrix} e^{i\phi_1} & 0 \\ 0 & e^{i\phi_2} \end{pmatrix}$$

where of course ϕ_1 and ϕ_2 are real. The hamiltonian in eq. 2.8 of FT is transformed to

$$H(\mathbf{k}_\pm) = \begin{pmatrix} 0 & -e^{i(\phi_1-\phi_2)}\gamma_0\alpha(\mathbf{k}_\pm) \\ -e^{-i(\phi_1-\phi_2)}\gamma_0\alpha(\mathbf{k}_\pm)^* & 0 \end{pmatrix},$$

with diagonal elements if present unaffected by the transformation, and the coefficient vector transformed to

$$\begin{pmatrix} e^{i\phi_1}c_A(\mathbf{k}_\pm) \\ e^{i\phi_2}c_B(\mathbf{k}_\pm) \end{pmatrix}.$$

It is evident that the choice $\phi_1 - \phi_2 = \pi/2$, i.e., $e^{i(\phi_1-\phi_2)} = i$, yields

$$H(\mathbf{k}_\pm) = \begin{pmatrix} 0 & \gamma_0 a\frac{\sqrt{3}}{2}(q_x \mp iq_y) \\ \gamma_0 a\frac{\sqrt{3}}{2}(q_x \pm iq_y) & 0 \end{pmatrix} \equiv \hbar v_F \begin{pmatrix} 0 & q_x \mp iq_y \\ q \pm iq_y & 0 \end{pmatrix} \equiv H_{\mathbf{K}_\pm}.$$

In other words,

$$H_{\mathbf{K}_+} = \hbar v_F \begin{pmatrix} 0 & q_x - iq_y \\ q + iq_y & 0 \end{pmatrix} = v_f \hat{\sigma} \cdot \mathbf{p} \tag{4.2}$$

and

$$H_{\mathbf{K}_-} = \hbar v_F \begin{pmatrix} 0 & q_x + iq_y \\ q_x - iq_y & 0 \end{pmatrix} = v_f \hat{\sigma^*} \cdot \mathbf{p} = H^t_{\mathbf{K}_-}, \tag{4.3}$$

with $\hat{\sigma} = (\sigma_x, \sigma_y, \sigma_z)$ and $\sigma_x, \sigma_y, \sigma_z$ the Pauli matrices; moreover,

$$v_F = \gamma a \frac{\sqrt{3}}{2\hbar}.$$

The two equations above do agree with those in FT, thanks to correct definition of $\mathbf{K}_\pm$.

4.1.2.2 Pseudospin

Pauli matrices above are used to describe a physical properties of electrons in one of the two inequivalent valleys, i.e., the coefficients of the linear combination of bloch sums at A and B, $c_A(\mathbf{k})$, $c_B(\mathbf{k})$. We shall say that Pauli matrices above describe a new property of electrons and name it *pseudospin.*They have no relation with the physical spin which, up to this point, has not yet entered the description of electrons in graphene! Has we have already noted, in the absence of intervalley transitions electrons can be assigned an additional discrete degree of freedom which specify to which valley they belong ($\mathbf{K}_+$ or $\mathbf{K}_-$); we again use Pauli matrices for this degree of freedom and we shall denote them by τ_x, τ_y, τ_z to distinguish them from thos describing pseudospin; this is the valley pseudospin.

4.1.2.3 Alternative choice of axes and resulting hamiltonians.

We shall now consider a rotation of the wavevector axes (see Fig.4.1) by 90^oclockwise yielding $q'_x = -q_y$, $q'_y = q_x$, which changes eq. 4.1 into

$$\alpha(\mathbf{k}_\pm) = 1 - 1 + iq'_y a\frac{\sqrt{3}}{2} \mp \frac{\sqrt{3}}{2} q'_x a = \mp a\frac{\sqrt{3}}{2}(q'_x - iq_y). \tag{4.4}$$

Let's drop the ' and write the hamiltonian with respect to the new axes

$$H_{\mathbf{K}_\pm} = \pm \begin{pmatrix} 0 & \gamma_0 a\frac{\sqrt{3}}{2}(q_x \mp iq_y) \\ \gamma_0 a\frac{\sqrt{3}}{2}(q_x \pm iq_y) & 0 \end{pmatrix} \equiv \pm\hbar v_F \begin{pmatrix} 0 & q_x \mp iq_y \\ q \pm iq_y & 0 \end{pmatrix},$$

or

$$H_\xi = \xi\hbar v_F \begin{pmatrix} 0 & q_x - i\xi q_y \\ q + i\xi q_y & 0 \end{pmatrix} = \xi v_F(\hat{\sigma}_x p_x + \xi\hat{\sigma}_y p_y), \quad \xi = \pm. \tag{4.5}$$

Consider now

$$H_- = -\hbar v_F \begin{pmatrix} 0 & q_x + iq_y \\ q - iq_y & 0 \end{pmatrix}.$$

Evidently, if we write the spinor as

$$\begin{pmatrix} c_{B-}(\mathbf{q}) \\ c_{A-}(\mathbf{q}) \end{pmatrix},$$

rather than

$$\begin{pmatrix} c_{A-}(\mathbf{q}) \\ c_{B-}(\mathbf{q}) \end{pmatrix},$$

we obtain for the hamiltonian

$$H_- = -\hbar v_F \begin{pmatrix} 0 & q_x - iq_y \\ q + iq_y & 0 \end{pmatrix} = -\hbar v_F(\hat{\sigma}_x p_x + \hat{\sigma}_y p_y),$$

or

$$H_\xi = \xi v_F(\hat{\sigma}_x p_x + \hat{\sigma}_y p_y), \quad \xi = \pm, \tag{4.6}$$

and the hamiltonian

$$H = \begin{pmatrix} H_+ & 0 \\ 0 & H_- \end{pmatrix} = \hbar v_F \begin{pmatrix} \hat{\sigma}\cdot\mathbf{p} & 0 \\ 0 & -\hat{\sigma}\cdot\mathbf{p}_- \end{pmatrix} = \hbar v_F \hat{\tau}\otimes\hat{\sigma}\cdot\mathbf{p} \tag{4.7}$$

acts on the four-spinor $(c_{A_+}(\mathbf{q}), c_{B_+}(\mathbf{q}), c_{B_-}(\mathbf{q}), c_{A_-}(\mathbf{q}))^t$.

4.1.2.4 Helicity

The helicity is defined as the projection of the pseudospin along the direction of momentum

$$\hat{h} = \hat{\sigma}\cdot\frac{\mathbf{p}}{|\mathbf{p}|}, \tag{4.8}$$

and is clearly proportional to the Hamiltonian of eq. 4.2, therefore one may choose common eigenstates for helicity and hamiltonian, i.e., one can simultaneously diagonalize the hamiltonian and the helicity. Sticking to the vicinity of the $\mathbf{K}_+$ point, with Hamiltonian 4.2, it can be easily shown that to the two energies eigenvalues $E_\pm(p) = \pm v_f|\mathbf{p}|$ it correspond to helicity 1 (spin parallel to $\mathbf{p}$) for electrons in the upper band ($E(p) = v_f|\mathbf{p}|$) and helicity -1 (spin antiparallel to $\mathbf{p}$) for holes in the lower band ($E_-(p) = -v|\mathbf{p}|$) (see, e.g., FT, pages 18,19.).

Let's derive the above result. We use the form of eq. 4.6 for the hamiltonians at the $\mathbf{K}_\xi$point, which we rewrite as

$$H_\xi = \xi v_F|\mathbf{p}| \begin{pmatrix} 0 & e^{-i\theta_p} \\ e^{i\theta_p} & 0 \end{pmatrix}, \tag{4.9}$$

where $\xi = \pm 1$, $p_x + ip_y = |\mathbf{p}|e^{i\theta_p}$, and $\theta_p \arctan(p_y/p_x)$. Consider the unitary transformation

$$U_\xi = \frac{1}{\sqrt{2}} \begin{pmatrix} -e^{-i\theta_p} & e^{-i\theta_p} \\ 1 & 1 \end{pmatrix}$$

and calculate $U_\xi^+ H_\xi U_\xi$:

$$H'_\xi = U_\xi^+ H_\xi U_\xi = \xi \frac{v_F|\mathbf{p}|}{2} \begin{pmatrix} -e^{i\theta_p} & 1 \\ e^{i\theta_p} & 1 \end{pmatrix} \begin{pmatrix} 0 & e^{-i\theta_p} \\ e^{i\theta_p} & 0 \end{pmatrix} \begin{pmatrix} -e^{-i\theta_p} & e^{-i\theta_p} \\ 1 & 1 \end{pmatrix} = -\xi v_F|\mathbf{p}| \begin{pmatrix} 1 & 0 \\ 0 & -1 \end{pmatrix} = -\xi v_F|\mathbf{p}|\hat{\sigma_z}.$$

Thus the energy eigenvalue are $E_\pm(p) = \pm v_f|\mathbf{p}|$, for $\sigma_z = \mp 1$. If we observe that the helicity may be written as

$$\hat{h_\xi} = \begin{pmatrix} 0 & e^{-i\theta_p} \\ e^{i\theta_p} & 0 \end{pmatrix},$$

it immediately follows that $U_\xi^+ \hat{h}_\xi U_\xi = -\hat{\sigma_z}$. Thus for $\xi = +1$ ($\mathbf{K}_+$ point) in the upper band ($\sigma_z = -1$, $E_+(p) = v|\mathbf{p}|$) the eigenstate has positive helicity, i.e. the pseudospin is parallel to the momentum and in the lower band ($\sigma_z = +1$, $E_-(p) = -v|\mathbf{p}|$) the eigenstates have negative helicity, i.e., pseudospin is antiparallel to the momentum. Clearly the situation is reversed for $\xi = -1$ ($\mathbf{K}_-$ point).

4.1.2.5 Absence of backscattering

As helicity is a good quantum number near a Dirac point, the conservation of helicity means that the change in sign of $\mathbf{p}$ implies also the flip of pseudospin (change of sign of the projection of the pseudospin along the momentum). Thus backscattering would be possible only in the presence of interactions that also flip the pseudospin.

4.2 Dirac Fermions in a magnetic field (FT 2.7.5)

4.2.1 Spectrum and spinors

What happens when graphene is placed into a perpendicular magnetic field $\mathbf{B} = (0, 0, B)$? Let's start from the linearized Hamiltonian, of eq. 4.6which we rewrite, as in Foa-Torres,

$$H^\xi = \xi v_F \begin{pmatrix} 0 & p_x - ip_y \\ p_x + ip_y & 0 \end{pmatrix} = \xi v_F(p_x\sigma_x + p_y\sigma_y),$$

where from now on we drop the hat operator symbol on both spin matrices and momentum. **According to the envelope function approximation we change $\hbar\mathbf{q}$, with $\mathbf{q}$ the small wavevector providing the departure from either $\mathbf{K}_+$ or $\mathbf{K}_-$, into the momentum operator $\mathbf{p}$**. The presence of the magnetic field can be taken into account by the minimal coupling $\mathbf{p} \to \mathbf{p} + e\mathbf{A}(\mathbf{r})/c \equiv \mathbf{\Pi}$. The Hamiltonian becomes

$$H_B^\xi = \xi v_F \begin{pmatrix} 0 & \Pi_x - i\Pi_y \\ \Pi_x + i\Pi_y & 0 \end{pmatrix} = \xi v_F(\Pi_x\sigma_x + \Pi_y\sigma_y). \tag{4.10}$$

Let's now study the commutation relations between the components of the generalize momentum $\mathbf{\Pi}$. We have

$$\begin{aligned}[\Pi_x, \Pi_y] &= [p_x + e\mathrm{A}_x(\mathbf{r})/c, p_y + e\mathrm{A}_y(\mathbf{r})/c] = \frac{e}{c}\left([p_x, A_y] + [A_x, p_y]\right) = \\ &= \frac{e}{c}\left([p_x, A_y] - [p_y, A_x]\right) = -i\hbar\frac{e}{c}\left(\frac{\partial_x A_y}{\partial x} - \frac{\partial_y A_x}{\partial y}\right) = -i\frac{\hbar eB}{c}.\end{aligned}$$

Introducing the magnetic length l_B as

$$l_B^2 = \frac{\hbar c}{eB},$$

we get

$$[\Pi_x, \Pi_y] = -i\frac{\hbar^2}{l_B^2}. \tag{4.11}$$

Considering the similarity with the p q commutation relation in the harmonic oscillator, we introduce the lowering and raising (destruction and creation) operators as

$$a = \frac{l_B}{\sqrt{2}\hbar}\left(\Pi_x - i\Pi_y\right), \qquad a^+ = \frac{l_B}{\sqrt{2}\hbar}\left(\Pi_x + i\Pi_y\right).$$

We easily verify the commutation relation of such operators using eq. 4.11.

$$[a, a^+] = \frac{l_B^2}{2\hbar^2}\left(i[\Pi_x, \Pi_y] - i[\Pi_y, \Pi_x]\right) = \frac{l_B^2}{2\hbar^2}\left(\frac{2\hbar^2}{l_B^2}\right) = 1.$$

Indeed they act as destruction and creation operators. Let's now rewrite the Hamiltonian in terms of such operators. Evidently

$$\Pi_x = \frac{\hbar}{\sqrt{2}l_B}(a + a^+), \qquad \Pi_y = i\frac{\hbar}{\sqrt{2}l_B}(a - a^+)$$

and

$$\begin{aligned}H_B^\xi &= \xi v_F(\Pi_x\sigma_x + \Pi_y\sigma_y) = \frac{\hbar}{\sqrt{2}l_B}\xi v_F[(a + a^+)\sigma_x + i(a - a^+)\sigma_y] \\ &= \frac{\hbar}{\sqrt{2}l_B}\xi v_F \begin{pmatrix} 0 & a + a^+ + (a - a^+) \\ a + a^+ - (a - a^+) & 0 \end{pmatrix} \\ &= \xi\sqrt{2}\frac{\hbar v_F}{l_B}\begin{pmatrix} 0 & a \\ a^+ & 0 \end{pmatrix}.\end{aligned}$$

Thus for $\xi = 1$ we get

$$H_B^+ = \sqrt{2}\frac{\hbar v_F}{l_B}\begin{pmatrix} 0 & a \\ a^+ & 0 \end{pmatrix},$$

and for $\xi = -1$ we get

$$H_B^- = -\sqrt{2}\frac{\hbar v_F}{l_B}\begin{pmatrix} 0 & a \\ a^+ & 0 \end{pmatrix} = -H_B^+.$$

Let's study H_B^ξ

$$H_B^\xi = \xi\sqrt{2}\frac{\hbar v_F}{l_B}\begin{pmatrix} 0 & a \\ a^+ & 0 \end{pmatrix} = \hbar\omega\begin{pmatrix} 0 & a \\ a^+ & 0 \end{pmatrix}.$$

Above we set $\omega = \sqrt{2}v_F/l_B$. The equation for the two-spinor is

$$H_B^\xi \psi_n = E_n \psi_n,$$

with

$$\psi_n = \begin{pmatrix} u_n \\ v_n \end{pmatrix}.$$

We get the two coupled equations

$$\xi\hbar\omega a v_n = E_n u_n \tag{4.12}$$
$$\xi\hbar\omega a^+ u_n = E_n v_n. \tag{4.13}$$

Using the first of the two equations in the second we get

$$\frac{1}{E_n}(\hbar\omega)^2 a^+ a v_n = E_n v_n$$

or

$$a^+ a v_n = \left(\frac{E_n}{\hbar\omega}\right)^2 v_n.$$

But we know that

$$a^+ a|n\rangle = n|n\rangle, \qquad n = 0, 1, 2, \ldots.$$

Thus we may take $v_n = |n\rangle$, which yields

$$a^+ a|n\rangle = \left(\frac{E_n}{\hbar\omega}\right)^2 |n\rangle = n|n\rangle,$$

which provides the eigenvalues

$$E_n = \pm\hbar\omega\sqrt{n}. \tag{4.14}$$

To get u_n we use eq. 4.12, which gives

$$u_n = \xi \frac{\hbar\omega}{E_n} a v_n = \pm\xi \frac{1}{\sqrt{n}} a|n\rangle.$$

Recalling that $a|n\rangle = \sqrt{n}|n-1\rangle$ and $a^+|n\rangle = \sqrt{n+1}|n+1\rangle$, we get

$$u_n = \pm\xi|n-1\rangle, \quad n > 0; \qquad u_n = 0, \quad n = 0.$$

Thus the spinor wavefunction is for $n = 0$

$$\psi_0 = \begin{pmatrix} 0 \\ |0\rangle \end{pmatrix},$$

and for $n > 0$

$$\psi_n = \begin{pmatrix} |n-1\rangle \\ \pm\xi|n\rangle \end{pmatrix}.$$

4.2.2 Wavefunctions and degeneracy

4.2.2.1 Wavefunctions and spectrum

In order to explicitly get spinors envelope wavefunctions and their degeneracy, we go back to eq. 4.10 and specialize to a particular choice of the gauge, the Landau gauge:

$$\mathbf{A}(\mathbf{r}) = B(-y, 0, 0).$$

Clearly, this implies

$$\begin{aligned} \Pi_x &= p_x - \frac{eB}{c} y \to -i\hbar\frac{\partial}{\partial_x} - \frac{eB}{c} y, \\ \Pi_y &= p_y \to -i\hbar\frac{\partial}{\partial_x}, \end{aligned}$$

which when used in eq. 4.10 yields:

$$H_B^\xi = \xi v_F \begin{pmatrix} 0 & \Pi_x - i\Pi_y \\ \Pi_x + i\Pi_y & 0 \end{pmatrix} = \xi v_F \begin{pmatrix} 0 & -i\hbar\frac{\partial}{\partial_x} - \frac{eB}{c} y - \hbar\frac{\partial}{\partial_x} \\ -i\hbar\frac{\partial}{\partial_x} - \frac{eB}{c} y + \hbar\frac{\partial}{\partial_x} & 0 \end{pmatrix}.$$

Recall that we have to solve the system

$$H_B^\xi \begin{pmatrix} \phi_A(\mathbf{r}) \\ \phi_B(\mathbf{r}) \end{pmatrix} = \xi v_F \begin{pmatrix} 0 & -i\hbar\frac{\partial}{\partial_x} - \frac{eB}{c} y - \hbar\frac{\partial}{\partial_x} \\ -i\hbar\frac{\partial}{\partial_x} - \frac{eB}{c} y + \hbar\frac{\partial}{\partial_x} & 0 \end{pmatrix} \begin{pmatrix} \phi_A(\mathbf{r}) \\ \phi_B(\mathbf{r}) \end{pmatrix} = E \begin{pmatrix} \phi_A(\mathbf{r}) \\ \phi_B(\mathbf{r}) \end{pmatrix},$$

with $\phi_A(\mathbf{r})$and $\phi_B(\mathbf{r})$ envelope functions, or defining $\epsilon = E/(\hbar\xi v_F)$

$$\begin{pmatrix} 0 & -i\frac{\partial}{\partial_x} - \frac{eB}{\hbar c}y - \frac{\partial}{\partial_y} \\ -i\frac{\partial}{\partial_x} - \frac{eB}{\hbar c}y + \frac{\partial}{\partial_y} & 0 \end{pmatrix} \begin{pmatrix} \phi_A(\mathbf{r}) \\ \phi_B(\mathbf{r}) \end{pmatrix} = \epsilon \begin{pmatrix} \phi_A(\mathbf{r}) \\ \phi_B(\mathbf{r}) \end{pmatrix};$$

this yields the system

$$\begin{cases} -i\frac{\partial\phi_B}{\partial_x} - \frac{y}{l_B^2}\phi_B - \frac{\partial\phi_B}{\partial_y} = \epsilon\phi_A \\ -i\frac{\partial\phi_A}{\partial_x} - \frac{y}{l_B^2}\phi_A + \frac{\partial\phi_A}{\partial_y} = \epsilon\phi_B \end{cases}.$$

Let's try with $\phi_A(\mathbf{r}) = e^{ik_x x}\varphi_A(y)$, $\phi_B(\mathbf{r}) = e^{ik_x x}\varphi_B(y)$. We get

$$\begin{cases} k_x\varphi_B - \frac{y}{l_B^2}\varphi_B - \varphi'_B = \epsilon\varphi_A \\ k_x\varphi_A - \frac{y}{l_B^2}\varphi_A + \varphi'_A = \epsilon\varphi_B \end{cases}, \tag{4.15}$$

with $\varphi'_A = \partial\varphi_A(y)/\partial y$, $\varphi'_B = \partial\varphi_B(y)/\partial y$. We now take the derivative with respect to y of the first equation to get

$$\left(k_x - \frac{y}{l_B^2}\right)\varphi'_B - \frac{\varphi_B}{l_B^2} - \varphi''_B = \epsilon\varphi'_A. \tag{4.16}$$

We then use (i) eq. 4.16 and (ii) the first equation in the system 4.15 in the second equation of the system to get

$$\left(k_x - \frac{y}{l_B^2}\right)\left[\left(k_x - \frac{y}{l_B^2}\right)\varphi_B - \varphi'_B\right] + \left[\left(k_x - \frac{y}{l_B^2}\right)\varphi'_B - \frac{\varphi_B}{l_B^2} - \varphi''_B\right] = \epsilon^2\varphi_B,$$

which simplifies to

$$-\varphi''_B + \frac{1}{l_B^4}(y - l_B^2k_x)^2\varphi_B = \left(\epsilon^2 + \frac{1}{l_B^2}\right)\varphi_B \equiv \tilde{\epsilon}_B\varphi_B. \tag{4.17}$$

In a similar fashion, taking the derivative of the second equation 4.15 and using it together with the second equation in the first one, one readlily obtains

$$-\varphi''_A + \frac{1}{l_B^4}(y - l_B^2k_x)^2\varphi_A = \left(\epsilon^2 - \frac{1}{l_B^2}\right)\varphi_A \equiv \tilde{\epsilon}_A\varphi_A. \tag{4.18}$$

Eq. 4.17 is the equation of a one dimensional harmonic oscillator, as it is clearly obtained by rewriting it as

$$-\frac{\hbar^2}{2m}\varphi''_B + \frac{\hbar^2}{2m}\frac{1}{l_B^4}(y - l_B^2k_x)^2\varphi_B = -\frac{\hbar^2}{2m}\varphi''_B + \frac{m\omega_c^2}{2}(y - l_B^2k_x)^2\varphi_B = \frac{\hbar^2}{2m}\left(\epsilon^2 + \frac{1}{l_B^2}\right)\varphi_B \equiv \tilde{\epsilon_B}\varphi_B,$$

where we have used the definition of the magnetic length to get the frequency of the oscillator $\omega_c = eB/mc$, i.e., the cyclotron frequency and $\tilde{\epsilon_B} = E^2/(2mv_F^2) + \hbar\omega_c/2$. Evidently $\tilde{\epsilon_B} = \hbar\omega_c(n_B + 1/2)$, $n_B = 0, 1, 2, \cdots$ and

$$\frac{E^2}{2mv_F^2} = \tilde{\epsilon_B} - \frac{\hbar\omega_c}{2} = \hbar\omega_c\left(n_B + \frac{1}{2}\right) - \frac{\hbar\omega_c}{2} = \hbar\omega_c n_B.$$

We get

$$E = \pm\sqrt{2mv_F^2\hbar\omega_c n_B} = \pm\sqrt{2mv_F^2\hbar eBn_B/(mc)} = \pm\hbar\sqrt{2v_F^2(eB/\hbar c)n_B}, \tag{4.19}$$
$$= \pm\hbar\sqrt{2n_B}v_F/l_B \equiv \pm\hbar\omega\sqrt{n_B} \tag{4.20}$$

in agreement with eq. 4.14, as $\omega = \sqrt{2}v_F/l_B$. Moreover $\varphi_B(y) = \varphi_{n_B}(y - y_0)$, $n = 0, 1, 2, \cdots$, with $\varphi_{n_B}(y)$ the oscillator wavefunctions centred at the origin and $y_0 = l_B^2 k_x$.

A similar result is obtained from eq. 4.18, which yields

$$\frac{E^2}{2mv_F^2} = \tilde{\epsilon_A} + \frac{\hbar\omega_c}{2} = \hbar\omega_c\left(n_A + \frac{1}{2}\right) + \frac{\hbar\omega_c}{2} = \hbar\omega_c(n_A + 1),$$

and E

$$E = \pm\hbar\omega\sqrt{n_A + 1}, \tag{4.21}$$

with $\varphi_A(y) = \varphi_{n_A}(y - y_0)$, $n_A = 0, 1, 2, \cdots$. Evidently from eqs. 4.19 and 4.21 one obtains $n_A = n_B - 1$. Thus, for $n_B > 0$ $\varphi_B(y) = \varphi_{n_B}(y - y_0)$ and $\varphi_A(y) = \varphi_{n_B-1}(y - y_0)$. However, for $n_B = 0$ $\varphi_A(y) = \varphi_{n_B-1}(y - y_0)$ is invalid, but substituting $\varphi_B(y) = \varphi_0(y - y_0)$ in the first equation in 4.15 one simply gets $\varphi_A(y) = 0$, in agreement with the results in the previous subsection. In order to write the spinor for given ξ, we observe that eqs. 4.15 fix the sign of the ratio $\varphi_A(y)/\varphi_B(y)$ for given value of E: recall that $\epsilon = E/(\hbar\xi v_F)$. Thus, if the energy is $\lambda\hbar\omega\sqrt{n_B}$, with $\lambda = \pm 1$, the spinor may be written, omitting the plane wave $e^{ik_x x}$, as

$$\begin{pmatrix} \phi_{n-1}(y - y_o) \\ \lambda\xi\phi_n(y - y_o) \end{pmatrix}, \tag{4.22}$$

for $n \neq 0$, and

$$\begin{pmatrix} 0 \\ \phi(y - y_o) \end{pmatrix} \tag{4.23}$$

for $n = 0$. You are urged to compare the results of the present subsection with those of 4.2.1

4.2.2.2 Degeneracy and filling factor

The one dimensional oscillators found above have centers in $y_0 = k_x l_B^2$ and the energy does not depend on k_x! Consider a sample with dimensions L_x, L_y and use periodic boundary conditions for the motion along x, so that $k_x = 2\pi n_x/L_x$, with $n_x = 0, \pm 1, \pm 2, \cdots$. Clearly the center of the oscillator must fall within the sample

$$0 \leq k_x l_B^2 \leq L_y,$$

or

$$0 \leq n_x \leq \frac{L_x L_y}{2\pi l_B^2}.$$

This implies that each oscillator state labelled with n has a degeneracy $g_n = L_x L_y/(2\pi l_B^2) = A/(2\pi l_B^2)$, where $A = L_x L_y$is the area of the sample. Lets consider a field $B = 1$ gauss. This yields $l_B = \sqrt{\hbar c/(eB)} = 2.56 \times 10^{-4} cm$. Thus for $B = 10$ tesla we get $l_B = 0.810 \times 10^{-6} cm = 8.1 nm$. Clearly if we take $A = 1 cm^2$ we get $g_n = 2.42 \times 10^{11}$, which is a huge number.

We note that

$$g_n = \frac{A}{2\pi l_B^2} = \frac{A\,B}{(hc/e)} = \frac{\Phi}{\Phi_0},$$

i.e., $g_n$is the ratio between the total magnetic flux through the sample and the quantum of flux $\Phi_0 = hc/e$ or the number of flux quanta within the sample surface.

One defines the flux density as the ratio between the level degeneracy g_n (or number of flux quanta) and the surface area, i.e. $n_B = 1/(2\pi l_B^2)$. Evidently one oscillator level may accomodate a maximum number of electrons of given spin and valley index equal to its degeneracy, i.e., An_B. Thus for $N \leq An_B$, one defines the filling factor of an oscillator level as $\nu = N/(An_B) \equiv \rho/n_B$,with $\rho = N/A$ the areal density of electrons. Evidently, by definition $0 \leq \nu \leq 1$.

5 Quantum Transport - additions to Foa-Torres

5.0.1 Additions to Landauer Buttiker

3 Quantum transport: general concepts

The previous sections have been devoted to the electronic structure of carbon-based materials. The rest of the book is now focused on their transport properties. This part is meant as a nexus, providing a brief reminder on quantum transport with a focus on the tools that are needed later in the book. After a discussion of the most relevant length scales and the different transport regimes, three different formalisms are reviewed, namely Landauer theory, the Kubo formalism and the semiclassical Boltzmann transport equation. More technical details concerning the use of Green's functions methods and the Lanczos method for computing the density of states and wave-propagation are discussed in Appendixes C and D respectively.

3.1 Introduction

3.1.1 Relevant time and length scales

Electron transport through a device is a phenomenon that takes place in time and space and as such there are relevant time *and* length scales. Given a device with characteristic dimensions L_x, L_y, and L_z, if the system is metallic then one has the Fermi wavelength $\lambda_F = 2\pi/k_F$ associated with its Fermi wave-number k_F. The elastic mean free path $\ell_{\rm el}$ can be defined as the distance that an electron travels before getting elastically backscattered (off impurities for example); $\ell_{\rm el} = v_F\tau_{\rm el}$, where $\tau_{\rm el}$ is the mean time between those elastic scattering events which are usually produced by defects or imperfections in the crystal structure. In disordered systems, when the disorder strength is such that $\ell_{\rm el} \sim \lambda_F$, the wavefunctions become localized on a length scale ξ, the localization length.

Analogously to $\ell_{\rm el}$, one can define the inelastic mean free path $\ell_{\rm in} = v_F\tau_{\rm in}$ as the mean distance between inelastic scattering events such as those due to electron–phonon or weak electron–electron interactions. Generically, it is usual to speak of the electronic mean free path ℓ, without discerning the specific source, elastic or inelastic.[1] The phase coherence length ℓ_ϕ (and corresponding coherence time τ_ϕ) is defined as the length over which the phase of the single-electron wavefunction is preserved (within an independent electrons approximation), which limits the scale of quantum phase interferences. Typical values for graphene, carbon nanotubes and other materials are given in Table 3.1.

[1] In graphene the main sources of scattering include charged impurities, defects in the crystal structure and microscopic corrugations of the graphene sheet (also called ripples). Their relative importance is still debated.

For graphene λ_F =35 ÷ 100 nm

Table 3.1 Typical magnitudes of the charge density (n), the mean free path ℓ, Fermi wavelength (λ_F) and the coherence length (L_ϕ) at 4 K in various materials.

	GaAs-AlGaAs	Metals	Graphene	SWNT	MWNT
n	4×10^{11} cm^{-2}	$10^{21} - 10^{23}$ cm^{-3}	$10^{11} - 10^{12}$ cm^{-2}	10^{11} cm^{-2}	,,
ℓ	$100 - 10^4$ nm	$1 - 10$ nm	50 nm to 3 μm[a]	1 μm	$10 - 40$ nm
λ_F	40 nm	0.5 nm	$2\sqrt{\pi/n}$	0.74 nm	,,
L_ϕ	100 nm	0.5 μm	0.5 μm[b]	3 μm[c]	100 nm

[a] In suspended graphene, mean free paths of about 100 nm were found at 4 K for $n \sim 10^{11}$ cm^{-2} (and about 75 nm at 300 K) in Du *et al.* (2008), while Bolotin *et al.* (2008) estimate ℓ of up to 1.2 μm for $n \sim 2 \times 10^{11}$ cm^{-2}. On the other hand, reported values for devices made from graphene sandwiched in between hBN crystals go up to 3 μm (Mayorov *et al.*, 2011).
[b] See Tikhonenko *et al.* (2009).
[c] See Stojetz *et al.* (2005).

3.1.2 Coherent versus sequential transport

Coherent or sequential? is probably one of the most crucial questions, since it dictates the general framework that better suits a particular system under investigation in a particular experimental condition (Weil & Vinter, 1987, Jonson & Grincwajg, 1987, Luryi, 1989, Foa Torres, Lewenkopf & Pastawski, 2003). Note, however, that the answer most probably lies in between these two extreme situations (see also Section 3.5).

Let us imagine that we start with the sample (nanotube, graphene ribbon, etc.) decoupled from the electrodes. As the coupling between them is turned on, there is an increasing escape rate which determines the intrinsic width (Γ_α) of the levels (ε_α) corresponding to the isolated sample. The more isolated is the sample from the electrodes, the longer the lifetime τ_D of an electron in any of those levels and the smaller the intrinsic level width $\Gamma_\alpha = \hbar/\tau_D$. If the lifetime associated with the intrinsic level width is longer than the coherence time (τ_ϕ), then the electrons will spend enough time inside the sample to suffer phase breaking events leading to a decoherent regime.

In the decoherent limit, one may use a *sequential picture* for transport, in which the electronic motion is divided, as in a theater play, into different parts:

1. *Tunneling in.* The electron is transmitted from the left electrode into the sample;
2. *Dwelling.* The electron dwells in the sample, eventually interacting with other electrons or with phonons/vibrational degrees of freedom;
3. *Tunneling out.* The electron tunnels into the right electrode or is reflected back to the left one.

A sometimes implicit assumption of such a picture is that transport is decoherent. Therefore, the description can be at a semiclassical level where only the occupation *probabilities* (and not the amplitudes) are taken into account into a set of rate equations. Typically, these rate equations take into account the different possible processes (tunneling in and out of the sample, electron–electron and inelastic interactions) through a Fermi golden rule for the associated transition rates. By solving these equations one gets

the occupation probabilities, from which the current and other quantities of interest can be computed. The widely used Boltzmann equation belongs to this class of schemes, and is introduced later in Section 3.3.

Transport in the Coulomb blockade regime (see also Section 5.8.1) is usually described by such a sequential picture (Beenakker, 1991). In this regime, the contacts to the electrodes are weak enough such that the charge inside the sample is well defined and quantified. One says that the transport is suppressed (or blocked) and is only possible at precise energies, which can be tuned by varying the gate voltage (conductance peaks). The energy scale governing such peaks is the charging energy (E_c): the energy necessary to compensate for the electron repulsion and add one more electron to the system.

When the coherence time is longer than the residence time in the sample, the tunneling processes through the contacts and dwell inside the sample cannot be treated in a separate fashion anymore. The picture is that of a coherent transport mechanism and the theater play becomes a weird quantum game. This is the realm where quantum interference effects and even more exotic phenomena involving correlated motion between electrons like the Kondo effect may take place.[2] The Landauer–Büttiker theory and the Kubo formalism, which are briefly introduced in Sections 3.2 and 3.4.4, provide an appropriate framework for coherent, noninteracting electrons.

A crucial magnitude controlling the transition between these regimes is the intrinsic energy level width Γ_α of the sample connected to outside world. As one moves from the coherent to the sequential regime, Γ_α is reduced until it becomes the smallest energy scale in the problem (the sample being more and more disconnected from the electrodes). Simultaneously, the value of the charging energy increases from zero to a value where it dominates over the mean level spacing Δ and dictates a sequential and discretized transfer of charges from a source to a drain electrode.

A beautiful experiment showing this transition is reproduced in Fig. 3.1 (Babic & Schönenberger, 2004). The coupling with the leads changes as the gate voltage V_g is varied, thereby producing a crossover from low transparency to high transparency contacts and allowing observation of the transition from coherent (lower V_g region in Fig. 3.1 (a) and (b)) to sequential tunneling (high V_g region in the figures, where isolated resonances are observed). The conductance accordingly exhibits a wealth of phenomena which includes, from higher to lower gate voltage: Coulomb blockade peaks, strong cotunneling, and Kondo effect, and destructive interference which is manifested as Fano resonances.[3] This experiment illustrates in a magnificent way that the occurrence and the

[2] The Kondo effect is one of the most studied many-body phenomena in condensed matter physics (for a review see Kouwenhoven & Glazman (2001)), and is also an active topic in graphene physics, both theoretically (Cornaglia, Usaj & Balseiro, 2009, Cazalilla *et al.*, 2012) and experimentally (Chen *et al.*, 2011).

[3] Fano resonances, also known as anti-resonances in the context of electronic transport (Guinea & Vergés, 1987, D'Amato, Pastawski & Weisz, 1989), are a coherent effect of destructive interference pioneered by Fano (1935) in spectroscopy and observed since then in many contexts in different nanostructures (Miroshnichenko, Flach & Kivshar, 2010).

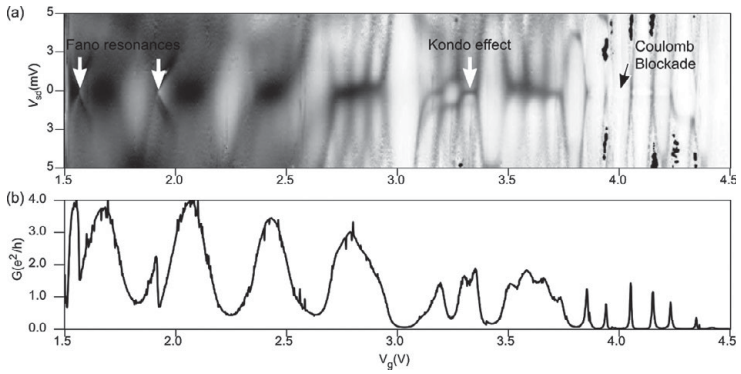

Figure 3.1 (a) Density plot of the differential conductance versus bias voltage V_{sd} and gate voltage V_g (high conductance in black and low conductance in white). (b) Linear response conductance versus gate voltage. The coupling to the leads strongly depends on the gate voltage, allowing for the observation of very different phenomena in the same experiment, namely, Coulomb blockade, Kondo effect and Fano resonances. (Adapted from Babic & Schönenberger (2004). Copyright (2004) by the American Physical Society. Courtesy of Christian Schönenberger.)

nature of quantum transport phenomena through a mesoscopic sample strongly depend on the conditions, the measurement setup, and the dominant energy scales of the system under study.

3.2 Landauer–Büttiker theory

One of the most influential frameworks for the study of quantum transport is Landauer theory, pioneered originally by Rolf Landauer in the early fifties (Landauer, 1957, 1970) and generalized later on by Büttiker and others (Büttiker *et al.*, 1985) for multi-lead systems. The simplicity of Landauer's picture for transport boosted it as a driving force in the field of nanoscale transport. As will be shown later, several reasons make it particularly useful in the context of graphene-based devices and therefore we dedicate the next pages to a brief presentation of its main points while trying to clarify the underlying assumptions and limitations.

Let us consider a sample or device that is connected through leads to reservoirs. A particular case with two leads is represented in Fig. 3.2. Within Landauer's approach conductance through a device is seen as a scattering process where electrons injected from the reservoirs are incident onto the device and then scattered back into the reservoirs. Landauer's theory relates the conductance, measuring the ease with which the electrons flow, with the transmission probability through the device. The current through electrode j (I_j) is given by

$$I_j = \frac{2e}{h} \int \sum_{i=1}^{N} \left[T_{j,i}(\varepsilon) f_i(\varepsilon) - T_{i,j}(\varepsilon) f_j(\varepsilon) \right] d\varepsilon, \tag{3.1}$$

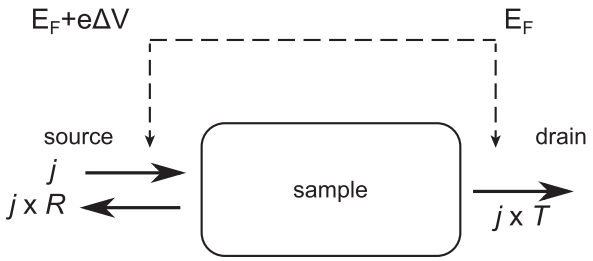

Figure 3.3 Scattering through a system with a single incoming and outgoing channel and an applied voltage difference ΔV. A current density j is injected from the source. The carriers are then scattered and a fraction R is reflected and a fraction T transmitted.

3.2.1 Heuristic derivation of Landauer's formula

Let us consider a one-dimensional metallic system coupled to two 1D electronic leads which drive incoming and outgoing currents as sketched in Fig. 3.3. The temperature of the system is set to zero, so only electrons at the Fermi level participate in the electronic current. This current originates from a potential difference between right and left leads with $e\Delta V \ll E_F$. Such potential difference is related to a density gradient $\delta n = n(E_F + e\Delta V) - n(E_F)$ ($n(E)$ being the electron density) which can be approximated, including spin degeneracy, by

$$\frac{\partial n}{\partial E}|_{E_F}.e\Delta V = 2e\Delta V/(\pi\hbar v_F). \tag{3.6}$$

On the other hand, this electron density difference δn can also be written in terms of the current densities in steady state as

$$\delta n = \frac{j + jR}{ev_F} - \frac{jT}{ev_F}, \tag{3.7}$$

introducing R and T, the reflection and transmission probabilities respectively. From Eq. (3.7) one infers that $\Delta V = [j(1 + R - T)/(ev_F)] \times \pi\hbar v_F/(2e)$. The total current $I = Tj$, so that the resistance of the system reads finally

$$\mathcal{R} = \Delta V/I = \frac{h}{2e^2}\frac{R}{T}. \tag{3.8}$$

Based on this derivation, the quantum conductance becomes $G = 1/\mathcal{R} = 2e^2/h \times T/R$, which has an ill-defined value in the limit of perfect transmission ($T = 1$). Indeed, given current conservation, $R + T = 1$, a perfect transmission through the system means $T = 1$ and $R = 0$, or $G \to \infty$ which is clearly unphysical. The reason for such a singularity comes from the neglect of contact effects. This problem was pioneered by Rolf Landauer (Landauer, 1970, Imry & Landauer, 1999) who demonstrated that in the situation of ballistic transport across a given (low-dimensional) system, the resistance and dissipation will take place at the interface between the measured system and the

metallic electrodes acting as charge reservoirs. This problem can be solved by rewriting the Landauer formula as

$$\mathcal{R} = \frac{h}{2e^2}\frac{1}{T} \tag{3.9}$$

$$= \frac{h}{2e^2} + \frac{h}{2e^2}\frac{1-T}{T}, \tag{3.10}$$

so that the quantum resistance is then seen to split into two parts for the single conducting channel case. The first term of Eq. (3.10) gives the contact resistance between the disorder-free one-dimensional metallic conductor and an electron reservoir with many more electron channels, whereas the second term of Eq. (3.10) actually provides information about the intrinsic resistance of the system, which can dominate the total resistance when the intrinsic transmission is very low. This second term is physically connected to the so-called four-points transport measurements, which allow access to such intrinsic resistance, by excluding contact effects.

3.3 Boltzmann semiclassical transport

The Boltzmann equation describes the transport properties of quantum particles (electrons, phonons) driven by a semiclassical dynamics. It determines how the particles of the system are accelerated in external fields, losing part of their accumulated energy through scattering-induced momentum relaxation. Scattering processes are determined by static (impurities, defects) as well as dynamical (phonons) disorders. The Boltzmann transport equation describes the dynamics of the distribution function $f_k(r,t)$, which gives the *probability* (and not the probability amplitude) of finding a particle in momentum-state $|\mathbf{k}\rangle$ in the neighborhood of $|\mathbf{r}\rangle$ and at time t. Its most general form states

$$\frac{\partial f_k(\mathbf{r},t)}{\partial t} + \mathbf{v}_k \cdot \nabla_{\mathbf{r}} f_k(\mathbf{r},t) + \mathbf{F} \cdot \nabla_{\mathbf{k}} f_k(\mathbf{r},t) = \left.\frac{\partial f_k(\mathbf{r},t)}{\partial t}\right|_{\text{coll}}, \tag{3.11}$$

with $\mathbf{F}$ describing external (Lorentz) forces acting on the particles, $\mathbf{v}$ denoting their velocity, and where $\frac{\partial f_k(\mathbf{r},t)}{\partial t}|_{\text{coll}}$ is the collision term which drives the system towards equilibrium, and depends on the sources of scattering and dissipation. The wave nature of electrons is accounted for in the collision term, as well as in the particles energetics (with $E(k)$ and $\mathbf{v}_k = \frac{1}{\hbar}\nabla_k E(k)$ given by the crystalline band structure of the clean system), but the particle dynamics is treated classically in the sense that quantum interferences between multiple scattering events are disregarded. The Boltzmann transport theory is therefore invalidated when localization phenomena enter into play and should instead be replaced by the Kubo approach (described in Section 3.4). In the regime of high charge density and high temperatures, the Boltzmann transport theory applies reasonably well, however, even in low-dimensional materials such as graphene.

In Eq. (3.11), the collision term describes the abrupt changes of momentum due to scattering of the particles. To keep the calculation simple, we hereafter consider only elastic scattering (particle momentum is changed in the scattering process but energy is

Chapter 1
Introduction

1.1 Quantum Transport in Mesoscopic and Nanoscale Systems

What systems, models and methods are considered in this book? What is the meaning of the term "nanoscale" and what is its difference from the other known term "mesoscopic"?

One can note that *nanoscale* simply assumes *nanometer scale spatial dimensions*, very often any structure with at least one spatial dimension smaller than 100 nm ($1\,\text{nm} = 10^{-9}\,\text{m}$) is considered as a subject of nanoscience. This definition, however, includes all types of nanostructures independently of their behavior and physical properties, which can be more or less quantum or quite the contrary (semi)classical in the sense of required physical models. Many nanostructures actually can be described by well established classical or semiclassical models.

We will focus on *quantum transport* of charge, spin and heat. *Nanoscale* in this respect characterizes not the size, but rather a specific type of systems and effects, which can be distinguished from both classical systems and mesoscopic quantum systems.

If you insert the word "nanoscale" into the search line of your internet browser, you will probably find about 10 times more links than for the word "mesoscopic". Nevertheless, about 20 years ago, when the first books about quantum transport in mesoscopic systems and nanostructures had been published [1–5], almost any quantum transport was considered as mesoscopic. Actually the term "mesoscopic" characterized the intermediate size between atomic (microscopic) and bulk (macroscopic). On the other hand, the main methods required to describe experiments in the eighties of the 20th century, first of all the experiments with semiconductor heterostructures with μm sizes in transport directions, were based on the quasiclassical methods for quantum systems with dense (or even continuous) energy spectra. Besides, the theoretical description was not based on discrete-level models and could be considered in the language of real-space propagation paths and phase shifts. As a result, nowa-

D.A. Ryndyk, *Theory of Quantum Transport at Nanoscale*,
Springer Series in Solid-State Sciences 184,
DOI 10.1007/978-3-319-24088-6_1

days, mesoscopic is associated with quasiclassical systems with continuous or dense energy spectra.

But in last years, due to development of molecular electronics and computational methods for direct modeling at the atomic level, the methods specific for discrete-level systems become more and more important. At present, quantum nanoscale transport constitutes its own field of research separated not by hard walls, but by some visible boundaries from the remaining field of quantum mesoscopic transport. Let's try to estimate the parameters responsible for this boundary.

To some extent, the classification can be given based on the characteristic lengths and times. The most important scales are:

L—the size of the system or characteristic internal length *in transport direction*;
l_p, τ_p—the elastic scattering length (mean free path) and time;
l_ε, τ_ε—the inelastic scattering (energy relaxation) length and time;
l_φ, τ_φ—the phase-decoherence length and time;
λ_B—the de Broglie wave length (depends on the kinetic energy, for electrons in metals it is taken at the Fermi surface).

Typically the characteristic lengths go in the following order

$$\lambda_B < l_p < l_\phi < l_\varepsilon.$$

For example, in semiconductor (GaAs, Si) 2D electron gas at low temperatures the values can be $\lambda_F \approx 0.05\ \mu\text{m} = 50\,\text{nm}$, $l_p \approx 0.5\ \mu\text{m}$, $l_\varphi \approx 1\ \mu\text{m}$, $l_\varepsilon \approx 3\ \mu\text{m}$. In metals the numbers are similar: $l_\varphi \approx 1\ \mu\text{m}$ in gold at $T = 1$ K. At room temperatures all these lengths in metals and semiconductors are very small and transport is described by semiclassical models. Note that this is not the case for carbon nanostructures like nanotubes, where even at room temperature both electron and phonon transport can be quantum.

Two scales: the de Broglie wave length λ_B and the phase-decoherence length l_φ are specific for quantum transport (other exist also in the classical limit) and are most important for classification of transport regimes. In the case

$$\lambda_B \ll L \leqslant l_\varphi$$

the motion of electrons is phase-coherent and can not be described by classical equations, but in most cases it is still quasiclassical, which means that classical trajectories can be used as a starting point and quantum effects are included mainly into the phases of quasiclassical wave functions. This is just a case of *mesoscopic* system.

Based on the definition of mesoscopic systems as the systems with continuous energy spectrum, we define *nanoscale* systems as the systems with essentially discrete energy spectrum in some parts. Usually it means that a discrete-level system is coupled to infinitely large electrodes (or substrate) with continuous spectrum.For example, assume that the characteristic size of the central region in *transport*

direction starts to be comparable with the electron wave length:

$$L \sim \lambda_B.$$

In this case quantization of the single-particle energy levels starts to be important.

Of course, we are interested also in other cases when some system is naturally represented by discrete-level models. In particular, molecular junctions are described using the basis of atomic or molecular orbitals. One more origin of discrete *many-body* energy spectra is Coulomb interaction (the charging energy) in quantum dots and small grains. Finally, nanostructured low-dimensional materials (e.g. short nanotubes, graphene flakes, etc.) are described by discrete tight-binding (lattice) models.

Thus, we suggest a point of view that the boundary between mesoscopic and nanoscale systems is mainly the boundary between: (i) a continuous energy spectrum and continuity in real space of the equations for wave functions in the mesoscopic case; and (ii) discrete energy spectrum and discrete basis wave functions in nanosystems. Of course, there is no strict separation between meso- and nano- transport and very often people actually mix these two terms. However, to have practical limits in the extremely wide field of nanoscience, I consider in this book only transport through *quantum nanosystems with discrete energy spectrum*, such as metal grains, semiconductor quantum dots and single molecules, coupled to one, two, or larger number of electrodes.

We *do not consider* in this book the methods and approaches, which are typical only for mesoscopic transport and focus instead specifically on nanoscale transport questions. In particular, the following topics are not included:

- quantum interference of Aharonov-Bohm type;
- weak localization;
- universal conductance fluctuations;
- random matrix theory;
- quantum Hall effect;
- quasiclassical and semiclassical transport.

I refer the readers to numerous special reviews on mesoscopic transport.

Still, there are some topics important for both quasiclassical (mesoscopic) and pure quantum (nanoscale) systems, for example the Landauer scattering approach. That is the reason why we start from the "mesoscopic" Landauer-Büttiker method in Chap. 2. However, in the next Chap. 3 we formulate the Landauer approach for discrete basis using the technique of matrix Green functions, in such a way we get a nanoscale version of this approach.

There is one other significant peculiarity of nanoscale systems: the enhanced role of interactions. The theory of mesoscopic transport is based usually on free particles or weakly interacting particles, the perturbation theory is widely used. At nanoscale, as we already mentioned, both electron-electron and electron-vibron interactions may be strong and the Landauer approach can not be used anymore. Fortunately, we can use the powerful methods of Nonequilibrium Green Functions and Quantum Master Equation, able to treat the many-body problems.

1.2 Nanojunctions

We focus on the models describing some *central system*, placed between two or many *ideal electrodes*, which are assumed to be noninteracting and being in thermal equilibrium. On the contrary, the central system can be interacting and can be nonequilibrium if finite voltage is applied. One can call such systems *nanojunctions*. Depending on the ratio between the energy scales associated with electron-electron or electron-vibron *interactions* in the central system (examples of these energy scales are the effective charging energy and the polaron energy) and coupling to the leads, nanojunctions can be classified in several groups.

In the case of strong coupling to the electrodes and weak interactions, the electronic states of the central system are hybridized with states in the electrodes, charge quantization is suppressed, transport is mainly coherent and the conductance is of the order of the conductance quantum $G_0 = 2e^2/h$. In some cases one can ignore completely the atomistic structure and formulate the model in the continuum medium approximation (a typical example is the nanojunction shown in Fig. 1.1), or use the lattice (tight-binding) model with given parameters. The basic way to understand quantum coherent transport in noninteracting systems is Landauer-Büttiker method (usually formulated for atomistic or lattice systems with Green function formalism). We consider coherent transport in Chaps. 2 and 3.

In the case of very weak coupling to the electrodes (Fig. 1.2), the electronic states of the central system are only weakly disturbed, strong charge quantization and Coulomb blockade take place and transport is mainly determined by sequential tunneling. The central region in this case is often called *quantum dot*. In this case the master equation for probabilities of the many-body states is a good starting point. We consider different examples of sequential tunneling through the systems with Coulomb blockade and polaron effects in Chaps. 5 and 6.

Besides, the important limiting case is a strongly asymmetric nanojunction (Fig. 1.3), when the central region is strongly coupled to one electrode and weakly coupled to other one. This is a typical situation for STM experiments. The peculiarity of this case is that the central region (quantum dot, molecule) is in equilibrium or weakly nonequilibrium state even at large voltage, because it keeps the state in

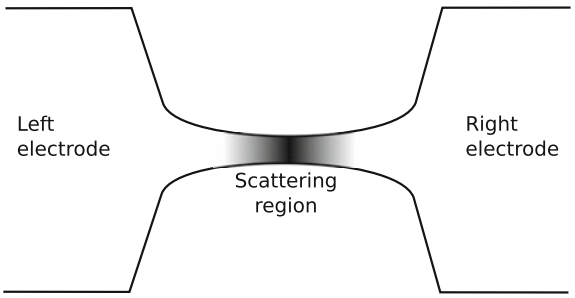

Fig. 1.1 Schematic picture of a nanojunction with strong coupling to the electrodes

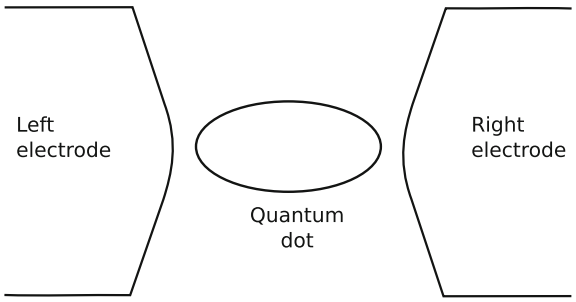

Fig. 1.2 Schematic picture of a nanojunction (quantum dot) with weak coupling to the electrodes

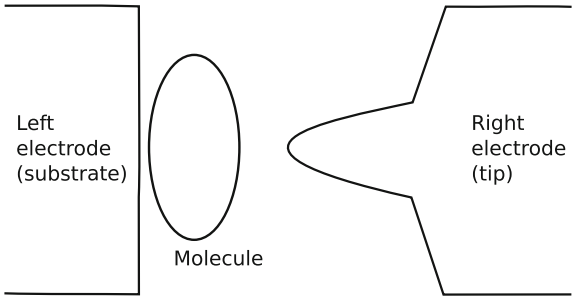

Fig. 1.3 Schematic picture of a strongly asymmetric nanojunction (STM set-up)

equilibrium with stronger coupled electrode. This type of junctions (as well as any direct contacts between two electrodes without any central region) can be describe by the so-called Tunneling (or Transfer) Hamiltonian method without use of more sophisticated methods. We consider tunneling in Chap. 4.

1.3 From Basic Concepts to Advanced Methods

The theoretical treatment of transport at nanoscale (see introduction in [1–12]) requires the combined use of different techniques and approximations. We will consider discrete-level models starting from few-level and tight-binding noninteracting models and going in the direction towards the many-body models with strong electron-electron and electron-vibron interactions. Let us now outline the main concepts.

Landauer-Büttiker method [13–22] establishes the fundamental relation between the wave functions (scattering amplitudes) of a junction and its conducting properties. The method can be applied to find the current through a noninteracting system or through an *effectively noninteracting* system, for example if the mean-field description is valid and the inelastic scattering is not essential. Such type of an electron transport is called coherent, because there is no phase-breaking and quantum interference is preserved during the electron motion across the system. In fact, coherence is assumed in many *ab initio* based transport methods using the density-

$$\boldsymbol{M}_T = \boldsymbol{M}\boldsymbol{M}_L\boldsymbol{M}' = \begin{pmatrix} M_{11} & M_{12} \\ M_{21} & M_{22} \end{pmatrix} \begin{pmatrix} e^{-ikL} & 0 \\ 0 & e^{ikL} \end{pmatrix} \begin{pmatrix} M'_{11} & M'_{12} \\ M'_{21} & M'_{22} \end{pmatrix}. \tag{2.62}$$

$$M_{T11} = M_{11}M'_{11}e^{-ikL} + M_{12}M'_{21}e^{ikL} \tag{2.63}$$

In the case of two identical barriers, for transmission coefficient we find

$$T(E) = \frac{T_1^2}{T_1^2 + 4R_1\cos^2(kL - \theta)}, \tag{2.64}$$

where θ is the phase of the complex M_{11}. T_1 and R_1 are transmission and reflection coefficients of the single barrier.

From this general expression one can see the important property of two-barrier structures: there are transmission resonances, at some specific energies E_n the transmission coefficient is large ($T(E_n) = 1$ in symmetric structures), while between resonances it can be small.

When the barriers are δ-functions $M_{11} = 1 + \dfrac{i}{K}$, $\theta = \arctan\dfrac{1}{K} = \arctan\dfrac{m\alpha}{\hbar^2 k}$ and the equation for resonances ($T = 1$) is

$$\tan kL = -\frac{\hbar^2 k}{m\alpha}. \tag{2.65}$$

Close to the resonance, around one of the resonance energies E_n, the transmission coefficient has a *Lorentzian* form

$$T(E) \approx \frac{\Gamma_n^2}{(E - E_n)^2 + \Gamma_n^2}, \tag{2.66}$$

where the width Γ_n is given for two δ-barriers as

$$\Gamma_n = \left(\frac{2\hbar^2 E_n T_1^2}{mL^2 R_1}\right)^{1/2}. \tag{2.67}$$

2.2 Landauer Formula

2.2.1 Single-Channel Formulas

The main idea of the scattering approach to the conductance was first formulated by Rolf Landauer [1, 2]. He proposed, that the conductance of some segment of a 1D channel with elastic scatterers is determined by the quantum mechanical probabilities of transmission (T) and reflection ($R = 1 - T$) through this segment. It

should be noted, that Landauer considered the local resistance of a system (the zero-temperature residual resistance), but not the resistance of a quantum system between two equilibrium electrodes. As a result, he got for the zero temperature one-channel (effectively one-dimensional) conductance the so-called "first Landauer formula"

$$G' = \frac{e^2}{h}\frac{T}{1-T} = \frac{e^2}{h}\frac{T}{R}. \tag{2.68}$$

The result, which seems to be reasonable at least in two limiting cases. At small transmission $T \to 0$, the conductance is also small and proportional to T, the result, which is well known from the perturbation theory. In the opposite case, when $T \to 1$, $R \to 0$, there is no scattering at all, so that the conductance should go to infinity, in agreement with (2.68). To take into account the spin degeneracy in this formula, one has to multiply the conductance (2.68) by 2.

However, the further investigations [3, 4] show that the conductance of a 1D system, calculated by the exact linear response method, can have also quite different form (depending on the boundary conditions)

$$G = \frac{e^2}{h}T. \tag{2.69}$$

This conductance is finite even in the case of the perfectly transparent junction ($T = 1$). Actually, there is no contradiction between these two formulas. It was shown that both are reasonable and give the same current, but correspond to the voltages, defined between different points. As we shall see below, the key difference between the formulas (2.68) and (2.69) is that the first one is for the conductance *inside* the junction (between points A and B, see Fig. 2.13 below), while the second gives the conductance related to the equilibrium electrodes (between points L and R in Fig. 2.13). In Sect. 2.2.4 we obtain both formulas and discuss the relation between them. The puzzle with finite resistance at $T \to 1$ is also understood, it is clear now that the current through a junction is always accompanied by the voltage drop at the boundaries between electrodes and leads. The physical reason is that the number of open electron transport channels is limited, while many other electrons reflect from the junction and create some charge distribution. Not so obvious is, however, that this contact resistance has the universal value $R_c = h/e$ for one spinless channel.

For the transport problems, considered in this book, the second type of the Landauer formula is more important usually. Besides, the first type formulas are not exact for finite-size nanostructures, because they are dependent on the particular electrical potential distribution inside the junction.

The important question, discussed in connection with the Landauer resistance, is the origin of dissipation in this approach. Indeed, finite dc current at finite dc voltage means that the energy is permanently dissipated. On the other hand, we consider only elastic scattering, so that the energy can not be dissipated in the scattering process. This problem is closely related to the phenomena of the residual resistance at low temperature, caused by impurities. In both cases we should introduce some thermal-

ization. In the case of transport between the *equilibrium* electrodes, this problem is resolved quite easy, the energy is dissipated in the electrodes, the details of the dissipation are not relevant. More precisely, the *incoming* from the electrodes particles are equilibrium distributed, while *outgoing* particles propagate into the electrodes and are thermalized here.

At finite temperature and finite voltage the Landauer formula (2.69) is transformed into the more general formula for the current:

$$I(V) = \frac{e}{h} \int_{-\infty}^{\infty} T(E, V) \, [f_L(E) - f_R(E)] \, dE, \tag{2.70}$$

where $T(E, V)$ is the *transmission function* describing the probability of transmission as a function of energy and voltage $V = \varphi_L - \varphi_R$, $f_s(E)$ are the distribution functions in the left ($s = L$) or right ($s = R$) electrodes. In equilibrium the Fermi-Dirac distribution functions with the chemical potential (Fermi energy) μ_s, the electrical potential φ_s and the temperature T_s are

$$f_s(E) = \frac{1}{\exp\left(\frac{E - \mu_s - e\varphi_s}{T_s}\right) + 1}. \tag{2.71}$$

2.2.2 Heuristic Derivation

Now we are ready to see in detail, how the transmission coefficient can be used to calculate the current through a quantum junction, in particular we will derive the Landauer formulas (2.69) and (2.70). We start from the mode-conserving scattering and use here the heuristic arguments. More rigorous methods are summarized in Sect. 2.3.

From the scattering picture it follows that all particles, coming from the left electrode, are transmitted through the junction with the probability $T(n, k_z)$ and, after that, their excess energy, phase coherence, and the memory of their previous state

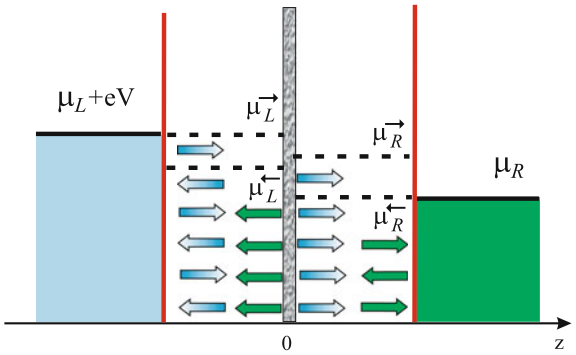

Fig. 2.9 Left-moving and right-moving particles in a wire with scatterer (energy diagram)

are lost in the right electrode. We assume in all cases, that an electron can go without scattering from the lead into the electrode, thus for incoming from the left electron there are only two possibilities: to go into right electrode with the probability T or to return back to the left electrode with the probability R. The same property takes place for all particles coming from the right and transmitted to the left. Transport through the junction is coherent in this model, energy E and transverse quantum number n are conserved (the case of the multi-channel scattering, when n is not conserved, will be considered later). Irreversibility is introduced through the relaxation in the electrodes. The main assumption is that *the right-moving particles in the left lead are populated with the equilibrium distribution function of the left electrode* $f_L^{eq}(E)$ and *the left-moving particles in the right lead are populated with the equilibrium distribution function of the right electrode* $f_R^{eq}(E)$ (see Fig. 2.9).

According to this model, the current of electrons, which enter from the left electrode is determined by the following expression

$$J_{L\to R} = e\sum_n \int_0^\infty T_{L\to R}(n,k_z)\upsilon_L(n,k_z) f_L(n,k_z)\frac{dk_z}{2\pi}, \tag{2.72}$$

where $\upsilon_L(n,k_z)$ is the group velocity of the particle with momentum k_z, $f_L(n,k_z)$ is the distribution function, the form of this function is considered below. The integration is only for right-moving particles with $k_z > 0$. Note, that it is not necessary to multiply this expression additionally by the factor like $(1 - f_R(n,k_z))$ as in the tunneling "golden rule" theory, because this factor describes the number of empty states in the right equilibrium electrode and should be included when the transition between left and right states is considered. Instead, in our approach we consider *scattering states in the leads*, which formally can be extended in the electrodes. The transmission coefficient from the left to the right is simply the probability to find a particle in the right part of this state.

Taking into account that

$$\upsilon(k_z) = \frac{\partial E_z(k_z)}{\hbar\partial k_z} = \frac{\partial E(k_z)}{\hbar\partial k_z}, \tag{2.73}$$

where $E(k_z) = E_n + E_z(k_z)$ is the full energy, we obtain

$$I_{L\to R} = \frac{e}{h}\sum_n \int_{E_{nL}}^\infty T_{L\to R}(n,E) f_L(E) dE, \tag{2.74}$$

and a similar expression for the current of right-incoming electrons

$$I_{R\to L} = \frac{e}{h}\sum_n \int_{E_{nR}}^\infty T_{R\to L}(n,E) f_R(E) dE. \tag{2.75}$$

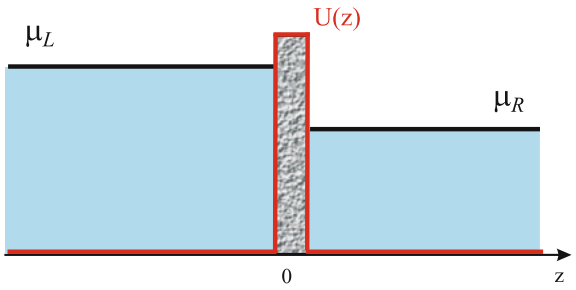

Fig. 2.10 Energy diagrams for chemical potential difference (the number of electrons in the band is changed, but not the potential)

Note that the integration in this expressions is done from the bottom of conduction band $E_{nL(R)}$. Taking into account the symmetry of transmission coefficients (2.28) we get the expression for the current

$$I = \frac{e}{h} \sum_n \int_{-\infty}^{\infty} T_n(E) \left[f_L^{eq}(E) - f_R^{eq}(E) \right] dE. \tag{2.76}$$

The limits of integration over E can be taken infinite, because the closed channels have $T_n(E) = 0$ and do not contribute to the current.

Finally, the distribution functions in this expression should be discussed. There are different possibilities to create a nonequilibrium state of the junction. In equilibrium the *electro-chemical potential* $\tilde{\mu} = \mu + e\varphi$ should be the same in both electrodes. Here μ is the *(internal) chemical potential*, which determines the filling of electron bands in the electrodes, and φ is the electrostatic potential. One can create a difference of only (internal) chemical potentials (Fig. 2.10) if one of the electrodes will be populated by extra particles. This case, however, is quite difficult to realize in nanostructures, because any change of the particle density causes the change in the electric field. Moreover, typically the external voltage is applied to the electrodes, while the (internal) chemical potentials of the electrodes far from the junction are not changed, $\mu_L = \mu_R = \mu$ (Fig. 2.11). More generally, one can say that the difference in the electro-chemical potentials between two points taken inside the equilibrium electrodes, is always produced by the external voltage ($\tilde{\mu}_L - \tilde{\mu}_R = eV$). To determine the exact distribution of the charge density and electrostatic potential near and inside the junction, the self-consistent solution of the coupled Schrödinger and Poisson equations is necessary. In this case the expression (2.76) should be used with care when the voltage is not small. Indeed, the potential $U(z)$ is now a function of the applied voltage, and consequently the transmission coefficient is a function of the voltage too.

The distribution functions in the general case are

$$f_L^0(E) = \frac{1}{\exp\left(\frac{E-\mu_L-e\varphi_L}{T_L}\right)+1}, \qquad f_R^0(E) = \frac{1}{\exp\left(\frac{E-\mu_R-e\varphi_R}{T_R}\right)+1}. \tag{2.77}$$

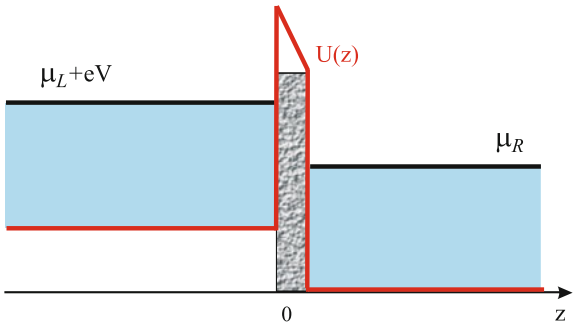

Fig. 2.11 Energy diagrams for voltage difference (the electron band is shifted up, the potential is modified)

The temperatures in the electrodes can be also different, but we consider it later. Usually the simplified form can be used, with explicitly written external voltage

$$I(V) = \frac{e}{h} \sum_n \int_{-\infty}^{\infty} T_n(E, V) \left[f_0(E - eV) - f_0(E) \right] dE. \tag{2.78}$$

where $f^0(E)$ is the Fermi-Dirac distribution function with the equilibrium chemical potentials $\mu_L = \mu_R = E_F$:

$$f_0(E) = \frac{1}{\exp\left(\frac{E - E_F}{T}\right) + 1}. \tag{2.79}$$

The distribution functions in the electrodes are the functions of energy E only, thus one can introduce *the transmission function*

$$T(E) = \sum_n T_n(E), \tag{2.80}$$

and obtain finally

$$I(V) = \frac{e}{h} \int_{-\infty}^{\infty} T(E, V) \left[f_0(E - eV) - f_0(E) \right] dE. \tag{2.81}$$

This formula can be wrong, however, if an external magnetic field is applied, because the magnetic field violates the time-reversal symmetry and the relation (2.28) may be violated too.

The conductance at zero temperature is given by

$$G = \frac{e^2}{h} \sum_n T_n(E_F). \tag{2.82}$$

2.2.3 Conductance Quantization

Perfect Wire

Consider now the conductance of a perfect wire adiabatically coupled to two electrodes. "Perfect wire" means that there are several open reflectionless channels with transmission coefficient $T_n(E) = 1$. Thus all right-going electrons inside the junction are populated only by the left electrode and left-going electrons are populated only by the right electrode (Fig. 2.12). We can say that right moving electrons have the (pseudo-) electro-chemical potential of the left electrode $\tilde{\mu}_L$, while left moving electrons of the right electrode $\tilde{\mu}_R$. Of course, the state of electrons inside the wire is not equilibrium, and these "left" and "right" chemical potentials give the number and energy of corresponding particles in the channel, but they are not usual thermodynamic potentials.

Now we simply use the expression for the current (2.81). The distribution functions in the electrodes at zero-temperature are the step-functions

$$f_L(E, V) = \theta(\mu + eV - E), \tag{2.83}$$

$$f_R(E) = \theta(\mu - E), \tag{2.84}$$

and for the current we obtain

$$\begin{aligned} I(V) &= \frac{e}{h} \sum_n \int_{-\infty}^{\infty} T_n(E, V) \left[\theta(\mu + eV - E) - \theta(\mu - E)\right] dE \\ &= \frac{e}{h} \sum_n \int_{\mu - E_n}^{\mu - E_n + eV} T_n(E, V) dE = \frac{e^2}{h} NV, \end{aligned} \tag{2.85}$$

where we used $T_n(E, V) = 1$, and N is the number of open channels between $\tilde{\mu}_L = \mu + eV$ and $\tilde{\mu}_R = \mu$. For the conductance one has

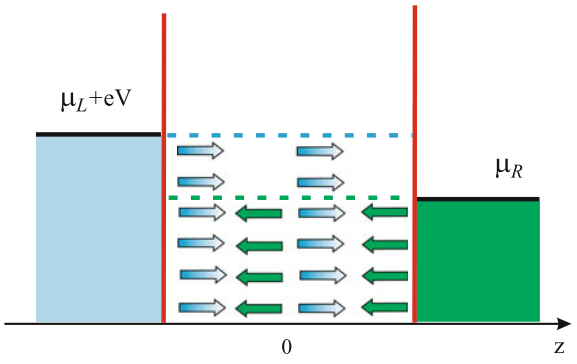

Fig. 2.12 Left-moving and right-moving particles in a perfect wire (energy diagram)

$$G = \frac{e^2}{h} N. \tag{2.86}$$

It is accepted to call the conductance of a single-channel perfect wire with spin *the conductance quantum*

$$G_0 = \frac{2e^2}{h} \approx 77.48\ \mu S = 7.748 \cdot 10^{-5}\ \Omega^{-1} \approx \frac{1}{12900}\ \Omega^{-1}. \tag{2.87}$$

The corresponding resistance is

$$R_0 = \frac{h}{2e^2} \approx 12.9\ k\Omega. \tag{2.88}$$

Where does the resistance of a *perfect* wire come from? The origin of this resistance is in the mismatch between the large number of modes in the electrodes and a few channels in the wire. So this is not the resistance of a perfect wire, but rather the contact resistance of the interface between electrodes and wire.

Quantum Point Contact

In quantum point contacts (QPC), which have usually the adiabatic form, the conductance at low temperatures is quantized in accordance with (2.86). In the spin-degenerate case it can be written as,

$$G = \frac{2e^2}{h} \sum_n \theta(E_F - E_n), \tag{2.89}$$

where E_F is the Fermi energy, and E_n is the maximum of the transverse energy $E_n(z)$. The Fermi energy in 2D electron gas can be changed by the gate voltage V_g, in this way the conductance quantization was observed experimentally in the form of steps at the function $G(V_g)$.

At finite temperature the conductance steps are smeared. Besides, the steps are not perfect, if the junction is not adiabatic. This can be seen from the exactly solvable model with the potential

$$V(x, z) = \frac{1}{2} m\omega_x^2 x^2 + V_0 - \frac{1}{2} m\omega_z^2 z^2. \tag{2.90}$$

The transmission coefficients have a simple form [5]:

$$T_n(E) = \frac{1}{\exp\left[-2\pi\ (E - V_0 - (n + 1/2)\hbar\omega_x)\ /(\hbar\omega_z)\right] + 1}. \tag{2.91}$$

At $\omega_z \ll \omega_x$ we return to the adiabatic approximation and well defined steps.

Classical Point Contact

It is interesting to compare the quantum conductance (2.86) with the conductance of a *classical* point contact with large width $d_0 \gg \lambda_F$, known as Sharvin conductance [6]. Following [7], this conductance for 2D ballistic channel with the width d_0 between two Fermi gases can be written as

$$I = \frac{e\upsilon_F}{\pi} d_0 \frac{\partial n}{\partial \mu} eV, \tag{2.92}$$

In 2D electron gas $\partial n/\partial \mu = m/\pi\hbar^2$, and we obtain (with spin degeneracy)

$$G_S = \frac{2e^2}{h} \frac{k_F d_0}{\pi}. \tag{2.93}$$

From quantum mechanical point of view $k_F d_0/\pi$ is the number of transverse channels N.

2.2.4 Contact Resistance

Consider now the single-channel case with the imperfect transmission $T \neq 1$, repeating the same calculation as in (2.85) we obtain

$$I = \frac{e}{h} T\,(\tilde{\mu}_L - \tilde{\mu}_R) = \frac{e^2}{h} TV, \tag{2.94}$$

$$G = \frac{e^2}{h} T. \tag{2.95}$$

This is the conductance between the reservoirs, e.g. between some two points "L" and "R" inside the electrodes (see Fig. 2.13). Now consider two other points "A" and "B" *inside the leads*. The distribution functions and corresponding "electro-chemical potentials" (these potentials are not true potentials, but give the correct number and energy of electrons, as we discussed before) are different for left and right moving electrons. Now, however, these potentials are different also at different sides of the scatterer (Fig. 2.12, right). The potential $\tilde{\mu}_L^{\rightarrow}$ of the right moving electrons is equal to $\tilde{\mu}_L$ only in the left part of the wire, as well as $\tilde{\mu}_R^{\leftarrow} = \tilde{\mu}_R$ in the right part. All other electro-chemical potentials are modified by the reflection from the barrier. Assume, that one can approximate the charge redistribution in the leads due to scattering by some quasi-equilibrium distributions with corresponding pseudo-potentials $\tilde{\mu}$. For example, only the part of right moving electrons is transmitted through the barrier and corresponding potential should be $T\tilde{\mu}_L$, but additionally $(1-T)\tilde{\mu}_R$ are reflected and move back. Finally, we obtain

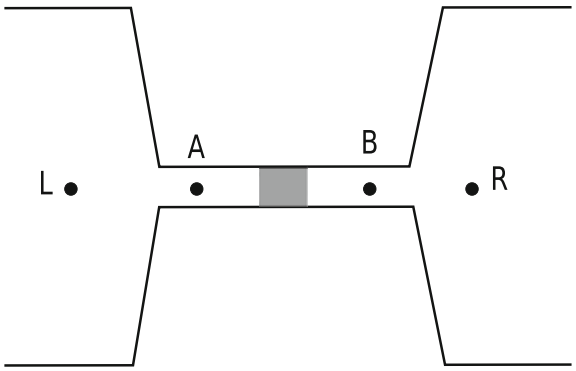

Fig. 2.13 The points of voltage measurement: L, R in the equilibrium electrodes; A, B inside the leads

$$\tilde{\mu}_L^{\rightarrow} = \tilde{\mu}_L, \quad \tilde{\mu}_R^{\rightarrow} = T\tilde{\mu}_L + (1-T)\tilde{\mu}_R, \tag{2.96}$$

$$\tilde{\mu}_R^{\leftarrow} = \tilde{\mu}_R, \quad \tilde{\mu}_L^{\leftarrow} = T\tilde{\mu}_R + (1-T)\tilde{\mu}_L. \tag{2.97}$$

The *difference* of both "left moving" and "right moving" chemical potentials across the barrier is the same

$$\tilde{\mu}_L^{\rightarrow} - \tilde{\mu}_R^{\rightarrow} = \tilde{\mu}_L^{\leftarrow} - \tilde{\mu}_R^{\leftarrow} = (1-T)(\tilde{\mu}_L - \tilde{\mu}_R). \tag{2.98}$$

We can identify this potential difference with the potential drop between points A and B

$$eV_{AB} = (1-T)(\tilde{\mu}_L - \tilde{\mu}_R). \tag{2.99}$$

Thus we can define the conductance (with the current (2.94))

$$G' = \frac{I}{V_{AB}} = \frac{e^2}{h}\frac{T}{1-T} = \frac{e^2}{h}\frac{T}{R}, \tag{2.100}$$

which is exactly "the first Landauer formula" (2.68). The voltage V_{AB} appears as a result of charge redistribution around the scatterer. Not surprising that for perfect wire with $T = 1$ and $R = 0$ this conductance is infinite.

The conductances (2.95) and (2.100) obey the following relation:

$$\frac{1}{G} = \frac{h}{e^2} + \frac{1}{G'}. \tag{2.101}$$

This result can be understood in the following way. G^{-1} can be considered as the full resistance of the junction, consisted from two sequential resistances of the scatterer (G'^{-1}) and of the contact resistance of the perfect wire (h/e^2).

Consider additionally the conductance of the *incoherent* series of N scatterers, each having the transmission coefficient T_1. If the phase coherence is broken, one

should summarize the probabilities of transmission instead of the quantum amplitudes. Thus, the transfer matrix method does not work in this case. Instead we use the probability theory. Let us consider first only two scatterers with the transmission coefficients T_1 and T_2. The probability of transmission trough both scatterers T is calculated as the sum of all possible (re)scattering processes

$$\begin{aligned} T &= T_1T_2 + T_1R_2R_1T_2 + T_1R_2R_1R_2R_1T_2 + \cdots \\ &= T_1(1 + R_1R_2 + (R_1R_2)^2 + \cdots)T_2 = \frac{T_1T_2}{1 - R_1R_2}, \end{aligned} \tag{2.102}$$

or

$$\frac{1-T}{T} = \frac{1-T_1}{T_1} + \frac{1-T_2}{T_2}, \tag{2.103}$$

which demonstrates the additivity of $(1 - T)/T$. Thus, for N scatterers we obtain

$$\frac{1-T}{T} = N\frac{1-T_1}{T_1}. \tag{2.104}$$

The resistance of the system is

$$R = \frac{h}{e^2}\frac{1}{T} = \frac{h}{e^2} + N\frac{h}{e^2}\frac{R_1}{T_1}. \tag{2.105}$$

We again obtain the series resistance of N Landauer scatterers and contact resistance.

2.3 Multi-channel Scattering and Transport

2.3.1 S-Matrix and the Scattering States

Consider now the general multi-channel case, when the scattering is possible between different modes. It is convenient to define separately left (L) and right (R), incoming (+) and outgoing (−) modes (Fig. 2.14). We assume that at $z < z_L$ and $z > z_R$ the leads have a constant cross-sections. To make the $\boldsymbol{S}$-matrix unitary, we introduce the normalization of incoming and outgoing modes, as was discussed in Sect. 2.1.4. Thus, outside the scattering region we define

$$\psi^{+}_{LnE}(\boldsymbol{r}) = \frac{1}{\sqrt{2\pi\hbar v_{Ln}}}\phi_{Ln}(x, y)A_{n+}e^{ik_n z}, \quad z < z_L \tag{2.106}$$

$$\psi^{-}_{LnE}(\boldsymbol{r}) = \frac{1}{\sqrt{2\pi\hbar v_{Ln}}}\phi_{Ln}(x, y)A_{n-}e^{-k_n z}, \quad z < z_L \tag{2.107}$$

Foa Torres 3.2.1

$$R = \frac{\Delta V}{I} = \frac{h}{2e^2}\,\frac{R}{T} \qquad G = \frac{1}{R} = \frac{2e^2}{h}\,\frac{T}{R}$$

Singolo canale tra fili ideali

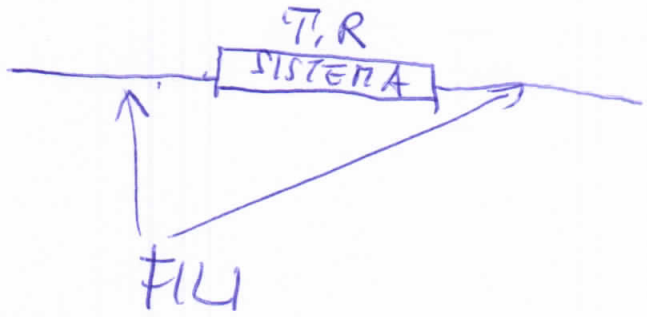

CONSIDERIAMO ORA GLI ELETTRODI

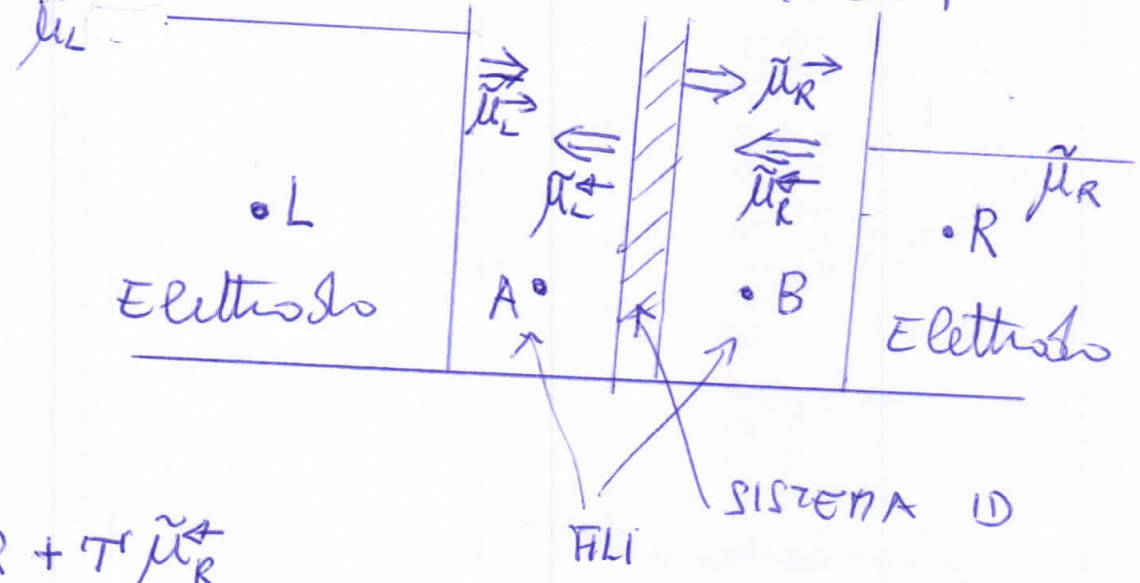

$$\vec{\tilde{\mu}}_L = \tilde{\mu}_L$$

$$\overleftarrow{\tilde{\mu}}_L = \vec{\tilde{\mu}}_L R + T' \overleftarrow{\tilde{\mu}}_R$$

$$\overleftarrow{\tilde{\mu}}_R = \tilde{\mu}_R$$

$$\vec{\tilde{\mu}}_R = \vec{\tilde{\mu}}_L \cdot T + R \overleftarrow{\tilde{\mu}}_R$$

CORRENTE TRA A e B

Assumiamo distribuzioni di quasi equilibrio nei fili

$$\vec{\tilde{\mu}}_L - \vec{\tilde{\mu}}_R = \tilde{\mu}_L (1-T) - (1-T)\tilde{\mu}_R$$

$$\vec{\tilde{\mu}}_L - \vec{\tilde{\mu}}_R = (1-T)(\tilde{\mu}_L - \tilde{\mu}_R)$$

$$\overleftarrow{\tilde{\mu}}_L - \overleftarrow{\tilde{\mu}}_R = \tilde{\mu}_L (1-T) - (1-T)\tilde{\mu}_R$$

$$\overleftarrow{\tilde{\mu}}_L - \overleftarrow{\tilde{\mu}}_R = (\tilde{\mu}_L - \tilde{\mu}_R)(1-T)$$

TRASPORTO/CORRENTE TRA 2 MARI DI FERMI ALL'EQUILIBRIO

(1D)

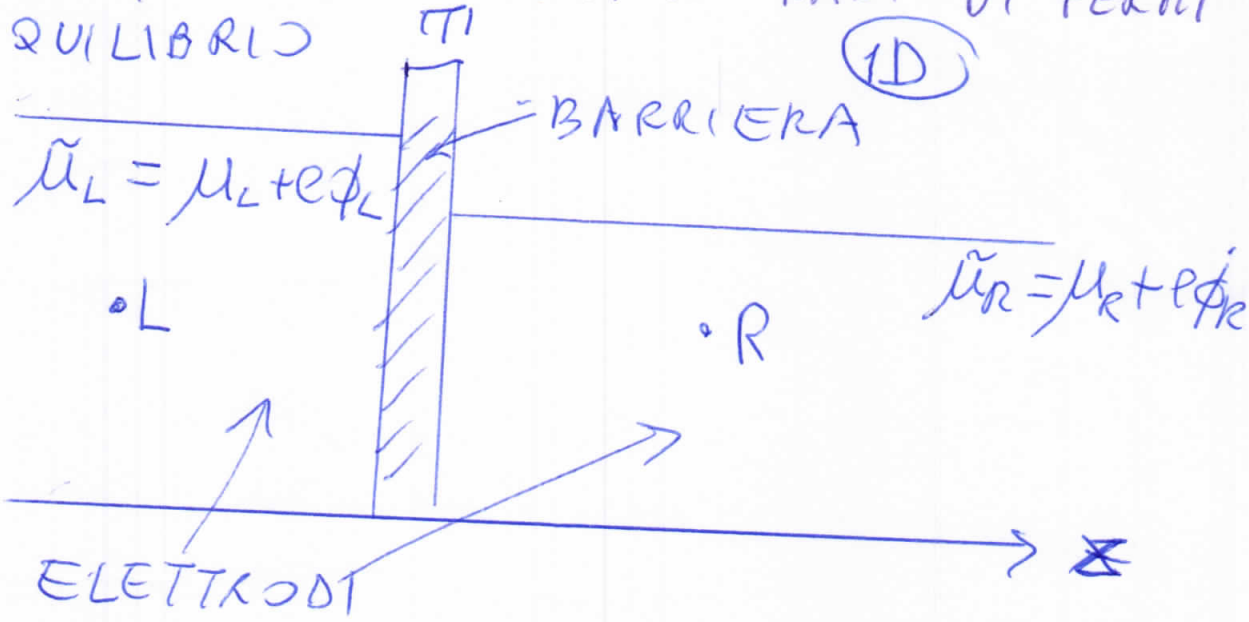

- CASO: $\mu_L = \mu_R = \mu$
- $E_n(k_z) = E_{nL} + \frac{\hbar^2 k_z^2}{2m}$ $\quad v_n(k_z) = \frac{1}{\hbar}\frac{\partial E_n(k_z)}{\partial k_z}$

$$dI_{L\to R} = 2e\frac{1}{L}\frac{dk_z}{\frac{2\pi}{L}} v(k_z) f_L(E_n(k_z))\, T(E_n(k_z))$$

$$I_{L\to R} = 2e\int \frac{dk_z}{2\pi}\frac{1}{\hbar}\frac{\partial E_n(k_z)}{\partial k_z} f_L(E_n(k_z))\, T(E_n(k_z))$$

$$= \frac{2e}{h}\int_{E_{nL}}^{\infty} dE\, f_L(E)\, dE\, T_n(E)$$

$$T_n(E) T_{LR}^{(n)}(E) = T_{RL}^{(n)}(E)$$

$$I_{R\to L} = \frac{2e}{h}\int_{E_{nR}}^{\infty} dE\, T_n(E) f_R(E)\, dE$$

- Stati di scattering nei fili + elettrodi identici $E_{nL} = E_{nR} = E_n$

$$I = I_{L\to R} - I_{R\to L}$$

$$= \frac{2e}{h} \int_{E_n}^{\infty} dE\, T_n(E) \left[f_L(E) - f_R(E) \right] dE$$

$$f_L(E) = \frac{1}{e^{\beta(E-\tilde{\mu}_L)}+1} \quad ; \quad f_R(E) = \frac{1}{e^{\beta(E-\tilde{\mu}_R)}+1}$$

$$f_{L,R}(E) = f_0(E - e\phi_{L,R}) \qquad f_0(E) = \frac{1}{e^{\beta(E-\mu)}+1}$$

$$I = \frac{2e}{h} \int_{E_n}^{\infty} dE\, T_n(E) \left[f_0(E - e\phi_L) - f_0(E - e\phi_L) \right]$$

$$\simeq \frac{2e}{h} \int_{E_n}^{\infty} dE\, T_n(E) \left. \frac{\partial f_0}{\partial E} \right|_E \left[-e(\phi_L - \phi_R) \right]$$

$$\phi_L - \phi_R = V$$

$$I = \frac{2e^2 V}{h} \int_{E_n}^{\infty} dE\, T_n(E) \left[- \left. \frac{\partial f_0}{\partial E} \right|_E \right]$$

$$I = \frac{2e^2}{h} V\, T_n(\mu) \qquad \frac{I}{V} = G = \frac{2e^2}{h} T_n(\mu)$$

- DATA la corrente tra L e R, la corrente tra A e B deve essere la stessa!

- La caduta di potenziale tra A e B è

$$\tilde{\mu}_L^{\rightarrow} - \tilde{\mu}_R^{\rightarrow} = \tilde{\mu}_L^{\leftarrow} - \tilde{\mu}_R^{\leftarrow} = (1-\pi)(\tilde{\mu}_L - \tilde{\mu}_R)$$
$$= (1-\pi)\, eV$$

- Quindi la conduttanza tra A e B è

$$\frac{I}{(1-\pi)V} = \frac{2e^2}{h}\frac{V\pi}{V(1-\pi)} = \frac{2e^2}{h}\frac{\pi}{R} = G'$$

in accordo con la prima formula di Landauer

- Infine notiamo che

$$\frac{1}{G} = \frac{h}{2e^2\pi} = \frac{h}{2e^2}\frac{R+\pi}{\pi} = \frac{h}{2e^2}\frac{1-\pi}{\pi} + \frac{h}{2e^2}$$

$$\boxed{\frac{1}{G} = \frac{1}{G'} + \frac{h}{2e^2}}$$

La resistenza totale è data dalla somma di $\frac{1}{G'}$ e la resistenza di contatto $h/2e^2$!

Resistenza di contatto: filo perfetto con $\pi = 1$

5.0.2 Additions to Kubo-Greenwood (in Foa-Torres 3.4)

As in Foa-Torres we consider a system in 1 dimension in an external electric field which in Coulomb gauge comes solely from a vector potential

$$A(t) = -\frac{E_0}{2i\omega}\left(e^{i\omega t} - e^{-i\omega t}\right),$$

yielding an electric field

$$E(t) = -\frac{\partial A(t)}{\partial t} = E_0 cos(\omega t).$$

Let's consider the dissipated power in the system due to the electric field, which causes transitions between eigenstate of the unpertubed hamiltonian ($H_0|n\rangle = E_n|n\rangle$). Evidently $P = J \cdot E$, but it can also be expressend as

$$P = \sum_{n,m}(E_m - E_{n)} f(E_n)[1 - f(E_m)]\tilde{p}_{n\to m},$$

where $\tilde{p}_{n\to m}$is the probability per unit time of the transition $|n\rangle \to |m\rangle$. Evidently when $E_m > E_n$ energy is *absorbed* by the system, while when $E_m < E_n$ energy is *emitted* by the system, thus the totale power is the difference between *absorbed* and *emitted* nenergy. To calculate P we need to calculate the $\tilde{p}_{n\to m}$. To this end we have to start from the coupling hamiltonian between the system and the electric field (in SI)

$$\delta\hat{H}(t') = e\hat{V}_x A(t).$$

Linear order time-dependent perturbation theory provides the expressions

$$a_{n\to m}(t) = \frac{-i}{\hbar}\int_0^t dt' e^{i(E_m - E_n)t}\langle m|\delta\hat{H}(t')|n\rangle,$$

$$\tilde{p}_{n\to m} = \lim_{t\to\infty}\frac{p_{n\to m}}{t} = \lim_{t\to\infty}\frac{1}{t}|a_{n\to m}(t)|^2 = \lim_{t\to\infty}\frac{1}{\hbar^2 t}\left|\int_0^t dt' e^{i(E_m - E_n)t}\langle m|\delta\hat{H}(t')|n\rangle\right|^2.$$

A simple calculations yields

$$\begin{aligned} a_{n\to m}(t) &= -\frac{eE_0}{2i\hbar\omega}\langle m|\hat{V}_x|n\rangle\left(\frac{e^{i(\omega+\omega_{mn})t} - 1}{i(\omega + \omega_{mn})} + \frac{e^{-i(\omega-\omega_{mn})t} - 1}{i(\omega - \omega_{mn})}\right) \\ &= \frac{eE_0}{2\hbar\omega}\langle m|\hat{V}_x|n\rangle\left(\frac{e^{i(\omega+\omega_{mn})t} - 1}{(\omega + \omega_{mn})} + \frac{e^{-i(\omega-\omega_{mn})t} - 1}{(\omega - \omega_{mn})}\right). \end{aligned}$$

Note that $\tilde{p}_{n\to m}$ does not vanish only if $a_{n\to m}(t)$ is diverging for large t. This happens if either $\omega + \omega_{mn} \to 0$ or $\omega - \omega_{mn} \to 0$; the two conditions are however mutually exclusive! Thus when we consider $|a_{n\to m}(t)|^2$ we can retain one term at time and get

$$|a_{n\to m}(t)|^2 = \frac{e^2E_0^2}{4\hbar^2\omega^2}|\langle m|\hat{V}_x|n\rangle|^2\left(2\frac{1 - \cos[(\omega + \omega_{mn})t]}{(\omega + \omega_{mn})^2} + 2\frac{1 - \cos[(\omega - \omega_{mn})t]}{(\omega - \omega_{mn})^2}\right).$$

Recall that $lim_{t\to\infty} 2[1 - \cos(\omega t)]/(\omega^2 t) = 4\pi\delta(\omega)$ to obtain

$$\tilde{p}_{n\to m}\lim_{t\to\infty}\frac{1}{t}|a_{n\to m}(t)|^2 = \frac{e^2E_0^2\pi}{2\hbar^2\omega^2}|\langle m|\hat{V}_x|n\rangle|^2[\delta(\omega + \omega_{mn}) + \delta(\omega - \omega_{mn})].$$

Thus, choosing $\omega > 0$ and setting $E = \hbar\omega$, we get

$$
\begin{aligned}
P &= \sum_{n,m}(E_m - E_n)f(E_n)[1 - f(E_m)]\tilde{p}_{n\to m} \\
&= \sum_{n,m}(E_m - E_n)f(E_n)[1 - f(E_m)]\frac{e^2E_0^2\pi}{2\hbar^2\omega^2}|\langle m|\hat{V}_x|n\rangle|^2[\delta(\omega + \omega_{mn}) + \delta(\omega - \omega_{mn}) \\
&= \frac{e^2E_0^2\pi}{2\hbar^2\omega^2}\sum_{n,m}|\langle m|\hat{V}_x|n\rangle|^2\left[-\hbar\omega f(E_n)[1 - f(E_m)]\delta(\omega + \omega_{mn}) + \hbar\omega f(E_n)[1 - f(E_m)]\delta(\omega - \omega_{mn})\right] \\
&= \frac{e^2E_0^2\pi}{2\hbar^2\omega^2}\sum_{n,m}|\langle m|\hat{V}_x|n\rangle|^2\left[-\hbar\omega f(E_n)[1 - f(E_m)]\delta(\omega + \omega_{mn}) + \hbar\omega f(E_m)[1 - f(E_n)]\delta(\omega + \omega_{mn})\right] \\
&= \frac{e^2E_0^2\pi}{2\hbar^2\omega^2}\sum_{n,m}|\langle m|\hat{V}_x|n\rangle|^2\left[\hbar\omega[f(E_m) - f(E_n)]\delta(\omega + \omega_{mn})\right] \\
&= \frac{e^2E_0^2\pi}{2\hbar^2\omega^2}\sum_{n,m}|\langle m|\hat{V}_x|n\rangle|^2\left[\hbar\omega[f(E_m) - f(E_n)]\hbar\delta(\hbar\omega + E_m - E_n)\right] \\
&= \frac{\pi\hbar e^2E_0^2}{2\hbar\omega}\sum_{n,m}|\langle m|\hat{V}_x|n\rangle|^2\left[[f(E_n) - f(E_m)]\delta(E_m - E_n - \hbar\omega)\right].
\end{aligned}
$$

This gives the conductivity in the RTA as

$$\sigma_{xx} = -\frac{e^2}{2\pi}\int kdk\left(\frac{\partial f_k^0}{\partial \varepsilon_k}\right)\tau_k v_k^2. \tag{3.28}$$

3.4 Kubo formula for the electronic conductivity

The conductivity of a bulk material is defined at finite frequency ω as the tensorial ratio between the applied electric field and the resulting electronic current: $\mathbf{J}(\omega) = \boldsymbol{\sigma}(\omega)\mathbf{E}(\omega)$. We assume that the transport measurement direction is along the (Ox) axis, so that only diagonal elements are taken into account: $\mathcal{J}_x(\omega) = \sigma(\omega)E_x(\omega)$. The Kubo approach is a technique to calculate linear response in materials (optical, electric, etc.). It is based on the *fluctuation–dissipation theorem* that establishes a correspondence between the *dissipative* out-of-equilibrium response (namely, the conductivity) and the *fluctuations* at the equilibrium (the correlation function of the charge carrier velocities).

We provide here a comprehensive derivation of the Kubo formula for electronic conductivity (Roche, 1996, Triozon, 2002, Lherbier, 2008), which is suitable for studying quantum transport phenomena in disordered graphene-based materials, based on numerical simulations. It is inspired by a derivation by Nevill Mott which calculates the absorbed power driven by electronic transitions induced by the exchanges between the system and the electromagnetic field (P).

Let us assume an electronic system described by the Hamiltonian $\hat{\mathcal{H}}_0 = \frac{\hat{\mathbf{P}}^2}{2m} + \hat{\mathcal{V}}$, where $\hat{\mathcal{V}}$ gives the crystal potential which can also include the effect of crystal imperfections. Then assume that its electronic spectrum is given by $\varepsilon_k, |\Psi_k\rangle$. By applying an external (weak) electric field, the system will undergo internal fluctuations, which are usually well captured by electronic transition between states of the system at equilibrium. To compute σ, we start with the equation $P = \mathcal{J}\cdot\mathbf{E}$ with $\mathcal{J} = \sigma\mathbf{E}$. The electric field $\mathbf{E}(t)$ is given by $E_0\cos(\omega t)\mathbf{u}_x$, but for computational convenience we use an oscillatory field throughout the derivation, while the limit to the static case is taken at the end ($\mathbf{E}(t) = E_0\mathbf{u}_x$) with $\omega \to 0$. The associated vector potential $\mathbf{A}(t)$ in the Coulomb gauge is

$$\mathbf{A}(t) = -\frac{E_0}{2i\omega}\left(\mathrm{e}^{\mathrm{i}\omega t} - \mathrm{e}^{-\mathrm{i}\omega t}\right)\mathbf{u}_x, \tag{3.29}$$

while the total power absorbed per unit time is

$$P_{\text{tot abs}} = \sum_{n,m} P_{\text{abs}}^{n\to m} - P_{\text{diss}}^{m\to n}. \tag{3.30}$$

The average power absorbed (P_{abs}) and dissipated (P_{diss}) per unit time can be estimated from the transition probabilities $\tilde{p}_{n\to m}$ from electronic states n to m (and inversely $(m \to n)$) and Fermi–Dirac distribution $f(E)$:

$$P_{\text{abs}}^{n\to m} = \left[\hbar\omega\, f(E_n)(1-f(E_m))\right]\tilde{p}_{n\to m}, \tag{3.31}$$

$$P_{\text{diss}}^{m\to n} = \left[\hbar\omega\, f(E_m)(1-f(E_n))\right]\tilde{p}_{m\to n}. \tag{3.32}$$

Such transition probabilities per unit time are derived from a first-order perturbation theory in the electric field as

$$\tilde{p}_{n\to m} = \frac{p_{n\to m}(t)}{t} = \frac{1}{\hbar^2 t}\left|\int_0^t dt' \mathrm{e}^{\mathrm{i}(E_m - En)t'/\hbar}\langle m|\delta\hat{\mathcal{H}}(t')|n\rangle\right|^2, \tag{3.33}$$

with $\delta\hat{\mathcal{H}}$ being the time-dependent perturbation of the total Hamiltonian. At first order it directly relates to the velocity operator $\hat{\mathbf{V}}$ and vector potential $\mathbf{A}$ through

$$\delta\hat{\mathcal{H}}(t') = e\,\hat{\mathbf{V}}\cdot\mathbf{A}(t'), \tag{3.34}$$

$$\delta\hat{\mathcal{H}}(t') = e\hat{V}_x A_x(t') \quad \text{(for the 1D case)}. \tag{3.35}$$

Using Eqs. (3.29–3.35) we obtain

$$P_{\text{tot abs}} = \frac{\pi\hbar e^2 E_0^2}{2\hbar\omega}\sum_{n,m}\left|\langle m|\hat{V}_x|n\rangle\right|^2\delta(E_m - E_n - \hbar\omega)\left[f(E_n) - f(E_m)\right], \tag{3.36}$$

and finally the total power absorbed per unit time and volume $P = \frac{P_{\text{abs}}}{\Omega}$ (Ω being the sample volume) is related to the conductivity by

$$P = \frac{P_{\text{tot abs}}}{\Omega} = \sigma\langle\mathbf{E}\cdot\mathbf{E}\rangle = \frac{\sigma E_0^2}{2}. \tag{3.37}$$

Using Eq. (3.37), where $\langle\cos^2(\omega t)\rangle$ has been replaced by its average value $1/2$, one gets the Kubo conductivity

$$\sigma(\omega) = \frac{\pi\hbar e^2}{\Omega}\sum_{n,m}\left|\langle m|\hat{V}_x|n\rangle\right|^2\delta(E_m - E_n - \hbar\omega)\,\frac{f(E_n) - f(E_m)}{\hbar\omega}. \tag{3.38}$$

Using the properties of $\delta(x)$ functions and rewriting the expression as a trace of operators the general expression becomes

$$\sigma(\omega) = \frac{\pi\hbar e^2}{\Omega}\int_{-\infty}^{+\infty} dE\,\frac{f(E) - f(E+\hbar\omega)}{\hbar\omega}\,\mathrm{Tr}\left[\hat{V}_x^\dagger\delta(E - \hat{\mathcal{H}})\hat{V}_x\delta(E + \hbar\omega - \hat{\mathcal{H}})\right]. \tag{3.39}$$

It is also instructive to rewrite this formula introducing the autocorrelation function of velocity ($C(E,t)$), together with the mean square spreading of wavepackets defined as ($\Delta X^2(E,t)$). Using

$$\delta\left(E + \hbar\omega - \hat{\mathcal{H}}\right) = \frac{1}{2\pi\hbar}\int_{-\infty}^{+\infty} dt\,\mathrm{e}^{\mathrm{i}\left(E+\hbar\omega-\hat{\mathcal{H}}\right)t/\hbar} \tag{3.40}$$

inside the trace, which is further denoted by $\mathbb{A}_1$:

$$\mathbb{A}_1 = \mathrm{Tr}\left[\hat{V}_x^\dagger\delta\left(E - \hat{\mathcal{H}}\right)\hat{V}_x\delta\left(E + \hbar\omega - \hat{\mathcal{H}}\right)\right], \tag{3.41}$$

$$\mathbb{A}_1 = \frac{1}{2\pi\hbar}\int_{-\infty}^{+\infty} dt\,\mathrm{e}^{\mathrm{i}\omega t}\,\mathrm{Tr}\left[\hat{V}_x^\dagger\delta\left(E - \hat{\mathcal{H}}\right)\,\hat{V}_x\,\mathrm{e}^{\mathrm{i}\left(E-\hat{\mathcal{H}}\right)t/\hbar}\right], \tag{3.42}$$

$$\mathbb{A}_1 = \frac{1}{2\pi\hbar}\int_{-\infty}^{+\infty} dt\,\mathrm{e}^{\mathrm{i}\omega t}\,\mathrm{Tr}\left[\hat{V}_x^\dagger\delta\left(E - \hat{\mathcal{H}}\right)\,\mathrm{e}^{\mathrm{i}\hat{\mathcal{H}}t/\hbar}\,\hat{V}_x\,e^{-i\hat{\mathcal{H}}t/\hbar}\right]. \tag{3.43}$$

The velocity operator in its Heisenberg representation being

$$\hat{V}_x(t) = \left(\mathrm{e}^{\mathrm{i}\hat{\mathcal{H}}t/\hbar}\, \hat{V}_x\, \mathrm{e}^{-\mathrm{i}\hat{\mathcal{H}}t/\hbar} \right), \tag{3.44}$$

we get

$$\mathbb{A}_1 = \frac{1}{2\pi\hbar} \int_{-\infty}^{+\infty} dt\, \mathrm{e}^{\mathrm{i}\omega t}\, \mathrm{Tr}\left[\hat{V}_x^{\dagger}(0)\, \delta(E - \hat{\mathcal{H}})\, \hat{V}_x(t) \right]. \tag{3.45}$$

Then, one uses the general definition of quantum average for a given energy E, from which any operator $\hat{Q}$ has

$$\langle \hat{Q} \rangle_E = \frac{\mathrm{Tr}\left[\delta(E - \hat{\mathcal{H}}) \hat{Q} \right]}{\mathrm{Tr}\left[\delta(E - \hat{\mathcal{H}}) \right]}. \tag{3.46}$$

Replacing $\hat{Q}$ by the product $\hat{V}_x(t)\hat{V}_x^{\dagger}(0)$,

$$\langle \hat{V}_x(t)\hat{V}_x^{\dagger}(0) \rangle_E = \frac{\mathrm{Tr}\left[\hat{V}_x^{\dagger}(0) \delta(E - \hat{\mathcal{H}}) \hat{V}_x(t) \right]}{\mathrm{Tr}\left[\delta(E - \hat{\mathcal{H}}) \right]}, \tag{3.47}$$

and using this result to rewrite $\mathbb{A}_1$,

$$\mathbb{A}_1 = \frac{1}{2\pi\hbar} \int_{-\infty}^{+\infty} dt\, \mathrm{e}^{\mathrm{i}\omega t}\, \mathrm{Tr}\left[\delta(E - \hat{\mathcal{H}}) \right]\, \langle \hat{V}_x(t)\hat{V}_x^{\dagger}(0) \rangle_E, \tag{3.48}$$

$$\mathbb{A}_1 = \frac{1}{2\pi\hbar} \mathrm{Tr}\left[\delta(E - \hat{\mathcal{H}}) \right] \int_{-\infty}^{+\infty} dt\, \mathrm{e}^{\mathrm{i}\omega t}\, \langle \hat{V}_x(t)\hat{V}_x^{\dagger}(0) \rangle_E, \tag{3.49}$$

$$\mathbb{A}_1 = \frac{1}{2\pi\hbar}\, \mathbb{A}_2\, \mathbb{A}_3, \tag{3.50}$$

$$\text{with} \quad \mathbb{A}_2 = \mathrm{Tr}\left[\delta(E - \hat{\mathcal{H}}) \right], \quad \text{and} \quad \mathbb{A}_3 = \int_{-\infty}^{+\infty} dt\, \mathrm{e}^{\mathrm{i}\omega t}\, \langle \hat{V}_x(t)\hat{V}_x^{\dagger}(0) \rangle_E. \tag{3.51}$$

Two interesting quantities emerge, with $\mathbb{A}_2$ the total density of states. The second quantity can be reformulated as ($\mathbb{A}_3$) using the definition of velocity autocorrelation function $C(E,t) = \langle \hat{V}_x(t)\hat{V}_x^{\dagger}(0) \rangle_E$, so that

$$\mathbb{A}_3 = \int_{-\infty}^{+\infty} dt\, \mathrm{e}^{\mathrm{i}\omega t}\, C(E,t), \tag{3.52}$$

$$\mathbb{A}_3 = \int_{-\infty}^{0} dt\, \mathrm{e}^{\mathrm{i}\omega t}\, C(E,t) + \int_{0}^{+\infty} dt\, \mathrm{e}^{\mathrm{i}\omega t}\, C(E,t), \tag{3.53}$$

$$\mathbb{A}_3 = \int_{0}^{+\infty} dt\, \mathrm{e}^{-\mathrm{i}\omega t}\, C(E,-t) + \int_{0}^{+\infty} dt\, \mathrm{e}^{\mathrm{i}\omega t}\, C(E,t), \tag{3.54}$$

and using $C(E,-t) = \langle \hat{V}_x(-t)\hat{V}_x^{\dagger}(0) \rangle_E = \langle \hat{V}_x(0)\hat{V}_x^{\dagger}(t) \rangle_E = C(E,t)^{\dagger}$, one gets

$$\mathbb{A}_3 = \int_{0}^{+\infty} dt\, \mathrm{e}^{-\mathrm{i}\omega t}\, C(E,t)^{\dagger} + \mathrm{e}^{\mathrm{i}\omega t}\, C(E,t), \tag{3.55}$$

$$\mathbb{A}_3 = \int_{0}^{+\infty} dt\, 2\Re\mathrm{e}\left(\mathrm{e}^{\mathrm{i}\omega t}\, C(E,t) \right). \tag{3.56}$$

One can easily show that the real part of the velocity autocorrelation function is proportional to the second derivative of the mean squared spread

$$\frac{\partial^2}{\partial t^2}\Delta X^2(E,t) = 2\Re\mathrm{e}\; C(E,t), \tag{3.57}$$

with $\Delta X^2(E,t)$ defined as

$$\Delta X^2(E,t) = \langle \left|\hat{X}(t) - \hat{X}(0)\right|^2 \rangle_E. \tag{3.58}$$

One can consequently rewrite $\mathbb{A}_1$ as follows:

$$\mathbb{A}_1 = \frac{1}{2\pi\hbar}\,\mathbb{A}_2 \int_0^{+\infty} dt\; 2\Re\mathrm{e}\left(\mathrm{e}^{\mathrm{i}\omega t}\; C(E,t)\right), \tag{3.59}$$

and $\mathbb{A}_1$ can be replaced in Eq. (3.39) to get another formulation of the Kubo conductivity (Roche, 1996, Triozon, 2002, Lherbier, 2008):

$$\sigma(\omega) = \frac{e^2}{2}\int_{-\infty}^{+\infty} dE\,\frac{f(E) - f(E+\hbar\omega)}{\hbar\omega}\;\frac{\mathrm{Tr}\left[\delta(E-\hat{\mathcal{H}})\right]}{\Omega}\int_0^{+\infty} dt\; 2\Re\mathrm{e}\left(\mathrm{e}^{\mathrm{i}\omega t}\; C(E,t)\right). \tag{3.60}$$

This last Eq. (3.60) is the total density of states per volume unit $\rho(E) = \mathrm{Tr}\big[\delta(E - \hat{\mathcal{H}})\big]/\Omega$. This is a general form for σ, which can now be simplified taking two limits. First, let us go to the static electric field limit $\omega \mapsto 0$,

$$\sigma_{DC} = -\frac{e^2}{2}\int_{-\infty}^{+\infty} dE\;\frac{\partial f(E)}{\partial E}\;\rho(E)\int_0^{+\infty} dt\; 2\Re\mathrm{e}\left(C(E,t)\right), \tag{3.61}$$

$$\sigma_{DC} = -\frac{e^2}{2}\int_{-\infty}^{+\infty} dE\;\frac{\partial f(E)}{\partial E}\;\rho(E)\int_0^{+\infty} dt\;\frac{\partial^2}{\partial t^2}\Delta X^2(E,t), \tag{3.62}$$

$$\sigma_{DC} = -\frac{e^2}{2}\int_{-\infty}^{+\infty} dE\;\frac{\partial f(E)}{\partial E}\;\rho(E)\lim_{t\mapsto\infty}\frac{\partial}{\partial t}\Delta X^2(E,t), \tag{3.63}$$

while the zero-temperature limit ($T \mapsto 0$) implies that $-\frac{\partial f(E)}{\partial E} \mapsto \delta(E - E_F)$, so that

$$\sigma_{DC}(E_F) = \frac{e^2}{2}\int_{-\infty}^{+\infty} dE\;\delta(E-E_F)\;\rho(E)\lim_{t\mapsto\infty}\frac{\partial}{\partial t}\Delta X^2(E,t), \tag{3.64}$$

$$\sigma_{DC}(E_F) = \frac{e^2}{2}\rho(E_F)\lim_{t\mapsto\infty}\frac{\partial}{\partial t}\Delta X^2(E_F,t). \tag{3.65}$$

This last expression means that $\frac{\partial}{\partial t}\Delta X^2(E_F,t)$ should converge in the limit $t \mapsto \infty$, to define a meaningful conductivity. The propagation of the wavepacket thus needs to establish a saturation regime before conductivity can be safely calculated. However, as shown in other chapters, the time-dependent scaling on the conductivity can be followed and allowed to follow localization phenomena as long as phase coherence is maintained. This formula, known as the Kubo conductivity (Kubo, 1966), is the most general starting point to study quantum (or classical) transport in any type of disordered materials, provided that electron–electron interaction can be described as a perturbation with

respect to the initial electronic structure, introducing additional transitions (inelastic scattering), but preserving the independent electron description of transport quantities.

3.4.1 Illustrations for ballistic and diffusive regimes

The behavior of $\Delta X^2(t)$ and related diffusion coefficient $D_x(t)$ defined by

$$D_x(t) = \frac{\Delta X^2(t)}{t} \tag{3.66}$$

is easily determined in two important transport regimes. Below we outline some consequences of the transport regime on the scaling property of the quantum conductivity, as computed from the Kubo formula.

Ballistic regime

First, in the absence of any structural imperfection, the electronic propagation remains ballistic with the mean square spread just defined by the initial velocity of the wavepacket $\Delta X^2(t) = v_x^2(0)t^2$, with $v_x(0)$ the velocity at $t = 0$. The diffusion coefficient is then linear in time, $D_x(t) = v_x^2(0)t$, while the Kubo conductivity is given by

$$\sigma_{DC}(E)_{\text{bal}} = \frac{e^2}{2}\rho(E)\lim_{t\mapsto\infty}\frac{\partial}{\partial t}\Delta X^2(E,t) = e^2\rho(E)\lim_{t\mapsto\infty} v_x^2(0,E)t, \tag{3.67}$$

so that $\sigma_{DC}(E)_{\text{bal}}$ diverges in the long time limit. This singularity is inherent to the fact that when deriving the linear response theory, a finite dissipation source, intrinsic to the sample, is introduced both physically and mathematically. The ballistic limit is therefore not well defined in this formalism, although as shown below a complete equivalence exists with the Landauer–Büttiker formulation, and the quantization of the conductance can be obtained from the Kubo formula with some extra assumptions. The conductance of the materials can indeed be derived from the conductivity through $G = \sigma L^{d-2}$, with d the space dimension. For one-dimensional systems $G = \sigma/L$. Dividing Eq. (3.67) by the relevant length scale L, we can recover a quantized conductance expected in a ballistic regime (when reflectionless contacts are assumed). By replacing L by $2v_xt$ (since the length propagated during t is $2\sqrt{\Delta X^2(t)} = 2v_xt$), the conductance then becomes

$$G(E) = e^2\rho_{1D}(E)\lim_{t\to\infty}\frac{v_x^2(E)t}{L} = e^2\rho_{1D}(E)\lim_{t\to\infty}\frac{v_x^2(E)t}{2v_x(E)t}, \tag{3.68}$$

$$G(E) = \frac{e^2}{2}\rho_{1D}(E)v_x(E) = \frac{2e^2}{h} = G_0, \tag{3.69}$$

using $\rho_{1D}(E) = 2/\pi\hbar v_x(E)$ and with G_0 the conductance quantum (spin degeneracy included). So even in the most unfavorable transport regime, the quantization of the conductance can be recovered and identified to the situation of perfect transmission through reflectionless contacts (Landauer–Büttiker approach, Section 3.2)

Diffusive regime

The velocity autocorrelation function in the time relaxation approximation is given by $\langle v_x(0)v_x(t)\rangle = v_x^2(0)\mathrm{e}^{-t/\tau}$ (introducing the transport time τ and restricting the discussion to elastic scattering events), which yields

$$\lim_{t\mapsto\infty}\Delta X^2(t) = \lim_{t\mapsto\infty} 2\tau v_x^2(0)\,[t-\tau] \longmapsto 2\tau v_x^2(0)t. \tag{3.70}$$

Similarly (using Eq. (3.66)) one gets $\lim_{t\mapsto\infty} D_x(t) \longmapsto 2\tau v_x^2(0)$. The Kubo formula for a diffusive regime then gives access to the semiclassical conductivity (σ_{sc}):

$$\sigma_{sc}(E) = \sigma_{DC}(E)_{\mathrm{diff}} = \frac{e^2}{2}\rho(E)\lim_{t\mapsto\infty}\frac{\partial}{\partial t}\Delta X^2(E,t), \tag{3.71}$$

$$\sigma_{sc}(E) = e^2\rho(E)\tau(E)v_x^2(0,E), \tag{3.72}$$

$$\sigma_{sc}(E) = e^2\rho(E)v_x(0,E)\ell_e(E), \tag{3.73}$$

where the mean free path $\ell_e(E)$ is introduced. For the diffusive regime,

$$\sigma_{sc}(E) = \frac{e^2}{2}\rho(E)\lim_{t\mapsto\infty} D_x(E,t) = \frac{e^2}{2}\rho(E)D_x^{\max}(E), \tag{3.74}$$

where $D_x^{\max}$ corresponds to the maximum value ($D_x^{\max} = 2\tau v_x^2(0)$). In this regime, by defining the charge density as $n(E) = \int dE\rho(E)$, the mobility μ is given by

$$\mu(E) = \frac{\sigma_{sc}(E)}{n(E)e}. \tag{3.75}$$

For free electrons $E(k) = (\hbar k)^2/2m$ and $v(k) = \hbar k/m$, with $\rho_{1D}(E) = \frac{2}{\pi\hbar}\left(\frac{m}{2E}\right)^{1/2}$ and $n_{1D}(E) = \frac{2}{\pi\hbar}(2mE)^{1/2}$, so that using Eq. (3.72) and Eq. (3.75), the mobility finally is given by

$$\mu(E) = \frac{e^2\rho_{1D}(E)\tau(E)v^2(E)}{en_{1D}(E)} = \frac{e\tau(E)v^2(E)}{2E}, \tag{3.76}$$

$$\mu(E) = \frac{e\tau(E)\hbar^2k^2}{2\left(\frac{\hbar^2k^2}{2m}\right)m^2} = \frac{e\tau(E)}{m}, \tag{3.77}$$

which are familiar expressions for semiclassical transport (absence of quantum interferences). One notes that estimation of the mobility becomes problematic for graphene-based materials for plenty of reasons. First, for clean graphene-based materials (nanotubes, graphene ribbons or two-dimensional graphene), the mean free path might become longer than the electrode spacing, so that the use (or even the definition) of Eq. (3.75) becomes inappropriate since it neglects contact effects. Additionally, in the presence of intrinsic disorder (vacancies, adsorbed adatoms, etc.), strong scattering and a significant contribution of quantum interferences occur, which again invalidate the use of Eq. (3.75). Quantum interferences up to 100 K have been measured experimentally in disordered graphene materials (see for instance Moser *et al.* (2010)), so even if inelastic scattering restores in principle the validity of Eq. (3.75), the experimental estimations have to be scrutinized with care. One general assumption is that the quality of the sample can be appreciated by estimating the mobility at a charge density

of (typically) 10^{11} cm^{-2} with varying temperature, and that the absolute value allows comparison of sample quality. In the numerical calculations (using the Kubo formula) that are discussed later, the estimations of mobility using Eq. (3.75) are made using the semiclassical conductivity computed at zero temperature.

3.4.2 Kubo versus Landauer

The Kubo approach is a quantum generalization of the semiclassical Bloch–Boltzmann approach for studying electron transport in materials, which includes all multiple scattering effects driven by disorder. The Kubo–Greenwood formalism (Kubo, 1966) is well suited for exploring the intrinsic transport properties of a given disordered material of high dimensionality. It mainly applies to the study of weakly or strongly disordered systems, characterized by a diffusive regime and localization phenomena in the low temperature limit. It gives all information on the intrinsic quantum conductivity which can be accessed experimentally by four-points transport measurements (meaning two electrodes for generating voltage drop and two others for measuring induced current). With this formalism, when the system is translational invariant, no scattering takes place, and the "intrinsic" mean free path is infinite. Differently, the Landauer–Büttiker transport formalism is directly linked with two-points transport measurements (meaning two identical electrodes for generating voltage drop and measuring induced current) and is proportional to the transmission probability for charges to be transfered through a given system connected to external electrodes. A connection between Kubo and Landauer can be made by rewriting the two-points resistance (computed with the Landauer–Büttiker method) as e.g. $R = R_0/T = R_0 + R_{\text{int}}$, making explicit the "intrinsic resistance" $R_{\text{int}} = R_0(1-T)/T$, which could be derived applying the Kubo–Greenwood approach.

Within this formalism, when the system is free of scattering, or when the density of impurities is sufficiently low such that $\ell_e \gg L$ (L is the distance between source/drain electrodes) the transport regime is ballistic, with a transmission probability at energy E entirely proportional to the number of propagating modes, that is $G(E) = G_0 N_\perp(E)$.

In the situation of a large amount of scatterers (such as chemical impurities), i.e. when $\ell_e \ll L$, the transport regime becomes diffusive and the conductance scales as $G(E) = G_0 N_\perp(E)\ell_e(E)/L$. An interpolation formula allows covering of the so-called quasiballistic regime with $T = N_\perp(E)/(1 + L/\ell_e)$. If the quantum transmission at the system/electrode interface is perfect (induces no scattering), then both Kubo and Landauer formalisms are totally equivalent, although some geometrical factors differentiate them if computed with the different formalisms (Akkermans & Montambaux, 2007). The extracted Landauer mean free path ℓ_e^L and Kubo mean free path ℓ_e^K are expected to be proportional, $\ell_e^L = \kappa \ell_e^K$ ($\kappa = 2$ for $d = 1$, $\kappa = \frac{\pi}{2}$ ($d = 2$), $\kappa = \frac{4}{3}(d = 3)$) (Akkermans & Montambaux, 2007). In the case of a rectangular waveguide, the κ coefficient depends on the dimensionality of the system (Datta, 1995).

For instance, to determine exactly the κ coefficient for a finite nanotube, one needs to solve the diffusion equation for the specified geometry and given boundary conditions (Datta, 1995). $\kappa = 2$ at the charge neutrality point. This can also be shown using the

Einstein relationship for conductivity, $\sigma_F = e^2 \rho_F D_F$, where $\rho_F = 4/\pi\hbar v_F$ is the total density of states at CNP, and $D_F = \ell_e v_F$ is the diffusivity coefficient at CNP. The total conductivity for the quasi-1D system is obtained by using Ohm's law, $G = G_0 N_\perp 2\ell_e/L$.

3.4.3 Validity limit of Ohm's law in the quantum regime

Ohm's law in the classical regime can be easily derived using the 1D formula for the conductance of a diffusive system, i.e. $G = \sigma_{sc} L^{d-2} = e^2 \rho(E) D/L$, with $\rho(E) = 2/hv_F$ and $D = \ell_e v_F$. Then $G = 2e^2/h\frac{\ell_e}{L}$ which uses the additivity rule of resistance, i.e. $\mathcal{R}(L_1 + L_2) = \mathcal{R}(L_1) + \mathcal{R}(L_2)$. In the quantum regime, if one uses the Landauer expression for the conductance/resistance, one demonstrates that the resistance $\mathcal{R}(L_1 + L_2) > \mathcal{R}(L_1) + \mathcal{R}(L_2)$ because of multiple scattering phenomena.

3.4.4 The Kubo formalism in real space

An efficient real space implementation of the Kubo formula was first developed by Roche and Mayou in 1997 for the study of quasiperiodic systems (quasicrystals) (Roche & Mayou, 1997). It was then adapted by Roche and coworkers to allow exploration of mesoscopic (magneto)-transport in complex and disordered mesoscopic systems including carbon nanotubes, semiconducting nanowires, and graphene-based materials (Roche, 1999, Roche & Saito, 2001, Roche *et al.*, 2005, Latil, Roche & Charlier, 2005, Lherbier *et al.*, 2008, Ishii *et al.*, 2009). The typical disordered samples studied with such methodology already contain several tens of millions of orbitals, and with the use of high performance computing resources, the simulation of samples with 1 billion atoms can be envisioned in the next decade. This numerical transport method therefore offers unprecedented exploration possibilities of complex quantum transport phenomena, not only in realistic models of disordered graphene-based materials, but also in any other types of materials of exciting scientific and technological interest (silicon nanowires (Persson *et al.*, 2008), organic crystals (Ortmann & Roche, 2011), topological insulators, etc).

We present here the basic ingredients of the numerical implementation and provide in further sections extensive illustrations of its use in the study of disordered graphene-based materials (Roche, 1996, Triozon, 2002, Lherbier, 2008). Appendix D provides an extensive technical derivation of such a real space (and order N) implementation using the Lanczos method, which is also reviewed in detail. We present here a summary of such a derivation, since it will help us to explore most quantum transport regimes in complex forms of graphene-based materials. We start again with the general form of the Kubo conductivity:

$$\sigma(\omega) = \frac{2\pi e^2 \hbar}{\Omega} \int_{-\infty}^{+\infty} \frac{f(E) - f(E+\hbar\omega)}{\hbar\omega} \mathrm{Tr}\left[\hat{\mathrm{V}}_x \, \delta(E - \hat{\mathcal{H}}) \, \hat{\mathrm{V}}_x \, \delta(E - \hat{\mathcal{H}} + \hbar\omega)\right] dE, \quad (3.78)$$

where $\hat{\mathcal{H}}$ is the Hamiltonian operator, $\hat{\mathrm{V}}_x$ is the operator for the electronic velocity along the x axis and $f(E)$ is the Fermi distribution function. The DC conductivity corresponds to the limit $\omega = 0$. Using the property